ABSTRACT

Title of Document: NATURAL VARIATION IN BIOLOGICAL AND SIMULATED CENTRAL PATTERN GENERATORS

David L Boothe, Doctor of Philosophy, 2007

Directed By: Professor Avis H. Cohen, Department of Biology

Here we analyze natural variability within two types of systems. 1, The output of the biological spinal central pattern generator for locomotion in the cat, and 2, Sets of stochastic neural networks giving an output qualitatively similar to that observed within the biological system.

Fictive locomotion contains asymmetric transitions between the flexion and extension phases. The transition from extension to flexion is: 1, Always strongly phase locked; 2, Composed of overlapping extensor burst offsets and flexor burst onsets; and 3, Invariant to changes in mean cycle period. The transition from flexion to extension is: 1, Weakly phase locked within bouts containing short cycle periods, and well phase locked in bouts containing long cycle periods; 2, Offset times of flexor bursts and the onset times of extensor bursts do not overlap; and 3, Strength of phase locking depends critically upon relative timing of flexor offset and extensor onset.

Stochastic neural networks that qualitatively reproducing the timing relationships observed within the biological system have outputs that depend upon both the architecture of the network as well as model neuronal type (oscillatory-non-

oscillatory). Within models designed to reproduce the bi-phasic activity observed in some muscles, correlation of the bi-phasic burst is strongly influenced by model connectivity. Additionally sets of leaky integrators have burst durations, which are sometimes well correlated even though they are well separated in time.

Half-center models producing alternating output are strongly influenced by the internal structure of simulated neurons. A half-center composed of a pair of leaky-integrators has transitions between phases which are always well phase locked, and overlapping. Half-centers composed of intrinsically oscillatory Morris-Lecar neurons have transitions between phases whose phase locking is parameter dependent. This parameter dependence is mainly due to changes in the timing of burst offset and burst onset.

We conclude that the output of the biological central pattern generator is likely to be strongly influenced by the intrinsically oscillatory properties of its neurons. Models containing non-intrinsically oscillatory simulated neurons are unable to account for observed variability within the output of the biological system.

NATURAL VARIATION IN BIOLOGICAL AND SIMULATED CENTRAL PATTERN GENERATORS

By

David L. Boothe

Dissertation submitted to the Faculty of the Graduate School of the
University of Maryland, College Park, in partial fulfillment
of the requirements for the degree of
Doctor of Philosophy
2007

Advisory Committee:
Professor Avis H. Cohen, Chair
Professor Todd W. Troyer
Professor Catherine Carr
Professor James Reggia
Professor John Jeka

Acknowledgements

I would like to thank:

My advisor Dr. Avis H. Cohen for all of her support over more years than I would like to admit, and for making her lab a positive environment for researchers who want to look at neuroscience from a different perspective.

My second and unofficial advisor Dr. Todd W. Troyer, for spending many many hours teaching me more math than I ever new existed, and for most importantly knowing when to slow down and explain things.

My parents and family for always believing in me, and being supportive.

All of my friends from University of Maryland, and elsewhere who kept me sane through the whole thing.

TABLE OF CONTENTS

List of Tables

List of Figures

CHAPTER ONE: GENERAL INTRODUCTION

The History of the Half-Center

Since the beginnings of the scientific study of the nervous system it has been observed that animal preparations, even though greatly reduced either through the elimination of higher centers or through lack of sensory input, could maintain a rhythmic motor output similar to that observed within walking in the intact animal (Brown, 1911, Sherrington, 1913). Brown proposed from this evidence that the nervous system contained intrinsically active 'centers' which alternated in activity and provided the source of the neural signal to the muscles necessary to maintain movement (Brown 1911). In modern terms this intrinsically active center is called the spinal central pattern generator for locomotion (sCPG).

The first theoretical model proposed to explain the persistence of rhythmic behavior within an animal preparation that was greatly reduced is the half-center (Lundberg, 1969). Lundberg hypothesized that the spinal cord contained a set of mutually inhibitory neurons which were activated in an alternating fashion. Activity within each set of neurons was associated with activity within either flexors (muscles causing lifting of the limb), or extensors (muscles causing protraction of the limb). For Lundberg, the isolated spinal cord within the reduced preparation was incapable of generating the complicated pattern of activity observed within the intact animal without sensory input into the network.

Subsequently, Grillner and Zangger (1979, 1984) observed that individual nerves within the ventral root retain a pattern of activation very similar to that observed within intact locomotion even when the spinal cord was isolated from sensory input. To account

for this complex pattern of activity Grillner hypothesized that the sCPG consisted of not just a single half-center but a collection of linked half-centers each controlling activity within single joints (Grillner, 1981). This framework with the half-center as the basic building block of the sCPG for locomotion continues to be the dominant paradigm in understanding the structure of the sCPG.

Ubiquity of Oscillation

Study of the structure of the mammalian sCPG for locomotion has been complicated by a variety of factors, but perhaps historically the most vexing is the ubiquity of oscillatory behavior within neurons of the spinal cord. This ubiquity has made identification of neurons making up the sCPG for locomotion difficult. This is most clearly evident in the work of Orlovskii and Feldman (1972). In a survey of 30 spinal interneurons the authors found that 11/30 were active during the stance phase of locomotion, 8/30 during the swing phase of locomotion and that the remaining 11/30 could not be categorized as associated with either the stance or the swing phase of locmotion. More modern approaches focus on molecular methods to identify sets of interneurons which are likely to have intrinsically oscillatory properties on the assumption that these neurons are likely part of the core sCPG within the spinal cord (Eide, et. a.l., 1999, Kiehn, 1996, Stokke, et. al., 2002).

Perturbation of the Network: The Modern Paradigm

Given the inaccessibility of sCPG to direct measurment, the dominant experimental paradigm for understanding network function is through analysis of its

response to perturbation. While recording intracellularly from motor neurons in a reduced preparation one stimulates a single nerve at high frequency (Burke et. al. 2001, Quevedo et. al. 2005a-b). Stimulation at the periphery causes sub-threshold excitatory and inhibitiory post synaptic potentials within the motor neuron of interest. An analysis of the timing and strength of theses PSPs allows one to make inferences about the details of the pathway from sensory interneurons to motor neurons.

Differential response to peripheral stimulation has led to the hypothesis that the sCPG for each limb is hierarchal, containing a feed-forward rhythm generator setting the overall timing for flexion and extension, and a separate pattern formation network that both shapes the output of rhythm generator and adapts that output to sensory inputs (Rybak et. al, 2006a-b, La Friene Roula et. al. 2005). Perturbation experiments like these form the main experimental evidence used to calibrate models of the mammalian sCPG for locomotion.

Previous and Current Models of the Mammalian CPG

Given the fact that the sCPG network is uncharacterized, construction of biophysical realistic models is impossible. Traditionally, models of the sCPG for locomotion have used the half-center organization as the basic building block of network connectivity. Sets of deterministic half-centers can then be coupled together to explain how coordinated activity across multiple joints is maintained (Taga. 1991), Rybak, 2006a-b). These models differ from one another in terms of connectivity, for instance order to account for responses to periphaeral perturbation the Rybak (2006a-b) model is hierachal with a separate half-center termed the rhythm generator connected in a feed

forward fashion to a set of lower level pattern formation neurons. The major weakness of these models and models like them is that model dynamics are sufficiently complicated that understanding their functioning is non-trivial.

Quantifying Natural Variance

Our approach to understanding the structure of the mammalian sCPG differs substantially from those described above. The current work focuses on using the natural variance within the output of both biological and simulated networks as a probe into the structure function relationships inherent within those networks.

Natural variation within the nervous system is derived from many potential sources the impacts of which are matters of much debate. Within model systems of simulated neurons natural variation is induced by the injection of noise into the network of interest. The natural variation of each system can then assessed through the use of identical statistical techniques.

The addition of noise to simulated neuronal networks is not new in and of itself, but the context within which it is used here is novel. Most of the current results focus on networks having some strong underlying asymmetry within their structure. These asymmetries allow noise to influence the output of the networks under study in interesting and previously unknown ways. At some points in the dynamics of these networks injected noise shows very little influence on model outputs, whereas at other times it might strongly influence the behavior of the network. The differences in the way noise interacts with network dynamics can then be observed in the relative timing of events within each models output. One can then track which set of asymmetries within

the internal structure of the networks creates which timing relationships within its output and compare these directly to the output of the biological system.

Unlike the lamprey system, the study of mammalian locomotion has been largely devoid of detailed mathematical analysis. This is likely due to the unreliability of most mammalian locomotion preparations making statistically significant data sets rare. As such even a basic analysis of the structure of natural variation within the output of biological system is currently unreported within the literature.

Here we report our analysis of natural variation within three systems 1, Two sets of stochastic neural networks designed to produce double-bursting. 2, The output of MLR induced fictive locomotion within the cat, and 3, Two stochastic half-centers, one composed of oscillatory and one composed of non-oscillatory units.

Models of Double Bursting (Chapter 2)

One important theoretical problem for models of the sCPG organized in a half-center fashion is double bursting. Many muscles within the hind limb of cat are active twice per cycle, once during flexion and once during extension. This pattern of activation is unlikely to be reproducible within a network composed of linked half-centers. We hypothesized two ways that the half-center could be modified to provide a double bursting output (Boothe, and Cohen, 2002, Chapter 2). Such modified half-centers could potentially be fit within a larger network like those proposed above (Taga 1991, Rybak. 2006). The set of models we present here, unlike previous models of mammalian locomotion, emphasize are mathematically tractable and transparent in their dynamics.

We report our analysis of how each model's architecture and dynamics determines the observed natural variabilitiy inherent in model outputs within Chapter 2.

Natural Variation within the Ouput of the MLR Induced Fictive Locomotion (Chapter 3)

Surprisingly, detailed analyses of the natural variability of fictive locomotion is unreported within the mammalian sCPG literature. Likely sources for this absence are as stated previously a lack of large data sets, and a focus on experiments involving perturbations of the system. The one previous study similar to that presented here focused on the relationships between burst durations and cycle period (Yakovenko, 2005). However this study left important aspects of the output of the fictive locomotor preparation unanalyzed, specifically the timing relationships between burst onsets and offsets. Chapter 3 provides a detailed study of these timing relationships and what sorts of inferences can be made regarding underlying sCPG structure. Unforunately, an in depth analysis of double bursting was impossible due to the lack of data.

The Influence of Model Neuronal Type on the Output of the Half-Center (Chapter 4)

Although the half-center has been well studied both as a mathematical object (Sommers and Kopell, 1994, Jung, et. al., 1996, Izhikevitch, 2001), and as the building blocks in more complicated networks (Taga, 1991, Rybak, et. al. 2006a-b), the impact of model neuronal type on the output of such networks is sparse. Here, we present a set of stochastic half-centers and report how model neuronal type influences network output. We then use these networks to flesh out hypotheses developed in Chapter 3 to explain our observations of the output of the biological sCPG

CHAPTER TWO: TEMPORAL CORRELATIONS IN A STOCHASTIC MODEL OF DOUBLE BURSTING

(Boothe DL, Cohen AH, Troyer TW (2006) Temporal correlations in a stochastic model of Double bursting. J Neurophysiol 95: 1556-1570)

Abstract

The output of the spinal central pattern generator for locomotion falls into two broad categories; alternation between antagonistic muscles, and double bursting within muscles acting on multiple joints. We first model an alternating half-center, and then present two different models of double bursting. The first double bursting model consists of a central clock with an explicit one-to-one mapping between interneuron activity and model output. The second double bursting model consists of a half-center with an added feedback neuron. Models are built using rate-coded leaky integrator neurons with slow self-inhibition.

Structure-function relationships are explored by the addition of noise. The interaction of noise with the dynamics of each network creates a unique pattern of correlation between phases of the simulated cycle. The effects of noise can be explained by perturbation of deterministic versions of the networks. Three basic results were obtained: 1) slow self-inhibitory currents lead to correlations between parts of the step cycle that are separated in time and network relative; 2) model outputs are most sensitive to perturbations presented just before competitive switches in network activity, and; 3) clock-like models possess substantial symmetries within the correlation structure of burst durations, whereas the correlation structure of feedback models are asymmetric.

Our models suggest that variability in burst length durations can be analyzed to make inferences about the structure of the spinal networks for locomotion. In particular,

correlation patterns within double bursting outputs may yield important clues regarding the interaction between more central, clock-like networks and feedback from more peripheral interneurons.

Introduction

The dominant behavior of electroneurograms (ENGs) recorded in the mammalian spinal cord during locomotion is an alternating output that occurs during walking. Generally, flexors are active during the swing phase of locomotion when the animal lifts its limb off the ground and extensors are active during stance when the animal makes contact with the ground and pushes itself forward. Many muscles display more complicated behaviors such as double bursting, in which a flexor is active during both the swing and the stance phases of locomotion (Grillner, 1979). Within intact animals the period of co-activation between flexor activity and extensor activity is thought to stabilize the limb upon contact with the ground and can be used to create additional force during extension (Grillner, 1975). The addition of a second flexion burst to the familiar alternation between flexion and extension results in an output pattern with four parts (Forssberg 1979): (F) flexor on alone; (E1) extensor on alone during the beginning part of extension; (E2) a second flexion phase cotemporaneous with extensor activity; and (E3) extensor on alone during the later part of extension.

Double bursting raises a key theoretical issue about the structure of the spinal central pattern generator (CPG) for locomotion: are the two bursts of flexion controlled by independent or overlapping sets of neurons within the CPG? According to one hypothesis, the CPG is a set of neurons working much like a clock whose timing is set

centrally (Burke et. al 2001, Burke 1999). The basic output pattern of this clock is then fine tuned by the many interneurons of the spinal cord, but the basic pattern of activity within the clock itself remains unchanged. Alternatively, the interaction between more centrally located interneurons and feedback from interneurons closer to the periphery may create the proper output (Shefchyk et. al. 1990, Edgley and Jankowska, 1987). Under this hypothesis, some spinal premotor interneurons are part of the central pattern generator and contribute to pattern formation even in the absence of sensory input.

Here we investigate three network models of the spinal CPG for locomotion built using mutually inhibitory leaky integrator neurons with slow self-inhibition. We first study the dynamic properties of these networks using a simple half-center model with two mutually inhibitory interneurons. We then extend the half-center to consider networks that embody the two hypotheses above for producing double bursting outputs. The closest point of experimental contact with our modeling work is the data obtained from fictive walking in which the spinal cord is isolated by removing descending motor commands and inputs from the periphery. Although fictive walking is often quite variable and sometimes non-functional, there are bouts of fictive locomotion where the CPG output is very similar to the output of the intact system (Grillner, and Zangger, 1984, Grillner, 1975).

To investigate structure-function relationships in our models, we injected white noise currents into the model interneurons and studied the resulting patterns of variability in motor neuron outputs. In particular, we measured patterns of variance and covariance in the durations of different parts of the step cycle. To further analyze the models, we performed a series of microstimulation experiments that allows the effect of a single

perturbation to be traced through time. Results from these experiments can then be reintegrated to understand the results from the noise-driven simulations.

Overall, we find three basic results. First, we find that the slow dynamics of self-inhibition can cause correlations that occur over more than a single cycle. For example, in one network model, the duration of the flexion burst F is strongly correlated with the last phase of extension E3, but is nearly independent of the intervening phases E1 and E2. Second, the microstimulation studies show that the networks are much more sensitive to perturbation at some time points than others. For the current class of models, this sensitivity is generally greatest during the period just before transitions between parts of the step cycle. Finally, we find that the underlying symmetry in the clock-based model is reflected in the variations of the durations of different phases of the cycle. In particular, all phases of the step cycle have similar variance, and the correlation between two phases is determined chiefly by the number of intervening phases of the step cycle rather than the identity of either phase. This pattern is not seen within the model based on feedback from interneurons closer to the periphery where correlations between bursts are specific to interactions between the underlying inhibitory interneurons. Our modeling results suggest that measurements of the noise-driven correlation structure may provide insight into the structure and function of the underlying spinal CPG for locomotion.

Methods

The main aim of the models presented here was to explore basic theoretical issues related to the production of double bursting outputs during locomotion. Given our limited knowledge concerning the neuronal properties and connectivity of mammalian pattern

generating circuits we have chosen to explore basic structure-function relationships in simplified models of the spinal CPG (for current debates see *e.g.* Eide, et. al. 1999, Huang, et. al, 2000). The connectivity and structure of the networks are shown in Fig. 1. The connectivity of the half-center model is similar to that proposed for the lamprey spinal CPG (Grillner, 1975). The connectivity of the clock model has been studied previously within the context of gait creation and symmetry (Golubitsky, et. al. 1999), and the connectivity of the feedback model is similar to the function proposed for some sensory interneurons of the spinal cord (Edgely and Jankowska, 1987).

Neuron Model

We used the well-studied lamprey system as a starting point for our networks (Williams, 1992, Jung et. al., 1996). Lamprey neurons are known to exhibit bursting behavior in which spikes ride on a wave of depolarization. This wave of depolarization is well correlated with the output of the motor neurons as recorded by ENGs (Grillner 1975, 1979 and 1999, Kiehn, et. al., 1999)**.** Therefore we used simple rate-coded neurons where the activity in a single model neuron represents the summed bursting activity of a population of functionally related neurons (Jung, et. al. 1996, Boothe and Cohen, 2001, 2002). Model neuron *i* is governed by two internal variables: a normalized membrane voltage variable V_i that takes values between -1 and 1, and a slow self-inhibitory conductance $g_{di}D_i$, where D_i ranges between 0 and 1. Voltage dynamics are based on the following differential equation:

$$(1) \qquad \frac{dV_i}{dt} = g_{ri}\,(0 - V_i) + g_{ti}\,(1 - V_i) + \sum_{j=1}^{n} h(V_j)\, g_{syn}^{ij}\,(v_{syn} - V_i) + g_{di}\,D_i\,(-1 - V_i) + I_i$$

The terms on the right hand side of equation (1) represent the following currents: a leak current with conductance g_{ri} and reversal potential V=0; a tonically active excitatory current with conductance g_{ti} and reversal potential V=1; synaptic input from other neurons as represented by the sigmoid firing rate function $h(V_j)$ times a maximal synaptic conductance g_{ij} and reversal potential v_{syn} (v_{syn} =1 for excitation, v_{syn} = -1 for inhibition); the slow self-inhibitory current with conductance g_{di} D_i and reversal potential V= -1; and a perturbation current I_i. Perturbation currents took one of two forms: a Gaussian white noise process η_i, or a short step of current applied at various phases of an ongoing deterministic system. The slowly acting inhibitory conductance $g_{di}D_i$ was governed by an exponential decay to a cells output firing rate $h(V_i)$ with time constant τ:

$$(2) \quad \frac{dD_i}{dt} = (h(V_i) - D_i)/\tau_i$$

A similar schema for self-inhibition was used in Pribe, et. al. (1997), where the slow self-inhibitory current was construed as an additional neuron providing inhibitory feedback.

The firing frequency of a simulated neuron is a function of the membrane voltage and is determined by a non-linear sigmoid rate function $h(V_i)$. We chose to use a piecewise polynomial function with the following properties (Jung, et. al. 1996): (i) outputs rates range from 0 to 1; (ii) there exists a true threshold (V_i = 0) below which output rate is equal to 0; (iii) the function is sufficiently smooth to facilitate currently unpublished bifurcation analyses.

$$(3) \quad h(V_i) = \begin{cases} 0 & if \quad V_i < 0 \\ -20\,V_i^7 + 70V_i^6 - 84\,V_i^5 + 35\,V_i^4 & if \quad V_i \geq 0 \end{cases}$$

Analysis of Network Behavior

Our analysis focused on changes in the durations of parts of the step cycle. All three of the networks analyzed (Fig. 1) included two excitatory interneurons that serve as the model's output, one to flexor motor neurons (E_f) and one to extensor motor neurons (E_e). The fractionation of the step cycle into parts was determined by time intervals during which these neurons were above a burst threshold. To avoid small noise fluctuations near threshold being registered as separate events, burst threshold was set at 0.1 simulated units of voltage. In addition, periods of threshold crossing shorter than .1 simulated seconds were not considered to be bursts and were ignored.

The flexor burst (F) and the extensor burst (E) were defined as the period of time in which activity in E_f and E_e, respectively, were above the burst threshold (see Fig. 2). A cycle is defined as the time from the beginning of one flexion phase (F) to the beginning of the next flexion phase (F). The two double bursting models have a second period of flexor activity that is cotemporaneous with extension. This splits the extensor period E into three parts. These are E1, which is the length of time from the beginning of the E burst (extensor on alone) until the beginning of the second flexor burst, E2 in which both E_e and E_f are above threshold, and E3 which is the length of time from the end of E2 to the end of extension. Note there may be short periods during transitions when neither neuron is active, so F+E1+E2+E3 is not always equal to the length of a full cycle. In practice, these small periods of time made little difference to the results.

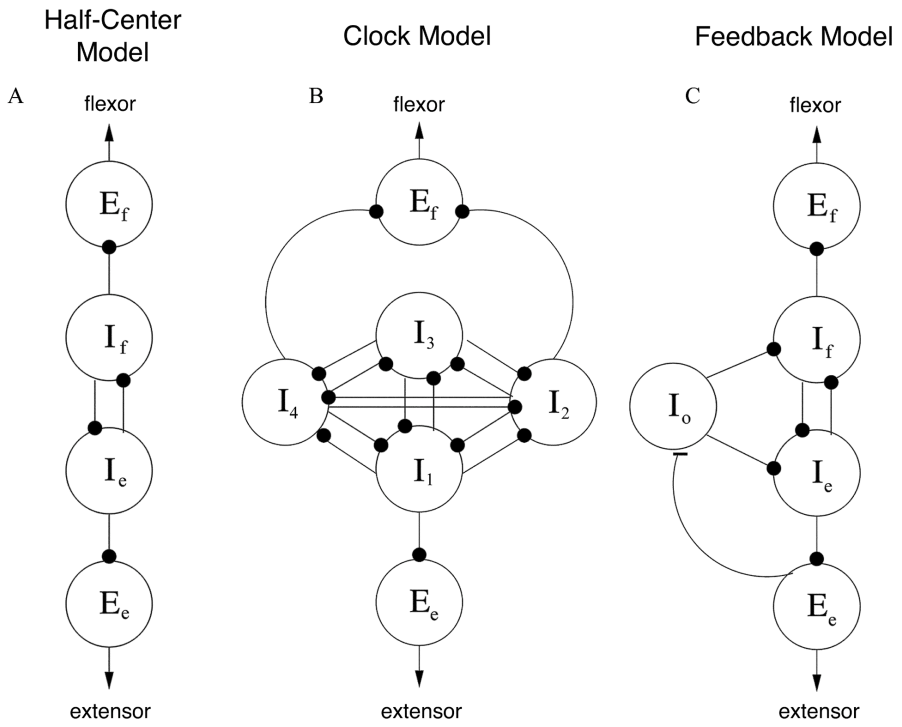

FIG. 2.1, Model Architectures. Excitatory/inhibitory connections are marked with a line/filled circle. Excitatory interneurons form the model output: E_f to flexors; E_e to extensors. A: Half-center model. Mutual inhibition biased by slow self-inhibition (not shown) causes alternation of the two central interneurons (I_e, I_f) and hence alternating flexion and extension. B: Clock model. Mutual inhibition with asymmetric weights causes serial activation of the four central interneurons, I_1 to I_2 to I_3 to I_4. When I_3 is active, neither E_f nor E_e is inhibited creating double bursting output. C: Feedback model, consisting of a half-center plus an additional "override" neuron I_o. Onset of extension activates I_o, inhibiting I_f and I_e simultaneously, creating double bursting output.

Model Parameters

The network architectures studied are shown in Fig. 1. Final parameter values were set with two basic aims: the burst durations should match the burst durations measured during fictive walking in the cat, and overall cycle variability should be similar across models (Boothe and Cohen, 2002). The need to control burst durations had to be

balanced with the need to achieve stable behavior in the face of added noise.

Overall, the half-center model and clock model (Fig. 1A, 1B) are more robust than the feedback model (Fig. 1C), giving functional outputs for many parameters varying over an order of magnitude. A number of parameters affect total cycle duration on both models but keep the basic activity patterns intact. The frequency of oscillation can be increased by raising the tonic drive to the inhibitory interneurons, g_{ti}, and/or by reducing the magnitude of either g_{di} or the time constant □ of the slow self-inhibition. Burst durations remain at a fixed relative phase during these changes.

In the clock model, the main difficulty in achieving stable output was a tendency for the model to have two simultaneous winners in the central square of inhibitory interneurons. This was counteracted by increasing tonic excitatory drive to these neurons while increasing the strength of the mutually inhibitory connections (see below). Since parameters affecting a single interneuron tended to change the durations of multiple phases of the cycle, achieving the appropriate fractionation of the step cycle required the simulataneous adjustment of several parameters..

In the feedback model, a mismatch between parameters affecting the override neuron and those affecting slow inhibition in the central inhibitory neurons I_e and I_f caused non-functional alternating outputs where flexion and extension overlap at the end of flexion and the beginning of extension. Due to the hierarchical nature of this model, it was relatively easy to independently adjust the durations of different parts of the step cycle.

Values of the parameters used are reported below. The rest conductance of all neurons in all models was set to g_{rI} , $g_{rE} = 3.5$. Synaptic conductances not represented in

Fig. 1 and not described below have been set at g^{ij}_{syn}=0, including g^{ii}_{syn}=0 for all simulated neurons.

The parameters of the half-center model were as follows: the tonic excitation to the excitatory interneurons, g_{tE}= 1.6; tonic excitation to the inhibitory interneurons, g_{tI}= 1.0; the conductance of the slow self inhibition, g_{dI}= 100; the conductance of the synaptic current from the inhibitory interneurons to the excitatory interneurons, g^{IE}_{syn}= 90; and the synaptic current between the mutually inhibitory interneurons, g^{II}_{syn}= 35; and the time constant of self-inhibiton on the inhibitory interneurons, □= 10.

The parameters of the clock model were as follows: the tonic excitation to the excitatory interneurons, g_{tE}= 2.0; the tonic excitation to the inhibitory interneurons, g_{tI}= 20; the conductance of the slow self inhibition, g_{dI}= 75; the conductance of the synaptic current from the inhibitory interneurons to the excitatory interneurons g^{IE}_{syn}= 20; and the strong synaptic current between the mutually inhibitory interneurons, g^{I1I4}_{syn}, g^{I2I1}_{syn}, g^{I3I2}_{syn}, g^{I4I3}_{syn}= 70; the medium synaptic current between the mutually inhibitory interneurons, g^{I1I3}_{syn}, g^{I2I4}_{syn}, g^{I3I1}_{syn}, g^{I4I2}_{syn}= 100; and the weak synaptic current between the mutually inhibitory interneurons, g^{I1I2}_{syn}, g^{I2I3}_{syn}, g^{I3I4}_{syn}, g^{I4I1}_{syn}= 65; and the time constants of self-inhibiton, □$_1$= 4, □$_2$= 3, □$_3$= 3, and □$_4$= 2.

The parameters of the feedback model were as follows: the tonic excitation to the excitatory interneurons, g_{tE}=1.6; the tonic excitation to the inhibitory interneurons, g_{tI}=3.5; the tonic excitation to the override neuron, g_{tO}=.7; the conductance of the slow self inhibition on the mutually inhibitory interneurons I_e and I_f, g_{dI}=100; the slow self inhibition on the override neuron, g_{dO}=150; the conductance of the synaptic current from the inhibitory interneurons to the excitatory interneurons, g^{IE}_{syn}=100; the synaptic current

between the mutually inhibitory interneurons, g^{II}_{syn}=35; the synaptic current between the flexor excitatory interneuron and the override neuron, g^{EeIo}_{syn}=15; and the synaptic current from the override neuron (I_o) to the mutually inhibitory interneurons, g^{IoI}_{syn}=150, the τ of self-inhibiton on the mutually inhibitory interneurons, τ=10, τ_O=9.

Simulations

Stochastic simulations were run on a Dec-alpha using xpp.aut (Bard Ermentrout, www.math.pitt.edu/~**bard**/xpp/xpp.html). Differential equations used in the model were solved numerically using the Euler-Maruyama method for solving stochastic differential equations (Oksendal, 2000). Simulations were originally run using a variety of time steps and methods with little change in model outputs; reported simulations used a time step *dt* =0.004. This noise takes the simplest possible form, an additive current into the membrane voltage. At each time step of width *dt,* noise values in the term ξ_i were drawn from a Gaussian distribution with standard deviation equal to one and then scaled by the quantity σ/sqrt(*dt*). The final value for σ was set so that the variability in cycle length was approximately the same for all models (σ=.03 for the half-center, σ=.04 for the clock model, and σ=.01 for the feedback model).

The deterministic microstimulation experiments were performed using the standard ODE solver available in matlab [ode23; Mathworks, Natick, MA]. Parameters of this model were identical to those used in the stochastic case. A small current was injected into each model for 10 time steps, or 0.04 simulated seconds. Due to their greater stability, the magnitude of injects current was larger for the half-center and clock model (0.3) than for the feedback model (0.1). For each of the central inhibitory interneurons

in each model, we performed 60 separate simulations in which microstimulation was initiated at regular 0.1 second intervals spanning the 6 second long prototypical cycle. Burst durations were then compared to perturbation-free simulations. Since perturbations of burst durations were small during the second cycle after the perturbation was given, we analyzed changes in burst duration for phases of the step cycle containing the pertubation as well as the phases in the next cycle.

Measuring and Predicting Correlations

Correlations between the lengths of different phases of the step cycle were quantified using Pearson's correlation coefficient, *r*. For any two variables X and Y the correlation coefficient ranges from –1 to +1 and is defined by

$$r = \frac{Cov(X,Y)}{\sqrt{Var(X)Var(Y)}}$$

where *Cov(X,Y)* is the covariance of X and Y and *Var(X)=Cov(X,X)* is the variance of X.

Correlation coefficients measured during the simulations with noise could be predicted from the results of the microstimulation simulations described above. We write the magnitude of burst duration perturbations as $\Delta\Delta_B(t, I)$. The subscript *B* refers to the burst phase for which perturbations are measured (F and E for the half-center model and F, E1, E2 and E3 for the double bursting models), the argument *t* refers to the time of the perturbation relative to the beginning of the cycle containing the burst, and the argument *I* is the label of the interneuron to which the stimulation was delivered (I_e and I_f for the half-center; I_1, I_2, I_3, and I_4 for the clock model; I_e, I_f, and I_o for the feedback model).

Since all perturbations decay to very small values by the second cycle after stimulation, we only computed values for times in the same and previous cycle as the burst in question, for all other times *t* we assumed $\Delta\Delta_B(t, I)=0$.

We view noise as a continuous bombardment of perturbations having amplitude *a(t,I)* delivered at time *t* to interneuron *I*. To the degree that perturbations are linear, this perturbation should change the lengths of bursts X and Y by amounts proportional to $a(t,I)\,\Delta t_X(t,I)$ and $a(t,I)\,\Delta t_Y(t,I)$ respectively. Implicit in this linearity assumption is the fact that negative perturbation have an equal and opposite effect as positive perturbations of the same magnitude. This assumption was examined for a sample of perturbations and found to hold to a reasonable degree.

We can perform a prediction *pCov*(X,Y) for the noise-driven covariance of burst phases X and Y, by noting that a given perturbation will contribute to the covariance of X and Y in proportion to the product of the effects of that perturbation on X and Y. Suppose X and Y lie in the same cycle and consider a perturbation delivered to interneuron *I* at time *t* relative to the start of that cycle. Let *a(t,I)* be the amplitude of the perturbation. This perturbation will contribute to the covariance of X and Y in proportion to $a^2(t,I)\,\Delta t_X(t,I))\,\Delta t_Y(t,I)$. A prediction *pCov*(X,Y) can be obtained by averaging these products over the distribution of noise amplitudes and summing these products over all perturbations that affect the lengths of both bursts. Since the noise injections are the same for all interneurons and uniform in time, the average of $a^2(t,I)$ is a fixed constant A. Then *pCov(X,Y)* is proportional to $A\sum_I\sum_s \Delta t_X(t,I)\,\Delta t_Y(t,I)$. If burst Y is in the cycle following burst X, then the expression becomes:

$$A\sum_I\sum_t \Delta t_{X,same}(t,I)\,\Delta t_{Y,next}(t-L,I)$$

where the time t is expressed relative to the cycle containing X and L is the length of an entire cycle. Finally,

$$r_{pred} = \frac{pCov(X,Y)}{\sqrt{pCov(X,X)pCov(Y,Y)}}$$

Note that in calculating the values for $pCov(X,Y)$, we sum over time at the resolution at which we delivered stimulation, *i.e.* time t covers the cycle in .1 sec intervals. To the degree that this resolution is sufficient to capture the behavior of the system, sampling time more finely should change the above expression by a constant factor. Since both this constant factor and the noise scaling A enter equally in the numerator and denominator, they do not affect our final predicted value for the correlation coefficient r_{pred}.

Results

We have analyzed three models of walking behavior. We begin with a detailed analysis of the simple half-center model in order to clarify and highlight basic behavioral principles that emerged from our analysis. We then explore two conceptually distinct mechanisms for the creation of double bursting each of which gives different predictions of the correlations structure between phases of the step cycle.

Half-Center Model

We start by exploring the behavior of a simple half-center oscillator, since it forms the basis for understanding fundamental properties of the double bursting networks presented later. The half-center model has been studied previously in the context of models of lamprey swimming (Bem et. al. 2003, Buchanan, 1992, Williams, 1992).

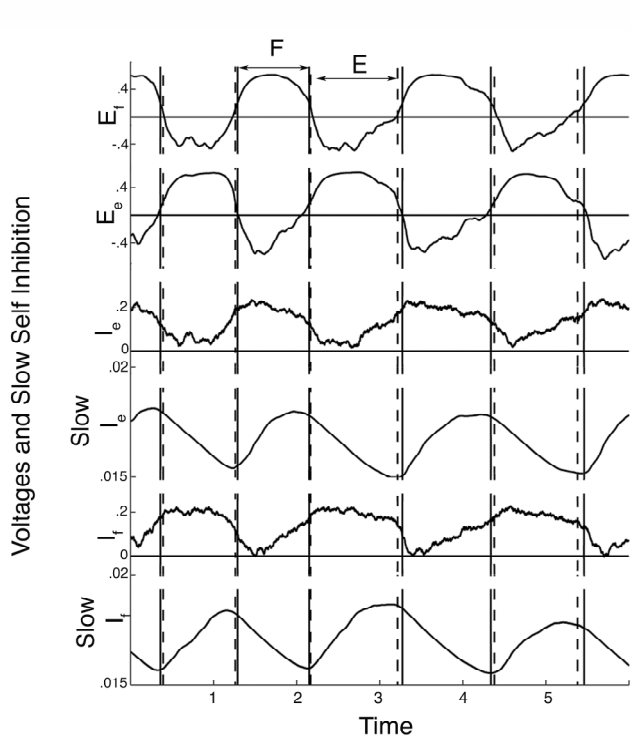

FIG. 2.2, Half-Center Output (noise level □ = 0.03). Voltage traces of the four interneurons, two excitatoy (E_e and E_f) and two inhibitory (I_e and I_f), plus slow self-inhibition in the two inhibitory neurons (Slow I_e and Slow I_f). The flexion burst (F; solid vertical lines) and extension burst (E; dashed vertical lines) are determined by activity in excitatory interneuron E_f and E_e being above threshold (=0.1). I_e suppresses extension and is active during F; I_f suppresses flexion and is active during E.

Dynamics of the half-center are characterized by the combined interplay of the fast winner take all interaction between the two mutually inhibitory interneurons (denoted I_e and I_f in Fig. 1A), and the slow dynamics of self-inhibition. Build up of slow inhibition in the currently active neuron eventually tips the competitive balance from one neuron to the other, resulting in alternating activity in the two mutually inhibitory interneurons (Fig. 2). The output of this central CPG is read out by corresponding excitatory interneurons (E_e and E_f in Fig. 1A). Note that since the actions of the central interneurons I_e and I_f are inhibitory, I_e is active during F (flexion) and I_f is active during E (extension).

To examine the dynamic structure within the network, we ran simulations in the presence of a white noise current injected into each of the two main inhibitory neurons I_e and I_f (see Methods) and measured overall variability and the correlation between the lengths of extension and flexion bursts in the same and surrounding two cycles (Fig. 3).

Correlation was quantified using the Pearson's correlation coefficient (see Methods). This correlation analysis reveals that F is positively correlated with adjacent parts of the step cycle (significantly different from 0; error bars show 2 standard deviations) and is uncorrelated with parts of the cycle further away. This means that a lengthening of F, rather than being correlated with a shortening of the adjacent E's, actually is correlated with their lengthening as well.

Microstimulation of the Half-Center Model

To understand the dynamic mechanisms underlying the correlation structure in the noisy case, we performed a series of microstimulation experiments in which single small perturbations were made to an otherwise noise free simulation (.2 amplitude current for .04 simulated seconds). Fig. 4a shows the reaction of the model to microstimulation of interneuron I_e delivered starting at time 2.5. The main effect of the microstimulation is to elongate the flexion burst F. This experiment was repeated, with microstimulation delivered at times evenly spaced throughout the step cycle. The changes in the flexion burst length (ΔF) were then plotted as a function of the time at which the stimulation of I_e was delivered (Fig. 4b). Thus, we see that perturbation of I_e late during F results in a relatively large lengthening of that phase, whereas stimulation early during F results in a moderate shortening.

This technique is generalized to examine how microstimulation of a given interneuron during one part of the step cycle affects the lengths of that and all subsequent parts of the cycle. Figs. 5Ab-5Ae show the effects of microstimulation of I_e on the length of four different burst phases: F and E during the current cycle and F and E during the

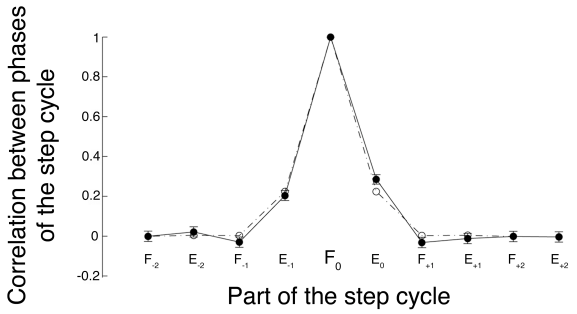

FIG. 2.3, Correlation Structure for the Half-Center Model (noise level □ = 0.03). Filled circles indicate Pearson correlation coefficients between flexion burst duration and other bursts for two cycles before and after. Error bars on correlation coefficients denote two standard deviations. Subscript denotes distance in cycles (0=current cycle, +1=next; -1=previous). F_0 indicates the correlation of F with itself (coefficient = 1). $E_{-1} > 0$ and $E_0 > 0$ indicate that the flexion burst is positively correlated with the length of the previous and subsequent extension. Open circles indicate linear prediction from microstimulation experiments.

next cycle (Fig. 5b is an extended version of Fig. 4b). Figs. 5Bb-5Be show the analogous results for stimulation of I_f. Notice that the plots in Figs. 5Ab and 5Bb fall to zero for times after the end of F, simply because microstimulation delivered after the end of F cannot affect its length. A similar causal relationship can also be seen at the right-hand side of Figs. 5Ac and 5Bc: microstimulation delivered after the end of E cannot affect the length of E. Note also that the symmetry of the underlying model is reflected in the perturbation results. For example, perturbations of I_f have the same effect on the length of E as do perturbations of I_e on the length of F.

The curves shown in Fig. 5 are related to the well-known phase response curve (PRC) commonly used to examine the behavior of coupled oscillators (Rinzel and Ermentrout, 1989; Winfree, 2001). However, the PRC measures the effect of a perturbation on the timing of the entire oscillation, whereas Fig. 5 separates out the effect of a given perturbation on the separate subparts of the oscillation over multiple cycles. The effects of microstimulation on the half-center oscillator can be understood by

considering three basic properties of networks using fast mutual inhibition and slow self-inhibition: (1) The dynamics are most sensitive to perturbation near the fast competitive events that happen at transition points in the step cycle; (2) the role for a given interneuron switches at these transition points; (3) microstimulation of a given interneuron has a relatively large immediate influence in one direction, followed by a rather long lasting inhibition that acts in the opposite direction.

The switch from excitation to inhibition is most clearly seen when examining the duration of the burst in which the microstimulation is applied. If the active interneuron is stimulated near the end of a burst, the fast resulting excitation extends that burst (stimulation of I_e extends F, Fig. 5Ab at time 1.2; stimulation of I_f extends E, Fig. 5Bc at time 2.2). This effect is relative large. If the stimulation of the active neuron comes near the beginning of the burst, the direct excitatory effects decay away and self-inhibition hastens the transition to the next phase of the cycle, shortening the ongoing burst (Fig. 5Ab at time .6; Fig. 5Bc at time 1.6).

Application of property 2 suggests that these effects should be reversed for stimulation of the opposite neuron. This is indeed the case for stimulation late in the burst phase: the fast excitation of the inactive interneuron favors this neuron in the upcoming competition, shortening the burst (Fig. 5Ac at time 2.2; Fig. 5Bb at time 1.2). However, for stimulation occurring early in the burst phase microstimulation of the inactive neuron does not push this neuron above threshold. As a result, no additional self-inhibition is recruited and stimulation has no effect on burst duration (Fig. 5Ac at time 2.1; Fig. 5Bd at time 1.1).

An important property of the slow self-inhibition is that a relatively brief stimulation can have effects that linger for multiple phases of the cycle. For stimulation late in the burst, the increase in activity that helps the neuron win the competition in the current burst leads to self-inhibition that hinders the neuron during the next cycle. For example, stimulation of I_e near the end of F lengthens that phase but also leads to greater inhibition within I_e. This increased inhibition hinders I_e during the subsequent competition and consequently lengthens E (Fig. 5Ab and 5Ac at time 1.1). Note that in this case the reversal from fast excitation to slow inhibition is accompanied by a reversal in role from the active to the inactive neuron during the transition from F to E. Thus, stimulation of the active neuron near the end of a burst increases the duration of both the ongoing and subsequent burst. The same combination of a reversal from excitation to inhibition and a role reversal happens for stimulation of the inactive neuron near the end of the burst, so this stimulation acts to shorten both the current and subsequent burst (5Ac and 5Ad at time 2.1; 5Bb and 5Bc at time 1.1).

Finally, we point out that the time course over which self-inhibition exerts its influence can be influenced by dynamic events that are influenced by the initial stimulation. For example, consider stimulation of the active neuron during the middle of a burst phase. The stimulation recruits additional self-inhibition that ends the ongoing phase early. However, this reduces the period during which self-inhibition accumulates, largely compensating for the initial increase in inhibition. As a result, after the competitive transition that ends the phase the system has returned to near its unperturbed trajectory and the effect of the perturbation on subsequent phases is negligible (5Ab-5Ae at time 1.1; 5Bc-5Be at time 2.1).

Correlation Structure of the Half-Center Model

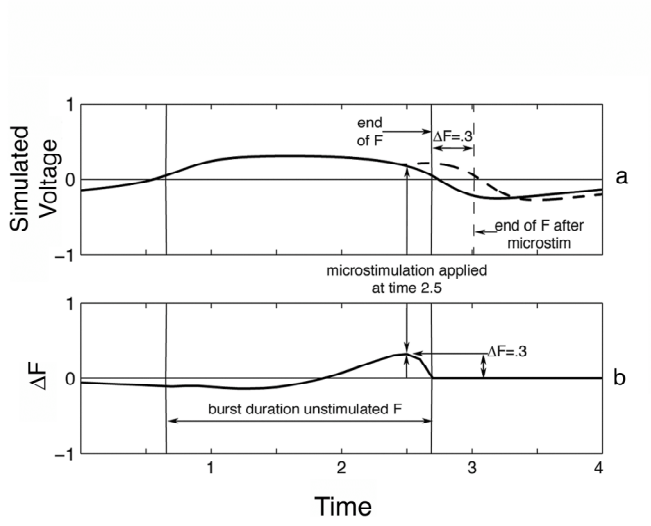

FIG. 2.4, Changes in Burst Duration Due to Microstimulation. Effects of microstimulation of I_e on the duration of F. (a) Voltage of E_f in the unstimulated condition (solid line) and with microstimulation starting at time 2.5 (dashed line). Vertical lines mark the end of F in the unstimulated (solid) and stimulated (dashed) simulations. The change in burst duration $\Delta F = 0.3$ sec. (b) ΔF as a function of the start time for microstimulation. Each point (0.1 sec intervals) shows ΔF for a single simulation, e.g. stimulation shown in (a) contributes the point at 2.5 sec. Stimulation of I_e early in the phase shortens F, whereas late stimulation lengthens F.

Taken as a whole, the microstimulation plots shown in Fig. 5 can be used to understand burst length correlations in the fully noise-driven model (Fig. 3). For example, consider the effects of microstimulating I_e near the end of F. As explained above, this stimulation will serve to elongate both F and E. That is, this common cause will tend to induce a positive correlation in the lengths of F and E. Viewing continuous noise perturbation as the sum of many small perturbations distributed in time, we can predict the net correlation between any two parts of the step cycle by computing the product of the effects of microstimulation on each part of the cycle, and summing these effects across all microstimulations (see Methods). Such a prediction assumes that the effects of perturbing different neurons sum linearly, as do the effects of perturbing the same interneuron at different times. It also assumes that effects scale linearly with the size of

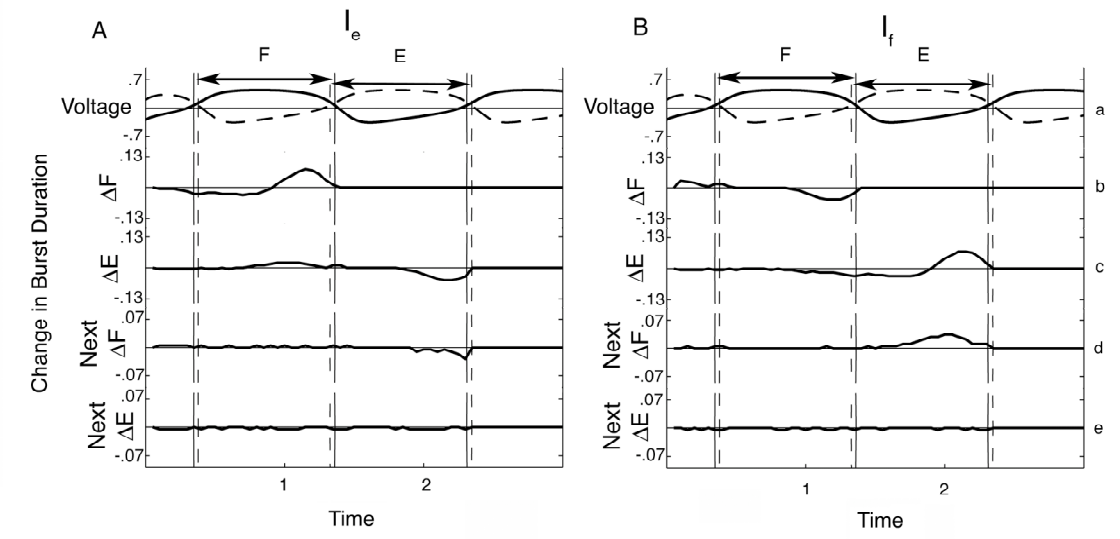

FIG.2.5, Microstimulation of the Half-Center. Effects of microstimulation of I_e (A) and I_f (B) on burst durations for the current and next cycle. a: Voltage traces of excitatory interneurons E_f (solid) and E_e (dashed). Vertical lines show limits of F (solid) and E (dashed). b,c: Change in F (□F) and E (□E) for the cycle undergoing microstimulation. Plots 5Aa and 5Ab are the same as in Fig. 4a and 4b. Stimulation of I_e near the end of F lengthens both F (time=1.1 Ab) and E (time=1.1 in Ac) in the current cycle. Stimulation of I_f near the end of E shortens F (time=1.1 in Bb) and E (time=1.1 Bc) in the current cycle. d,e: The change in burst durations of F and E in the cycle following microstimulation (labeled Next □F and Next □E above). Stimulation of I_e during E shortens E in the current cycle (time=2.1 in Ac) and F in the next cycle (time=2.1 in Ad). Stimulation of I_f during F lengthens F in the current cycle (time=2.1 in Bc) and E in the next cycle (time=2.1 in Bd). Influence of microstimulation on Next E is negligible (Ae and Be).

the perturbation, and that injecting a negative current has the opposite effect of injecting a positive current. Fig. 3 demonstrates that departures from these linearity assumptions are relatively minor.

Clock Oscillator Model

Like the half-center, the clock oscillator is constructed from a group of mutually inhibitory interneurons acting in a winner-take-all fashion. In generalizing the alternating half-center to a four phase output, the number of inhibitory neurons is increased from two to four (labeled I_1 to I_4, Fig. 1B). The weights within the network are biased such that

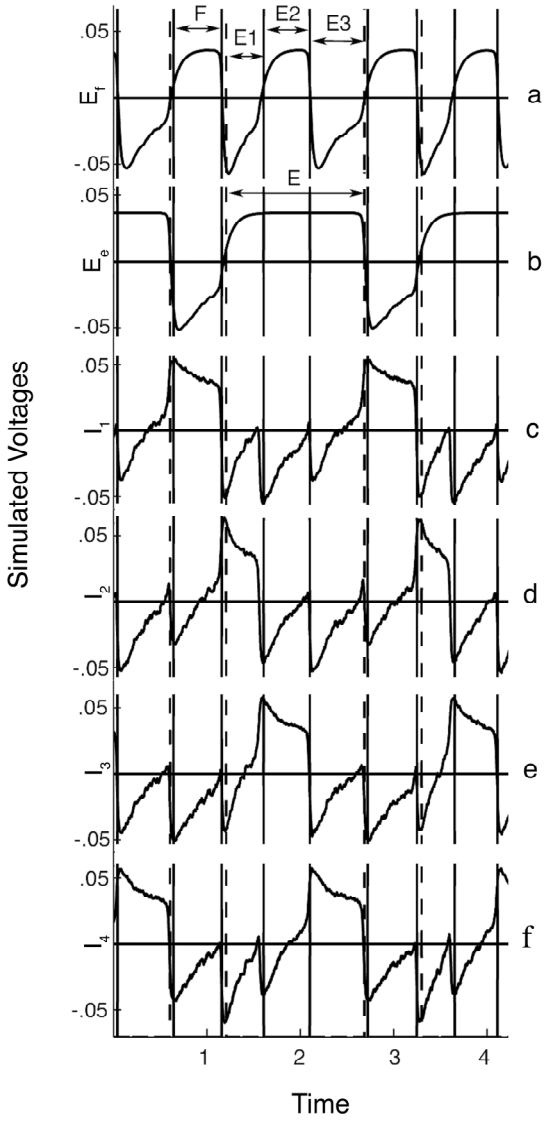

FIG. 2.6, Clock Model Output (noise level □ =04). a,b: Vertical lines show limits of F and E2 (solid) and of E1 and E3 (dashed) in the output of the excitatory interneurons (E_f and E_e). c-f: Activity in the four central inhibitory interneurons I_1, I_2, I_3 and I_4 correspond to phases F, E1, E2 and E3 in serial order.

activity patterns proceed in a single direction around the clock, I_1 to I_2 to I_3 to I_4 (Fig. 6). Each part of the cycle corresponds to activity within a single interneuron. In this sense, the central set of interneurons acts like a clock, marking off the four parts of the cycle. As in the half center model there are two excitatory interneurons E_f and E_e providing output to the flexor and extensor motor neurons. Activation of neuron I_1 corresponds to part F (flexor on alone), activation of I_2 to part E1 (extensor on alone), activation of I_3 to part E2 (double bursting), and activation of I_4 to E3 (extension alone).

Dynamics within the clock model have the property of rotational symmetry. For example, interneuron I_1 has a similar relationship with its neighbors I_4 and I_2 as interneuron I_2 has with its neighbors I_1 and I_3. More generally, rotating the labels in Fig. 1B would not

qualitatively change the pattern of relationships between the four central interneurons of the model. Since activity in each interneuron is associated with one burst phase of the cycle, we expect that the relationship of phase E1 with the surrounding phases F and E2 should resemble the relationship of phase E2 with its surrounding phases E1 and E3, etc. Note that because the time constants for the slow self-inhibition were altered to roughly match the experimentally measured burst lengths, the underlying symmetry of the dynamics is only approximate.

As a first step in analyzing output variability in the clock model, we set the noise level so that the coefficient of variation (CV = standard deviation divided by the mean) in overall cycle length was approximately 1.5% (noise level s=0.04 gave CV of the cycle = 1.45%). We then measured the CV for each part of the step cycle. All parts of the cycle showed similar degrees of variability as measured by the CV (F: 3.48%; E1: 2.50%; E2: 3.65%; E3: 2.78%). If the parameters of all neurons and connections were exactly symmetric, then the CVs would be identical (up to sampling noise).

We also measured the correlation for each part of the step cycle with all parts of the step cycle one cycle before and one after (Fig. 7). Each of the four subplots in Fig. 7 shows the correlation with a given phase of the step cycle. The dotted curve shows the correlations predicted from applying the linearity assumption to the perturbation results presented below. The basic pattern of correlation is similar for all four phases of the step cycle, *i.e.* the curve in each of the subplots has roughly the same shape when centered over the phase in question. This means that the strength of the correlation between any two phases of the step cycle is determined mostly by the number of intervening phases of the cycle, rather than on the specific phases being compared. Again, this is to be

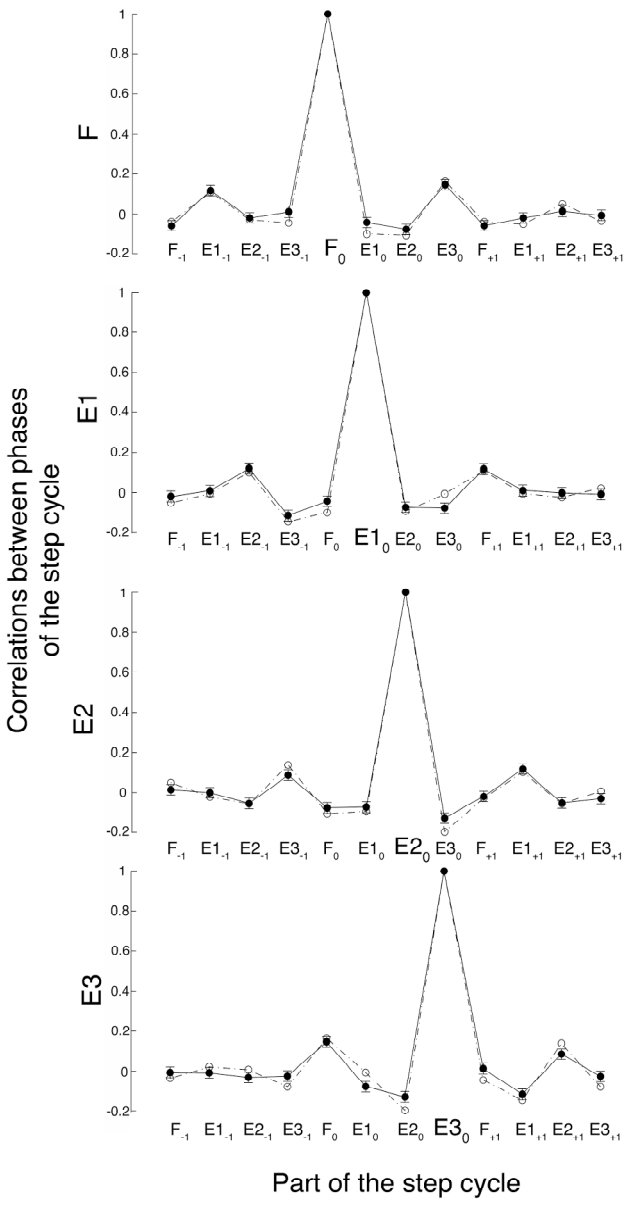

FIG. 2.7, Correlation Structure of the Clock Model. Correlations with noise shown as solid circles and solid line; error bars indicate 2 standard deviations. Each plot shows correlation of one phase of the cycle (F (a), E1 (b), E2 (c), E3 (d)) with other phases in the current, next and previous cycles (subscript = 0,+1,-1, resp.). All phases show the same basic pattern of correlation. Parts of the cycle separated by two intervening bursts have the strongest correlation, e.g. F_0 is most strongly correlated with $E3_0$, $E1_0$ with the next F_{+1}, etc. Open circles and dashed line show linear predictions from microstimulation.

expected from the approximate rotational symmetry of the underlying clock network. Second, the strongest correlations are between phases of the cycle that are separated by two intervening phases. This effect is moderately strong, yielding correlation coefficients in the range of 0.05-0.2 (Fig.7).

We explore the underlying dynamics of the clock model by examining the

effect of microstimulation on the central inhibitory neurons driving the oscillation. Fig. 8 shows the effect of microstimulation on interneurons I_3 and I_4. These plots again reveal the underlying rotational symmetry of the clock model, with stimulation of neuron I_3 having the same qualitative pattern as stimulation of I_4, just shifted in time and phase.

All the main features of the microstimulation experiments can be understood from direct application of the three properties outlined for the half-center model above. Stimulation of the active neuron results in the same large lengthening when delivered near the end of the burst and a moderate shortening when delivered earlier (Figs. 8Ac at times 2 to 2.8, and 8Bd at times 3 to 4). Like the half-center, the shortening of the phase from early stimulation largely compensates for an increase in self-inhibition so that early stimulation has little effect beyond the current phase. Also, stimulation of an inactive neuron near the end of a given phase aids this neuron in the upcoming competition and hence shortens that phase (Figs. 8Ab at time 1.9, and 8Bc at time 2.9).

The main difference between the models is that the clock model contains a greater variety of functional role reversals at competitive transition points between bursts. In particular, a neuron that has just been active does not participate in the competitions that determine the onsets of the next two burst phases. Therefore, the measurable output of the oscillator is not affected until the next cycle, where self-inhibition delays the onset of the corresponding burst. The delayed onset results in a lengthening of the burst before the neuron becomes active. The link between the extension of a burst and the delayed onset of the same burst in the next cycle results in a positive correlation between the length of that burst and the length of the preceding burst in the next cycle (Fig. 7). Negative

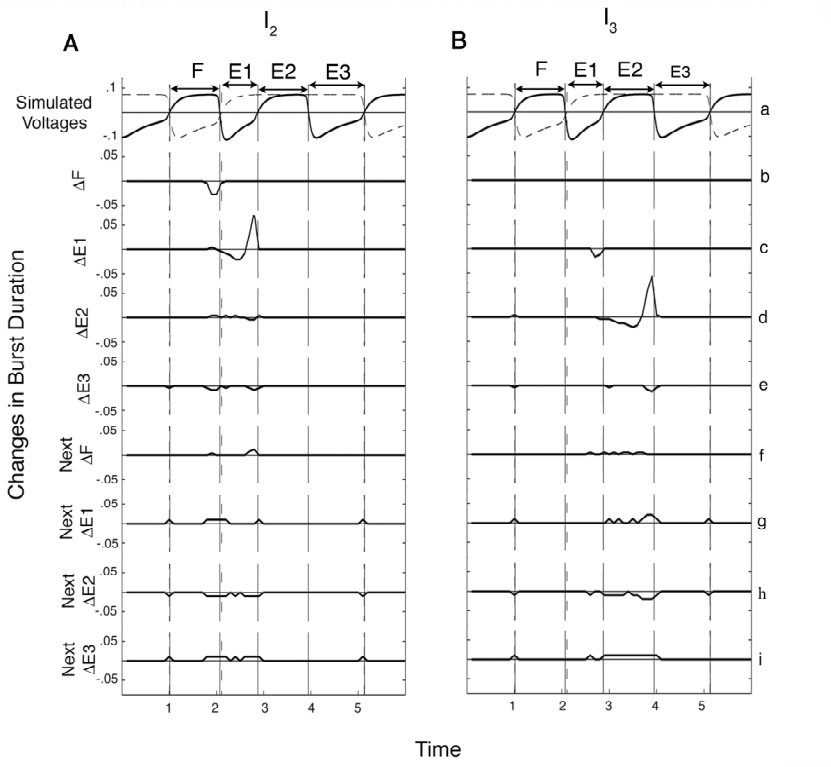

FIG. 2.8, Microstimulation of Clock Model. Stimulation of I_2 (Aa to Ai) and I_3 (Ba to Bi) in the clock model. Stimulating I_2 and I_3 lead to similar patterns of effects relative to the phase in which neuron is active (ΔE1 (Ac) and ΔE2 (Bd) resp.). Effects are similar to the half-center model. Stimulation of the active interneuron late in its active phase causes lengthening of that phase (time=2.8 in Ac, and time=4 in Bd); early stimulation causes shortening (time =2.4 in Ac and time=3.5 in Bd). Late stimulation also delays the onset time of activity in this interneuron in the next cycle which causes a lengthening of the previous phase (time=2.8 in Af and time=4 in Bg).

correlations between remaining bursts are a consequence of mutual inhibition between the inhibitory interneurons of the network.

Feedback Oscillator

The feedback oscillator is also a generalization of the basic half-center circuit. But rather than incorporate more neurons within a single winner take all dynamics, this

model retains a single pair of mutually inhibitory neurons that control flexor and extenor motor neurons. The basic alternation between flexion (F) and the period of extension (E1-E3) results from the mutual inhibitory dynamics between these two neurons. Double bursting is caused by a separate inhibitory neuron called the override neuron, that inhibits both I_f and I_e (I_o; Fig. 1C). High activity in this cell shuts down activity in all central inhibitory neurons. This releases all excitatory interneurons from inhibition, leading to co-activation of flexor and extensor motor neurons. The override neuron receives excitatory input from E_e. When E_e becomes active at the beginning of extension it excites I_o, which in turns inhibits I_f leading to a second flexion burst (I_e is already inhibited). This marks the end of E1 and the beginning of E2. Self-inhibition then accumulates in I_o, releasing I_f from inhibition, ending the second flexion burst and terminating phase E2. Voltage traces from the feedback model are shown in Fig. 9.

Unlike the clock model, the feedback model is hierarchical, and different mechanisms contribute to the transition between different phases of the step cycle. In particular, the transitions from F to E1 and from E3 to F are determined by mutual inhibition between I_e and I_f, the transition from E1 to E2 is determined by the buildup of activity in I_o, and the transition from E2 to E3 is determined by the decay of inhibition from I_o as well as the ability of I_f to escape from this inhibition. As a result of this heterogeneity, the different parts of the step cycle show very different degrees of variability. Again we adjusted noise level so that the CV of cycle length approximated 1.5% (noise level s=0.01 gave CV of the cycle = 1.71%). Unlike the clock model, the different parts of the step cycle in the feedback model have widely different CVs (F: 2.97%; E1: 1.09%; E2: 3.19%; E3: 4.86%). Fig. 10 shows the pattern of correlation

between different phases of the step cycle. As in Fig. 7, each subplot shows the pattern of covariance with a particular phase of the cycle. In contrast to the clock oscillator, each phase of the step cycle shows a distinct pattern of covariance. Of particular note is the correlation between E3 and the next F, which reaches almost 0.6 (Fig. 10a and 10d).

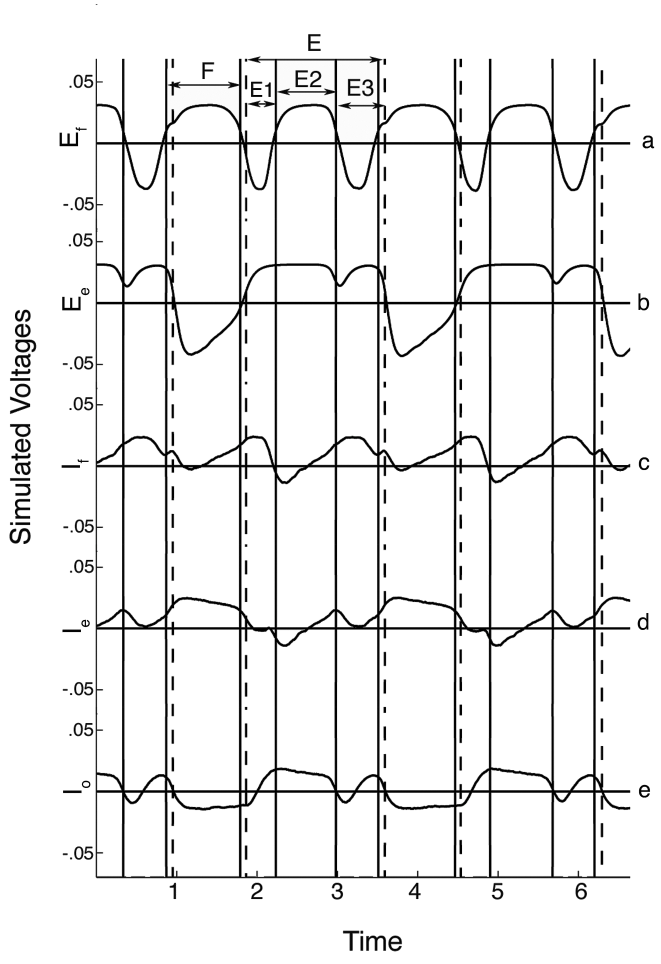

FIG. 2.9, Feedback Model Output (noise level □ = 0.01). Vertical lines show limits of F and E2 (solid) and of E1 and E3 (dashed)(a-e). Top two traces show excitatory (E_f (a) and E_e (b)) voltages. Bottom three traces show activity in inhibitory interneurons I_f (c), I_e (d) and I_o(e). I_o becomes active at the beginning of extension creating the second flexor burst (time=2.2 in e). Note the small period of I_e activity near the onset of E3 (time=3 in d). This is a third period of competition between I_e and I_f but one where I_e always loses. This adds significant complexity to the dynamics of the feedback model.

Microstimulation in the Feedback Oscillator

We describe the behavior of the feedback model in the context of how the model responds to micro-stimulation (Fig. 11), with a focus on each phase of the cycle, starting with the flexion phase F. The transition from F to E1 is governed by the competitive dynamics between I_e and I_f and

hence is influenced by the same mechanisms important in the half-center model. In particular, stimulation of I_e (the active neuron) late in the phase extends F, whereas stimulation early recruits self-inhibition and shortens F (Fig. 11Bb). Conversely stimulation of I_f (the inactive neuron) near the end of F shortens F (Fig. 11Ab). The only departure from the behavior of the half-center is that stimulation of I_e near the end of F does not result in a lengthening of the subsequent phase of extension, but rather has a slight shortening effect on E3. This results from a complex interaction between slow self-inhibition in I_e and other dynamic events occurring during extension and will be explained below. Note that the override neuron I_o is below threshold during F, so small stimulations of this neuron have no effect.

Next we examine the initial phase of extension, E1. Looking at the voltages in Fig. 9, we see that the onset of extension is marked by a rapid rise of activity in the excitatory extensor interneuron E_e (Fig. 9b, time 2), followed with a short delay the rapid rise in the override neuron I_o (Fig. 9f). This causes a rapid decline in I_f activity (Fig. 9d), leading to double bursting. Note that all transitions are strong and rapid. That means that even though perturbations may have a significant impact on voltage, these changes will be converted into rather minor differences in the time at which threshold is crossed. Consistent with this, stimulation of all interneurons, including the override neuron I_o, has a very small effect on the length of E1, explaining why E1 is the least variable phase in this model.

The double burst phase, E2, is terminated by the increasing self-inhibition in I_o that reduces inhibition to the central half-oscillator, allowing I_f to escape from inhibition and end E2. Stimulation of I_o shows the familiar pattern. Stimulation near the end of E2

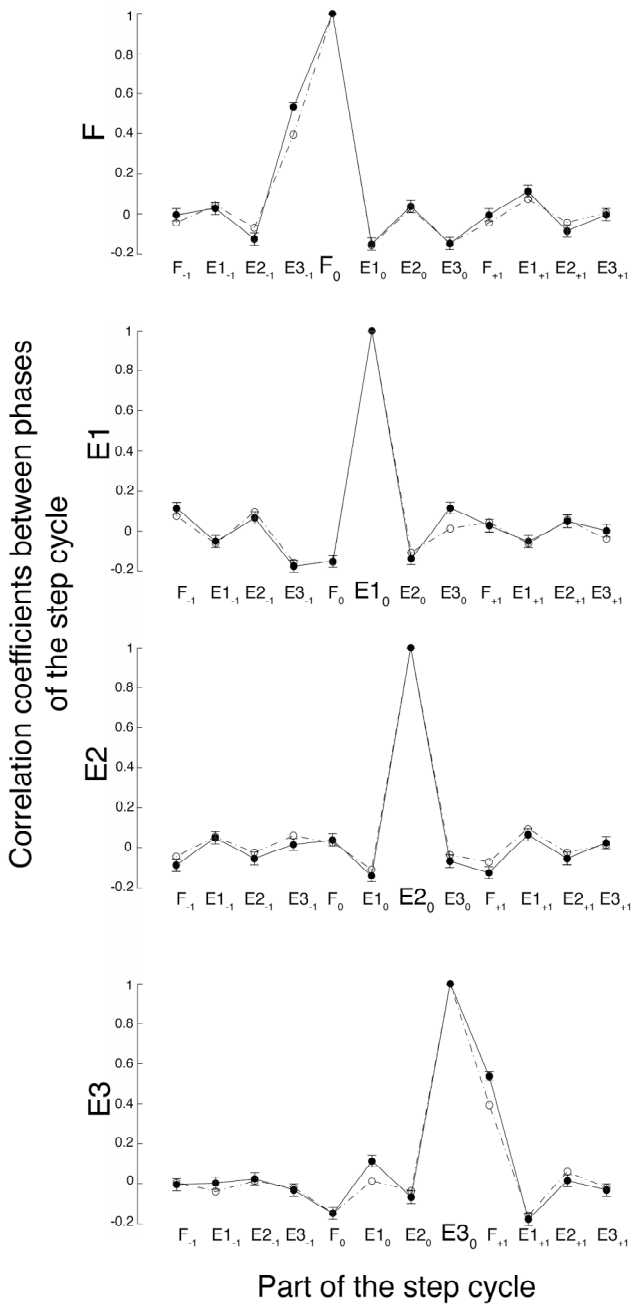

FIG. 2.10, Correlation Structure of the Feedback Model. Correlations with noise shown as solid circles with solid lines. Errorbars indicate two standard deviations. Phases are labeled as in Figs. 3 and 7. Each individual phase of the step cycle has a specific pattern of correlation with the other parts of the step cycle. Note the very strong correlation between F_0 and $E3_0$, and the different patterns of correlations between the graphs from top to bottom. Open circles and dashed line show linear predictions from microstimulation.

extends activity in I_o and hence extends E2 (Fig. 11Cd at time 4.5), whereas stimulation of I_o early during E2 recruits greater self-inhibition in I_o and shortens E2 (Fig. 11Cd at time 3.7). If we look at I_f, the effects are in the opposite direction and significantly smaller (Fig. 11Ad). A close examination of the voltage traces during the transition from E2 to E3 (Fig. 9f) reveals that I_e also increases its activity at this time, initiating another bout of competition between I_e and I_f and causing a dip in the output of E_e. I_f always has the upper hand in this competition (Fig. 9d), and activity in E_e quickly

recovers to support the rest of phase E3. However, the time it takes for I_f to escape from suppression by the override neuron is influenced by competition with I_e. As a result, microstimulation results in a typical half-center pattern, with stimulation of I_e late in the burst extending E2 and stimulation early shortening E2 (Fig. 11Bd). Conversely, stimulation of I_f late in the burst shortens E2 while stimulation early has little effect (Fig. 11Ad).

Finally, we turn our attention to the other transition governed by competition between I_e and I_f: the transition between E3 and F. Again we see the familiar half-center pattern near the end of E3 with stimulation of I_f (the active neuron) extending E3 and stimulation of I_e (the inactive neuron) shortening E3 (Figs. 11Ae and 11Be). We also see that stimulating I_o near the end of E3 extends E3. I_o inhibits both I_f and I_e (Fig. 11Ce), and so one would not necessarily expect I_o to bias the competition between them. However, a small increase in inhibition has a relatively minor impact on the already active neuron (I_f), whereas I_e is just beginning its rise in activity and the same small increase in inhibition has a relatively large impact. So although I_o sends increased inhibition to both I_f and I_e, it has a larger impact on I_e, delaying the onset of F. If we look further back in time, we see that the length of E3 is also highly sensitive to stimulation of I_e and I_f near the end of E2 (figs. 11Ae and 11Be). Interactions between all three interneurons contribute to ending both of the phases E2 and E3. The sensitivity of the dynamics at these two points in the cycle explains the relatively large effects of microstimulation at these times, as well as the fact that phase E3 is relatively more variable than the other phases in the cycle.

As pointed out above, the length of E3 is also reduced by stimulation of I_e near the end of F (Fig. 11Be). Note that this shortening runs counter to expectations derived from the half-center model: stimulation of I_e near the end of F should recruit more self-inhibition in I_e and this delay the onset of the next F, thereby lengthening E3. The reversal in the effect of slow inhibition is due to an interaction between the slow inhibition and the complex competitive event at the end of E2. With greater inhibition, I_e is less active during this event and this has a net effect of reducing the self-inhibition and hence shortens E3. This illustrates how interactions between long-lasting inhibition and subsequent dynamic events can lead to complex dependencies that span multiple phases of the step cycle.

The correlations seen in the structure in the noise-driven condition (Fig. 10) are entirely consistent with the microstimulation experiments. In particular, note that perturbation of all three interneurons has a similar effect on the length of E3 and the next F. Given the sensitivity of E3 to perturbation, this results in a very large correlation between these two phases. The microstimulation results also reveal that dynamic influences can work in opposition. For instance, for each of the mutually inhibitory interneurons, perturbation during E2 affects the length of both E2 and E3 in the same direction, leading to a positive correlation. However, perturbation of the override neuron in latter half of E2 lengthens E2 significantly, but acts to shorten E3 (Figs. 11 A-C, d and e). This induces a negative correlation. The fact that the net correlation between E2 and E3 is negative indicates that the influence of I_o on this correlation is stronger than the combined influence of I_e and I_f.

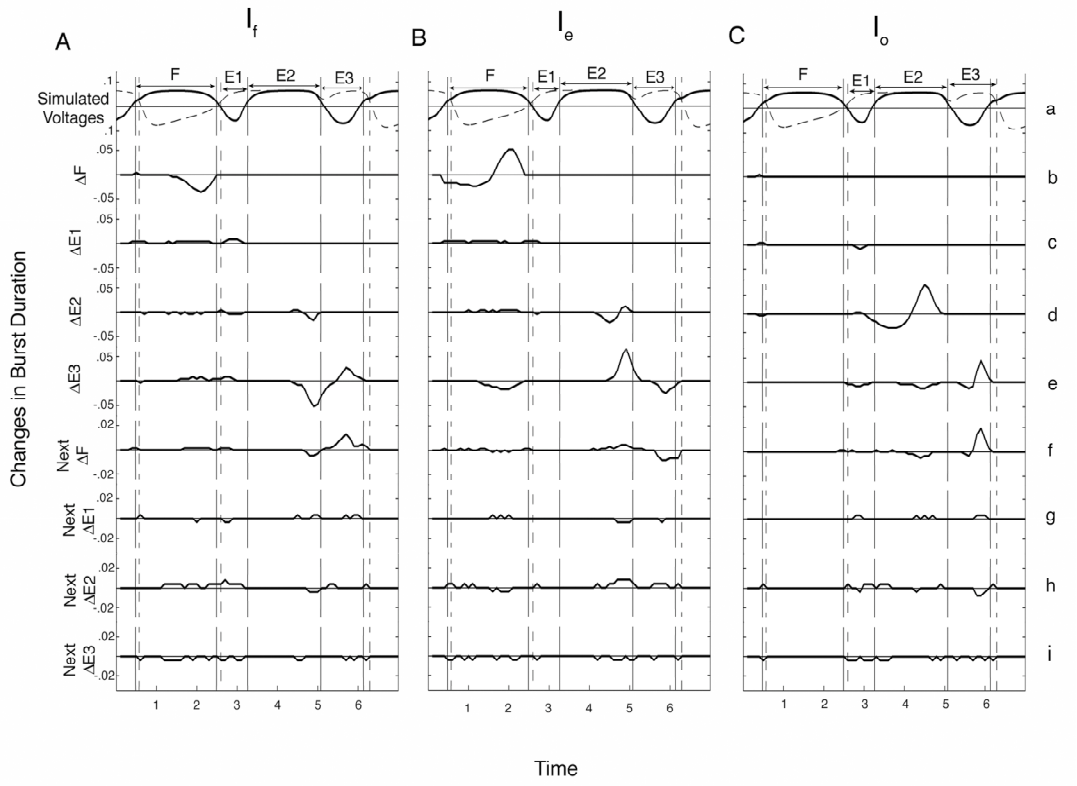

FIG. 2.11. Effects of Microstimuation on the Feedback Model. Stimulation of the central inhibitory interneurons I_f (Aa-i), and I_e (Ba-i), have similar effects on extenstion and flexion as in the half-center model (compare with Fig. 5). Stimulation of I_0 (Ca-i) has the largest effect on the duration of the double burst phase E2 (Cd), but also has an affect on the transition from E3 to F (Ce). Note that stimulation of all three neurons lead to a similar pattern of deviations in the lengths of E3 and the next F (Ad-e, Bd-e, Cd-e), accounting for the strong positive correlation between these phases (figure 10a, column $E3_{-1}$ and 10d, column F_{+1}).

Microstimulation Effects on Extension Length in Double Bursting Models

Differences between the output of the feedback and clock models can also be seen in the influence of microstimulation on the burst duration of the whole of extension (E) (Fig. 12). These results are interesting in light of recent results published by Saltiel and Rossignol (2004a, 2004b; see Discussion). When comparing changes in the duration of extension (E) across models under the effects of microstimulation, three differences are apparent:

First, microstimulation of some interneurons in the feedback model affect the length of E across a large portion of E (microstimulation of I_o in Fig. 12Bc), while the

same stimulation in the clock model only alters E if delivered in a small portion of the burst (microstimulation of I_3 in Fig. 12Ab).

Second, in the clock model, microstimulation affects the total length of E in a symmetric manner, i.e. stimulation of any of the three interneurons active during E leads to a part of the phase where E is initially shortened followed by a phase where E is lengthened (compare Fig. 12Aa to 12Ac). The same type of stimulation of the feedback model leads to multiple different responses (Fig. 12B). For instance stimulation of interneuron I_o shortens E if delivered at the beginning of E2, elongates E when delivered at the end of E2, and lengthens E when delivered during E3 (Fig. 12Bc). Compare this with microstimulation of I_e where stimulation during E2 acts like stimulation of I_o, but stimulation during E3 gives the opposite effect.

Third, within the feedback model there are times of the step cycle when stimulation of any of the interneurons of the model can influence the burst duration of E, (Fig. 12Ba-12Bc, times 3.2 to 5.1). Within the clock model there are points in the step cycle perturbable by more than one interneuron (Fig. 12Ab and 12Ac at time 2.8) but these make up only a fraction of the entire cycle, and there are no times where all of the three interneurons influence the burst duration of E.

Discussion

The current study explored three models of the spinal CPG for locomotion. Fundamental properties of networks based on fast competitive inhibition and slow self-inhibition were explored in the context of a simple half-center model. For this model, we find that excitatory perturbation of the active interneuron within a burst has differing

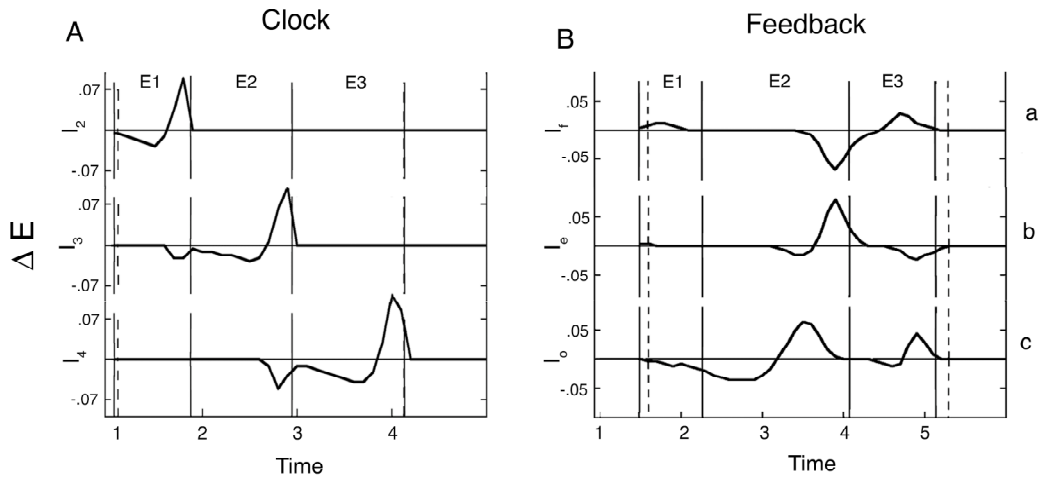

FIG. 2.12. Effects of Microstimulation on Extension. Change in total length of extension (ΔE) during microstimulation of interneurons in both the clock (A) and feedback (B) models. For the clock model (A) stimulation of the interneurons all effect ΔE in the same manner i.e. stimulation of I_3 during E and I_4 during E always shortens E first and then lengthens it, while stimulation of the interneurons of the feedback model each effect ΔE in a unique way, i.e. stimulation of I_0 first lengthens E during E2 and latter lengthens E during E3, while stimulation of I_f produces the opposite effect.

effects depending on when in the burst it is given: (1) perturbation early in the burst causes a moderate shortening of the ongoing burst and does not affect subsequent burst durations, and (2) perturbation late in the burst causes a relatively large lengthening of the ongoing burst and a moderate delay in the onset of the corresponding burst in the next cycle. We also find that (3) excitatory perturbation of the inactive interneuron is only effective near the end of the burst, and serves to shorten both the current burst and subsequent bursts. Effects 2 and 3 cause adjacent burst durations in the half-center model to either lengthen or shorten together, resulting in a positive correlation between these durations in the simulations with noise (Fig. 3). This positive correlation results from an

alignment of the reversal between initial excitation and delayed self-inhibition with the competitive reversal experienced by the stimulated interneuron at the boundary between bursts.

We then generalized the half-center, considering two architectures that give double-bursting output in flexor muscles. In the clock model, the two interneurons of the half-center are replaced by a ring of four mutually inhibitory interneurons, with activity proceding around the ring. The main predictions related to this model stem from the symmetry of the underlying architecture. In particular, all phases of the output have similar CVs, and the strength of correlation between any two phases depends chiefly on the number of intervening phases rather than the particular phases being compared. In the feedback model, a delayed feedback loop interacts with the mutual inhibition underlying flexion and extension to produce double bursting outputs. The main predictions of this model are that the E1 phase should be relatively insensitive to noise (low CV) whereas phase E3 should have relatively high noise sensitivity (high CV), and that correlations between the burst durations will not depend directly on the temporal relationship between the bursts being compared but upon which bursts are being examined as well.

Class of Models Studied

From a strictly theoretical perspective, the current models expand our understanding of how noise affects the output of neuronal networks that act like relaxation oscillators (Bem, et. al., 2003; Skinner, et. al. 1994; Traven, et. al., 1993; Wang and Rinzel, 1995). These models are characterized by large state changes at

specific times during the cycle, and have distinct fast and slow state variables that provide an explicit substrate for dynamic influences spanning multiple burst phases. The other main approach to modeling spinal CPGs has been to look at the class of oscillators with phase-difference coupling (Kiemel et. al., 2003; Kiemel and Cohen, 1998). Such phase oscillators are characterized by a single variable (the phase) and generally have state changes that are more continuous.

Although the slow self-inhibition in our models is most commonly attributed to neuronal adaptation via voltage or calcium dependent potassium channels (Rinzel and Ermentrout, 1989; Grillner 1999), slow inhibition could result from synaptic mechanisms such as g-protein coupled inhibition and/or from synaptic facilitation in mutually inhibitory synapses. Since the exact temporal profile of the self-inhibition is unlikely to qualitatively alter model behavior, we expect the qualitative predictions derived from our models to apply to a broad class of networks where mutual inhibition and slow self-inhibition drive the dynamics (Morris and Lecar, 1981).

Phase Dependent and Temporally Extended Responses

We have shown that the correlation between burst lengths in our models can be accurately predicted by integrating results obtained from microstimulating the interneurons that make up the simulated CPG. In the half-center model, the direct effect of stimulating either central inhibitory interneuron matches the most common action of proprioceptive feedback onto the mammalian CPG (Rossignol and Drew 1988; Hiebert, et. al. 1996; Whelan, 1996). For example, stimulating either Ia or Ib receptors of a given muscle during locomotion tends to enhance activity in the stimulated and active muscle

and inhibit activity in muscles antagonistic to them. Stimulation of the inactive muscle (e.g. flexor Ia receptors during extension) can end the current phase early and reset the step cycle to begin the next phase (Hiebert, et. al. 1996; Whelan, 1996). In our model, these results follow directly from the half-center architecture in which flexor and extensor inhibitory interneurons compete for activation.

In addition to the immediate effect on the interneurons driving the oscillation, microstimulation of our models has extended effects that are mediated by slow self-inhibition. For example, the build-up of inhibition in our half-center model leads to the curious property that microstimulation of the active interneuron early in a burst results in a shortening of the current burst duration. A similar difference between early and late perturbation has recently been reported for phasic retraction of a cat's shoulder during fictive locomotion (Saltiel and Rossignol, 2004b; see also Duysens, 1977; Duysens and Stein, 1978). A similar effect that spans adjacent phases of the step cycle can be seen within the stumble corrective reflex in the context of stumble prevention (Forssberg, 1979; Quevedo, et. al. 2005a). Transient stimulation to the superior peritoneal nerve during extension serves to elongate the extension ipsilaterally and to induce an increase in burst duration of the subsequent flexion (Quevedo, et. al., 2005a). Our half-center model shows a similar increase in extension and the following flexion after stimulation of I_f near the end of extension (Fig. 5Ab, 5Ac). The fact that both phases are elongated is due to the temporal alignment between the reversal from excitation to slow inhibition in I_f and the change in I_f 's state from active to inactive at the onset of extension.

Because long-lasting effects in our half-center model are sustained by slow self-inhibition, short-term and long-term effects must be functionally opposed. Thus, our

model cannot explain long-lasting alterations in the CPG that consistently favor extension or flexion. For example, our models cannot explain the fact that stimulation of the sural nerve during flexion elongates that flexion burst and also shortens the following extension phase (Duysens, 1977), or that stimulation of the superior peritoneal nerve during flexion elongates the current flexion but has no effect on the length of the following extension (Quevedo, et. al. 2005b).

Transition Points in the Dynamics of the Double Bursting Models

In a pair of recent papers, Saltiel and Rossignol (2004a, 2004b) argue for the existence of discrete 'critical points' within the locomotor output that correspond to the dynamics within bursts rather than the edges of bursts alone. These critical points occur at times when an animal must coordinate changes in activity within multiple muscle groups, and are associated with changes in the way the CPG responds to phasic perturbations. Although outputs in our model are restricted to a single pair of antagonistic muscles, the underlying dynamics have two properties that are similar to critical point behavior. First, the major transitions in the dynamics result from strong interactions between interneurons controlling different outputs. As a result, it is possible to alter when these transitions occur but it is impossible to decouple them without changing the basic behavior of the models. Second, like the results of Saltiel and Rossignol (2004a and 2004b), these coupled events often demark changes in how the models respond to microstimulation. Fig. 12 shows the effects of perturbations on the length of extension in our double bursting models. The length of extension is most

sensitive to perturbation near the dynamic transitions associated with the double bursting events.

Coordination of Complex Movements

The complexity and time course of the effects within our models suggest how transient inputs could aid in the coordination of complex movements. For example, transient sensory input to the spinal cord might trigger a series of dynamic changes that alter muscle activity over time periods extending into the next step cycle. Alternatively, temporally localized inputs from higher centers could trigger chains of functionally related effects to coordinate voluntary movements such as obstacle avoidance (Drew, et. al. 2004). Such long-lasting effects from transient stimulation have been observed under conditions of very strong stimuli from motor cortex (see Fig. 10 in Bretzner and Drew, 2005) and may explain why a complicated behavioral repertoire remains in animals without extraspinal inputs (*e.g.* Forsberg, 1979). Of course not all coordination will be accomplished within the spinal CPG, as it is well known that both motor cortex and sensory information modulate the CPG on a cycle-by-cycle basis (reviewed in Cohen and Boothe, 2002; Drew, et. al., 2004).

Such extended changes in burst lengths due to perturbation are often attributed to the triggering of complex activity patterns within excitatory and inhibitory interneurons (Bretzner and Drew 2005; Quevedo 2005b). Our simplified models raise the possibility that some of these functional reversals may reflect the shift from transient excitation to the dominance of slow self-inhibition. Moreover, our double bursting models demonstrate that simple switches from immediate excitation to long-lasting inhibition can

have complex and surprising effects that depend on the functional architecture of the model. In the clock model, for example, each interneuron only participates in the competitions at the boundaries of a single phase of the cycle. Therefore, perturbation of a single interneuron changes the length of the current burst, has very little effect on the two intervening bursts, and then another substantial effect on burst length. Somewhat surprisingly, this temporally separated interaction is not seen between the same phase across cycles, but rather a given phase in one cycle and the preceding phase in the next cycle. This is because burst durations are not coded per se, but rather are determined by competition-driven state transitions at the beginning and end of each phase. A different form of complexity is demonstrated by the feedback model, in which a short period of activity in one of the central interneurons (I_e) at the end of phase E2, has a very minor effect on the output of the CPG but serves to 'reverse the sign' of the effect of slow inhibition on later parts of the step cycle (see Results).

Clock-like vs. Feedback Model of Double Bursting

Much of the research on spinal CPGs addresses two basic questions. What controls the timing relations between various motor outputs? Is the same circuit or different circuits used to accomplish qualitatively different behaviors? The phenomenon of double bursting allows one to study a blend of these questions within the same basic behavior. In particular, it raises the question of whether the same or different parts of the spinal CPG drive the two bursts of flexion. A more specific, but related question is whether the CPG is dominated by a clock-like mechanism. If the dynamical mechanism is simply marking out time, one expects an underlying symmetry in the dynamics in

which distance in time, rather than similarity in peripheral effect, is the dominant variable determining the dynamic structure of the network (*c.f.* Golubitsky *et. al*, 1999).

Although quantitative predictions cannot be drawn from the abstract models considered here, the models do suggest a number of qualitative predictions. Most generally, a clock hypothesis predicts that correlation patterns for all phases of the cycle should be qualitatively similar (*e.g.* Fig. 7). More specifically, in a double bursting system the phases of flexor activation (F and E2) lie on 'opposite sides' of the step cycle. Under a clock hypothesis, these phases are expected to be 'maximally different' and have little correlation. One also expects that perturbing the CPG during these two phases should lead to quite different effects. In contrast, in a model in which the two phases of flexor activation are driven by the same part of the CPG, one would expect commonalities between these two phases, such as perturbations having similar effects in phase F and E2 (e.g. compare the effect of stimulating I_e and I_f during F on ΔF and stimulation during E2 on ΔE in Fig. 9).

Measuring Correlations as well as Perturbations

A classic method for studying a system is to perturb it and observe the pattern of effects. We have shown that noise-driven variability can also reveal useful information about the structure of the underlying system. In our models, stimulating distinct populations of interneurons within of the CPG cause perturbations that are generally consistent with these noise-driven correlations. In fact, the noise-driven correlations can be predicted by combining the perturbations from all components that drive the oscillation. In the actual system, however, little is known about the correlation structure

of burst lengths during fictive walking, and whether particular physiological perturbations act in concert with or in opposition to the natural variability within the system. It also an open question whether perturbations, in addition their effect on mean burst length, act to change patterns of subsequent variability in the system. Our approach suggests that analyzing the trial-to-trial variability under a number of experimental conditions may shed light on the structure of the underlying CPG.

CHAPTER THREE: ASYMMETRIES IN THE FICTIVE LOCOMOTOR CYCLE OF CAT

Abstract

Here we have performed a detailed statistical study of the natural variation occurring during midbrain locomotor region (MLR) induced flexor dominated fictive locomotion. We find strong asymmetries between the two main transitions of the step cycle; the transition from extension to flexion (E to F) and flexion to extension (F to E). Phase locking at the E to F transition is always strong. This strong phase locking is associated with periods of overlapping bursts between the offset of extensors and the onset of flexors. Phase locking at the F to E transition is variable. Bouts (3 out of 7) having short cycle periods (<.65 seconds) are associated with weak phase locking between flexor burst offsets and extensor burst onsets. Weak phase locking is associated with flexor burst offsets and extensor burst onsets that are separated in time. Bouts containing long cycle periods (4 out of 7) have increased levels of phase locking at the F to E transition, associated with shortening of latency between flexor burst offset and extensor burst onset. Overall we find that latency between burst terminations and onsets is a stronger indicator of strength of phase locking than either burst durations or cycle period.

We conclude that observed asymmetries in the fictive locomotor cycle are likely due to underlying asymmetries in the network making up the spinal central pattern generator for locomotion (sCPG).

Introduction

There is broad agreement that the core of the spinal locomotor system consists of an intrinsically oscillatory network or spinal central pattern generator (sCPG). However, the functional organization of the sCPG remains illusive. Early on, it was hypothesized that the structure of the sCPG consisted of two mutually inhibitory oscillators, each producing one of the two dominant phases of locomotion: flexion and extension (Brown, 1911, Lundberg, 1969). The central representations of these two phases were presumed to be unitary, with the more complex cycle fractionation in intact animals resulting from the interaction of the sCPG with sensory feedback. Subsequently, Grillner and Zangger (1979, 1984) showed that individual nerves retain their patterns of activation even when the spinal cord is isolated from sensory input. To account for this complex pattern Grillner hypothesized that the sCPG consisted of a collection of semi-independent sub-oscillators each controlling activity within single joints (Grillner, 1981).

Recently it has been shown that while stimulation of many sensory nerves can evoke changes in sCPG output (Burke et. al. 2001.), only a small subset of nerves are capable of resetting the phase of the overall step cycle (Lafriere-Roula and McCrea, 2005, Quevedo, et. al. 2005a-b, Rossignol, et. al. 2006). Differential response to peripheral stimulation has led to the hypothesis that the sCPG for each limb is hierarchical, containing a feed-forward rhythm generator setting the overall timing for flexion and extension, and a separate pattern formation network that both shapes the output of rhythm generator and adapts that output to sensory inputs (Rybak et. al, 2006a-b, La Friene Roula et. al. 2005).

Models based on mutual inhibition such as those described above have treated the sCPG as symmetric, with flexion and extension created by sub-networks having the same

connectivity and function (Lundberg, 1969, Grillner, 1981, Rybak, et. al. 2006a-b, Yakovenko, 2005). Asymmetries observed within intact locomotion such as changes in phase duration as animals increase or decrease their speed have been attributed to the influence of sensory input on a symmetric sCPG network (Rossignol, 2006). Recently it has been shown that flexor and extensor burst durations have a symmetric relationship with changes in cycle period (Yakovenko, et. al., 2005). However, in analyzing burst lengths only, other flexor/extensor asymmetries in the sCPG may have been overlooked.

Here we measure the degree of phase locking between previous burst offset and subsequent burst onset at transitions between flexion and extension. We find: 1, The transitions from extension to flexion (E to F) and flexion to extension (F to E) are qualitatively different, with E to F having strong phase locking across all experiments and F to E having weak phase locking for a subset of experiments; and 2, the latencies between burst onset/offset times are a critical determinant of the level of phase locking observed.

Methods

Experimental Procedures

Midbrain locomotor region (MLR) induced fictive locomotion reported here was kindly provided to the authors by Dr. David McCrea. The current data set has been previously published using a different set of statistical methods (Yakovenko, et. al., 2005). Experimental procedures used to obtain ventral root ENGs appear in Yakovenko, et. al. 2005, where different ENGs received by the authors were linearly rectified, filtered between 30 hz and 3 khz, low pass filtered at 100 hz and then digitized at 500 hz (Yakovenko, et. al. 2005).

Data Selection

MLR induced fictive locomotion is often noisy and inconsistent making choice of proper data to be analyzed an important aspect of reporting observations. We focused our analysis on ENG recordings that display consistent and regular bursting, selecting 10 bouts of fictive locomotion derived from 21 episodes of fictive locomotion. Bouts consisted of a continuous stretch of bursting activity fulfilling the following criteria: 1, Each bout contains a sufficient number of cycles (minimum= 17); 2, Bouts contain no phase resetting deletions (c.f. La Friene-Roula, et. al. 2005 for a discussion on deletions); 3, Bouts have bursts with high slope onsets and offsets with peak activity well above background noise, making them easily detectable using a threshold; and 4, All bouts contain both Sart and SmAB (the flexor and extensor nerves occurring most frequently within this data set), for determination of relative phase (see below). Out of the 11 bouts not reported here 6 were discarded because they lacked either Sart or SmAB. 2 were discarded because Sart or SmAB contained weak bursting, and 2 were discarded because sets of continuous bursts contained deletions, and one was discarded because it had an insufficient number of continuous bursts.

Some nerves within the 10 selected bouts were not analyzed due to three non-exclusive reasons: there were not enough bouts with consistent bursting; the nerves had inconsistent fractionation, i.e. they sometimes were active during flexion, sometimes during extension; or they were active only at the beginning of the flexor or extensor subphase. For example the posterior biceps semitendinosis appears in 6 bouts, however in 3 of those bouts it is weakly activated and inconsistent, in 1 bout it is double bursting,

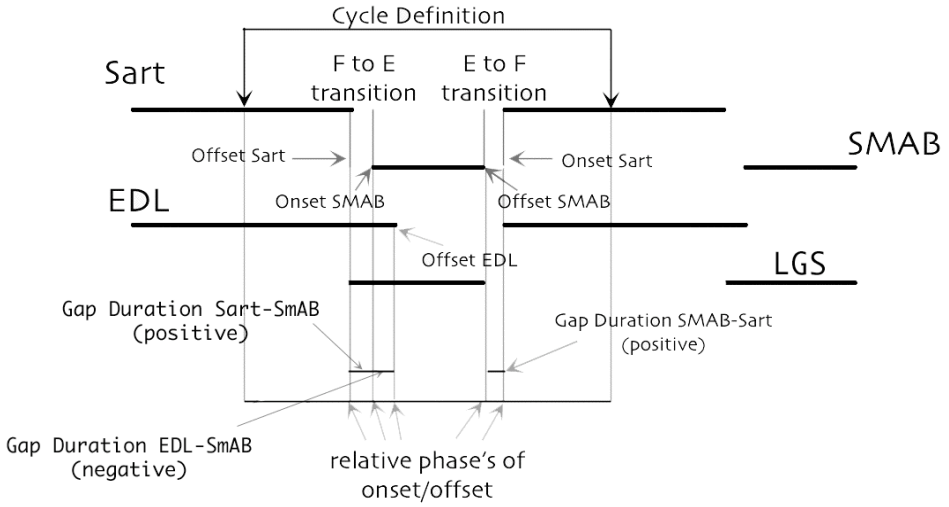

Fig. 3.1, Schematic of Cycle: Definition of Terms. Cycle is defined as the length of time from midpoint Sart burst to midpoint next Sart burst. Relative onset and offset times of bursts are then calculated in relative phase coordinates. The transition from the end of the flexion phase to the beginning of the extension phase is termed the F to E transition. The opposing transition from extension to flexion is termed the E to F transition. 'Gaps' or 'latencies' are the difference in sec between burst onset and offset times. Latencies with negative sign indicate a period of burst overlap (c.f. Gap EDL-SmAB above). Latencies with a positive sign indicate a period of time where both bursts are off (c.f. Gap SmAB-Sart above).

and in 2 bouts it is active during extension. The flexor digitorum longus appears in 6 bouts, out of which its bursting is weak and noisy in 3, and is active during flexion in two bouts and during extension in one. Quadriceps appears in 6 bouts, however its activation is often weak, and the shape of its burst with a long low slope onset beginning in the middle of flexion is poorly amenable to analysis using the thresholding method described below. Additional nerves present in the data but not analyzed were: Iliopsas; gastrocnemius soleus; flexor hallucis longus; flexor digitorum longus; and flexor digitorum hallucis longus. The final subset of nerves with consistent bursting properties included the knee flexor sartorious (Sart), the ankle flexors tibialis anterior (TA) and

peroneous longus (PerL), the ankle and toe flexor extensor digitorum longus (EDL), the hip extensor semimembranosus anterior biceps (SmAB), and the ankle extensors lateral gastrocnemius and soleus (LGS) and medial gastrocnemius (MG).

Burst Detection and the Determination of Relative Phase

All analyses were performed on a LINUX based Dell personal computer using MATLAB (Mathworks, Natick MA).

Continuous stretches of data were first obtained by visual inspection. Burst onset and offset times within individual ENGs were then determined by the crossing of a hand-set threshold. To eliminate small jumps above or below threshold caused by noise, super-threshold crossings less than .05 sec, and sub-threshold crossing less than .1 sec were discarded , except for within one bout where .4 sec was used.
We have applied similar methods previously within the context of lamprey ENGs (Mellen, et. al. 1995).

Since the absolute time at which an experiment was performed is arbitrary, timing of an event must be taken relative to other time points to have meaning. For example, burst duration measures the relative timing of burst onset and burst offset. To characterize the relative timing of individual events during a cycle with respect to a common frame, we used a relative phase measure of burst onset and burst offset times. For convenience, we used the midpoints of bursting activity within sartorious to define the beginning and end of a cycle (Fig. 1). Relative phase, which takes on values between 0 and 1, was defined as the time difference between the beginning of the cycle and the features of interest (in this case burst onset and burst offset), divided by the duration of that cycle.

Qualitatively similar results were obtained using slight variations of the method described above for determining relative phase including: 1, Defining two different cycle lengths each used to compute relative phase of a single transition, i.e. Sart onset to onset of next Sart for the F to E transition and SmAB onset to onset of the next SmAB for the E to F transition; 2, Computing the times of burst onset and offset relative to the midpoint onset and offset times for Sart and SmAB; and 3, Defining cycle onset/offset as the mean midpoint of all flexors. While absolute values of several statistical properties depended upon their method of measurement, relationships between the measurements were consistent across methodologies. We view the statistics reported here to be useful for purposes of comparison across nerves and across conditions, not as absolute measures of the underlying phenomena.

Data Analysis

Correlations between variables were reported using Pearson's correlation coefficient, *r*. To eliminate correlations resulting from slow drift in variables over the course of a bout, all variables were detrended by subtracting from each value x_i the average of all values within a 13 data point window centered on x_i. For any two random variables X and Y the Pearson's correlation coefficient *r* ranges from –1 to +1 and is defined by $r=Cov(X,Y)/(\sigma_X\sigma_Y)$, where $\sigma_X=sqrt(\Sigma(x_i-\mu_X)^2/(n-1))$ is the standard deviation of X (μ_X is the mean of X), and $Cov(X,Y)=\Sigma(x_i-\mu_X)(y_i-\mu_Y)/(n-1)$ is the covariance of X and Y. However, since the correlation coefficient is bounded between 1 and –1, comparisons across coefficients can be affected by floor/ceiling effects (e.g. it is impossible to get a correlation more than .05 higher than a value of .95). Therefore, all

statistical arguments relating to relative degrees of correlation used *z'* (z-prime), Fisher's z-transform of the correlation coefficient *r*: $z' = \log((1+r)/(1-r))/2$. This manuscript focuses on patterns of the correlations between measurements extracted from several nerves. Since a single nerve can be paired with several other nerves, pair-wise correlation values can not be assumed to be independent. Therefore, statistical comparisons are based on the less stringent, non-parametric Wilcoxon Rank Sum (WRS) test, and the Wilcoxon Ranked Pairs (WRP) test when paired measurements are reported.

To retain the intuitive power of the more familiar raw Pearson measure, we converted means and differences of *z'* back to the corresponding *r* value before reporting values in the text. For example, to report the mean difference between two sets of correlations A and B, all correlations in both A and B would be converted to *z'* scores, the mean difference between to *z'* scores in A and B would be calculated, and the mean difference in correlation would be reported as the *r* value that corresponded to this mean difference *z'* score.

Results

Previous statistical surveys of fictive locomotion have focused on the relationship between burst durations and cycle periods (Yakovenko, 2005). Here we focus on phase locking between burst onset and offset. We report four statistical properties of fictive locomotion: 1, Overall variance of burst durations and cycle periods; 2, Correlation between burst durations; 3, Phase locking of burst onset and offset times, and 4, Latencies of burst onset and offset times.

Data Analyzed

Qualitatively the output of MLR induced fictive locomotion can be placed into two broad categories: flexor dominated fictive locomotion where the flexor phase is longer than 1/2 of the cycle, and extensor dominated fictive locomotion where the extensors are active for more than 1/2 of the cycle. We have analyzed 474 cycles of flexor dominated locomotion from 7 bouts and 157 cycles of extensor dominated locomotion from 3 bouts, and present their statistics below. Different sets of nerves were recorded across bouts (Table 1). However, all bouts included the flexor Sart and the extensor SmAB.

Flexors	Mean Cycle Duration (seconds)	Extensors	Mean CycleDuration (seconds)
Sart	All	SMAB	All
TA	.639, .812, .909, 1.05 .855*, .995*	LGS	.534, .686, .812, .901 .995*
Perl	.522, .812, .855*, .995*	MG	.522, .554, .686
EDL	.522, .639, .734* .855*, .995*		

Variances of Burst Durations and Cycle Periods

We began by measuring the variability of cycle period, quantified using the coefficient of variation (CV is equal to the standard deviation divided by the mean). Because it lends itself to reliable measurements of the transitions between extension and flexion, we chose the midpoint of bursting in the flexor sartorius as the start of the cycle. Variation of cycle length in the 3 extensor dominated bouts was much greater than in the 7 flexor dominated bouts ($p = 1.85 \times 10^{-6}$); mean = 8.45%, range = 4.81 to 17.86% for

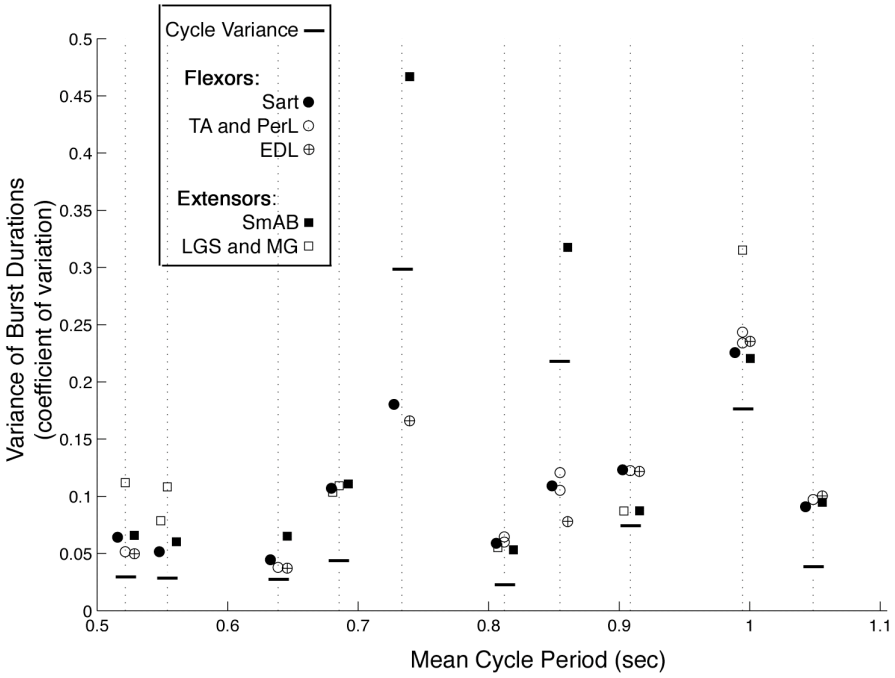

Fig. 3.2, Variance of Burst Durations. Each data point indicates coefficient of variation (y-axis) within each bout identified by mean cycle period (x-axis). Overall burst durations within the three extensor dominated cycles (mean cycle lengths .734, .855, .995 sec) are much more variable than those within flcxor dominated locomotion (all of other bouts). Variance of burst durations within all bouts is of similar magnitude for all flexor dominated bouts.

flexor dominated, mean = 22.45%, range = 7.81 to 46.68% for extensor dominated; Fig. 2). For all bouts, extensor bursts were proportionally more variable on average than the flexor bursts (mean CV of flexor/extensor bursts = 7.55/9.35% respectively during flexor-dominated bouts, and 16.98/31.56% during extensor-dominated bouts). Given the high variability seen in extensor-dominated bouts, all analyses reported below concern flexor-dominated locomotion unless otherwise specified.

Within the n=7 bouts containing flexor-dominated fictive locomotion, there appeared to be a systematic dependence of variability on mean cycle duration. Bouts containing short cycle periods (<0.65 sec; n=3) have flexor bursts which are less variable than longer cycle period bouts ($p = 4.136 \times 10^{-4}$; mean flexor CV for short-cycle bouts =

4.81%, range = 3.71% to 6.42%; mean flexor CV for long-cycle bouts = 9.46%, range = 5.89% to 12.32%; Fig. 2). The variability of extensor burst durations did not change across bouts (p=.4043).

Correlations Between Burst Durations

In order to examine the functional coupling between different components of the motor output, we calculated pairwise correlations between burst durations, measured using the Pearson correlation coefficient. Because it leads to more uniform measures of correlation, we used Fisher's z-transform of the correlation coefficient for figures and statistical comparisons (see Methods). However, given the intuitive nature of the raw Pearson values, we use these for reported values in the text and on axis labels. For simplicity, we will use "burst correlation" to refer to the correlation between burst durations.

As expected, flexor burst durations are positively correlated with other flexor bursts, and extensor burst durations are positively correlated with other extensor bursts (Fig. 3). The one exception is the bout containing cycles with the shortest period, where correlations between extensor bursts are not significantly different from zero.

Correlation between cotemporaneous extensor (SmAB, MG, and LGS) bursts are weak within short cycle bouts (p=.0159; mean correlation between extensors = .430 , range = -.084 to .778 for short-cycle bouts; mean correlation between extensors = .9051, range = .851 to .962 for long-cycle bouts). The same differences in burst correlations hold for cotemporaneous flexor nerves (Sart, TA, and PerL) with shorter cycle bouts having weaker correlations ($p=3.996 \times 10^{-4}$; mean correlation between flexors = .534,

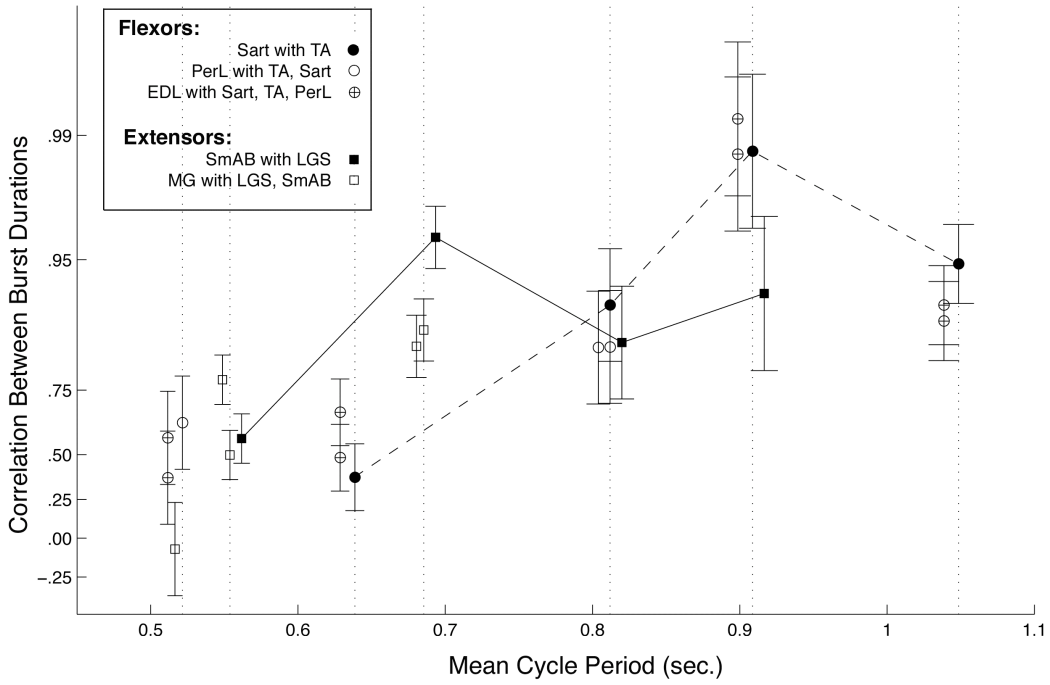

Fig. 3.3. Correlations Between Burst Durations. Error bars denote one standard deviation. Bouts having short cycle periods (mean cycle period <.65) tend to have burst durations within a phase which are weakly correlated ($p=.0159$ for extensors; $p=3.99\times10^{-4}$ for flexors). Solid line indicates connects correlation between SmAB and LGS burst durations in short and long cycle period bouts. Dashed line indicates strength of correlation between the flexors Sart and TA.

range = .378 to .680 for short cycle bouts; mean correlation between flexors = .952 seconds, range = .849 to .992 for long cycle bouts).

One possible explanation for differences in correlation between bouts with long and short cycles is that different collections of nerves are recorded in different bouts. To exclude this possibility, for each pair of nerves, we found the average correlation between those nerves in short-cycle bouts and in long-cycle bouts (n=7 pairs appeared in at least one short-cycle and one long-cycle bout; averaging was performed on z-transformed coefficients). Long-cycle correlations were larger in 7 out of 7 pairs.

The correlation coefficient between variables X and Y is a normalized measure equal to the covariance between X and Y divided by the product of the standard deviations of X and Y. Therefore, the smaller correlation in short-cycle bouts could be

due to an overall increase in standard deviation, and/or a decrease in covariance. Using the same pairings as above, we found that from long to short cycles the proportion of decrease in the average covariance was higher than the proportion of decrease in the product of the standard deviation in all nerve pairs observed. Thus, the decrease in correlation in short-cycle bouts is mainly due to a net decrease in covariance between burst durations. Therefore changes in correlation between bouts having short and long cycles cannot be explained simply as an increase in random noise.

In contrast to generally strong burst correlations between nerves belonging to the same phase, the correlation between flexor and extensor burst durations is weak. The mean correlation of a flexor burst with the following extensor burst is -.0944; the mean correlation of an extensor burst with the following flexor burst is .0633. These correlations are not significantly different from zero, and are not significantly different from one another.

Correlation Between Burst Onsets/Offsets

Conceptually, a weak correlation in the durations of two bursts could result from a weak correlation between burst onsets, a weak correlation between burst offsets, or both. Since measurements of timing require a standard (i.e. a time that is considered time zero), we characterized burst onset and burst offset using a normalized phase measure, based on a standard cycle starting and ending in the middle of the flexor Sart (see Methods). We will use the term "phase locked" to describe two events that are strongly correlated according to this measure. However, since changes in the duration of flexion and/or extension will shift the measured timing of events during the cycle, this measure

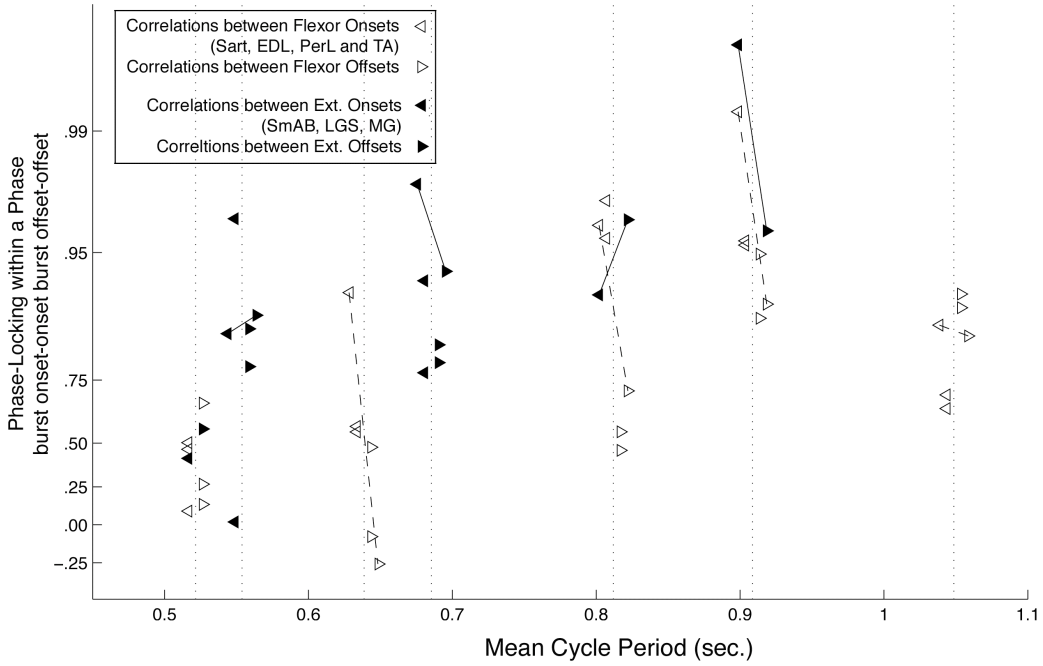

Fig. 3.4. Phase-Locking within a phase. Each data point represents correlation between a pair of burst onsets or burst offsets each within the same phase (flexion or extension). Correlation strength between pairs of extensor onsets and pairs of offsets are approximately the same (c. f. solid line between black triangles connecting correlations between SmAB and LGS). Pairs of flexor burst onsets are more well correlated than pairs of flexor burst offsets (p = .0156, c. f. dashed line indicates correlations between Sart and TA onsets and offsets). Overall correlation between the offset times of flexors is weak.

generally leads to positive correlations between events that occur at similar normalized phase. Therefore, we focus on the relative degrees of phase locking between different event pairs, rather than the phase-locking of any particular pair.

For different extensors recorded in the same bout, we find burst onsets having approximately the same degree of phase locking as burst offsets (p=.0742; onset correlation minus offset correlation equals .3368 +/- .4999; see Fig. 4). For cotemporaneous flexors (Sart, TA, and PerL), there is a strong asymmetry in strength of phase-locking, with the onsets of different flexors being significantly more phase-locked than offsets (p=.0156; mean onset correlation minus offset correlation .7910, range .0731 to .9483).

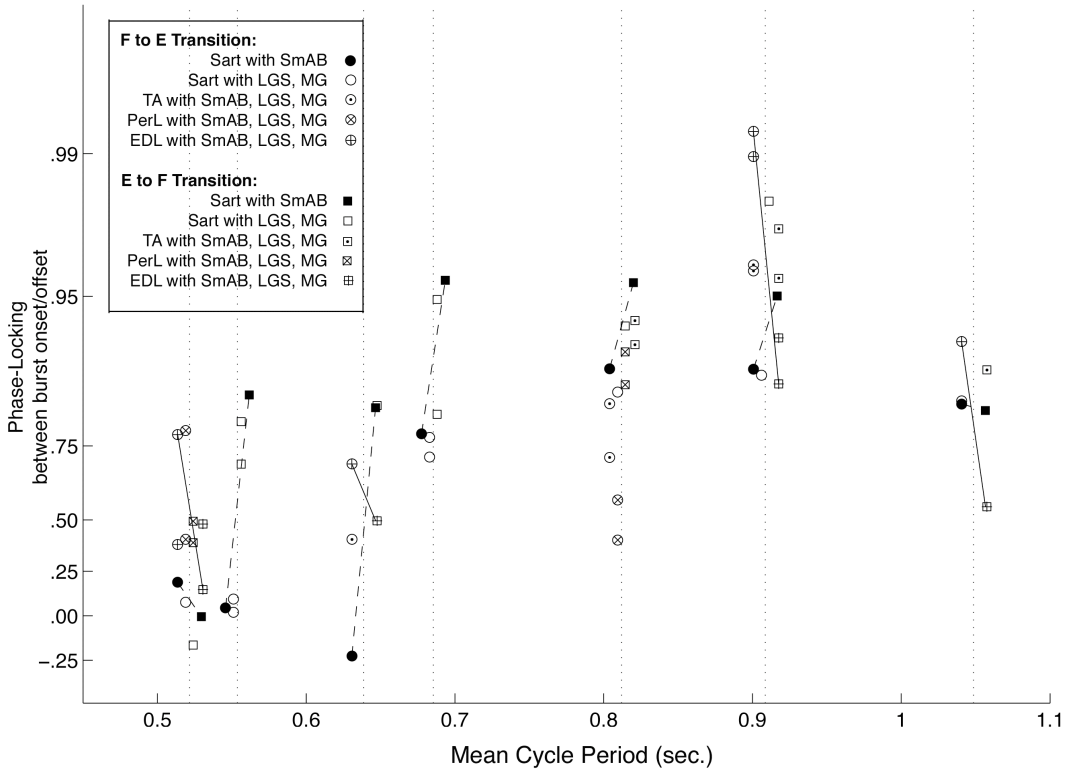

Fig. 3.5, Phase-Locking Between Burst Offsets/Onsets. Circles above represent correlation of relative phase of flexor offset with relative phase of the following extensor onset (F to E transition). Squares indicate opposite transition between extensor offset and flexor onset (E to F transition). Phase-Locking (correlation between burst offset and onset) between Sart and SmAB (shown as black circles/squares connected by dashed line) is weaker at the F to E transition, than at the E to F transition. This trend holds for all nerves observed with the exception of EDL. Phase-Locking between EDL and SmAB, is stronger at the F to E transition (+ inside of circles and squares connected by solid line), and weaker at the E to F transition.

Additionally EDL onset is less well phase locked with onset and offset of cotemporaneous flexors. For the 3 bouts containing Sart, TA, and EDL (Fig. 4, mean cycle length .63; .91; 1.06) phase locking between Sart onset and TA onset is stronger than phase locking between Sart onset and EDL onset.

Phase-locking at Transitions Between Flexion and Extension

Our analysis thus far has focused on flexion and extension as events that make up a given cycle. For the remainder, we adopt a complementary perspective that places a primary focus on the transitions *between* flexion and extension. Across our data set, transitions between cotemporaneous flexors and extensors are strongly asymmetric, with the transition from extension to flexion (E to F) more strongly phase locked than the transition from flexion to extension (F to E). The one exception to this is the bout having the shortest cycle period, This particular bout is unique in this set of data since it contains bursting within the posterior biceps-semitendinosis nerve during both flexion and extension. Due to its qualitatively different pattern of activation we do not include this bout in the remaining reported statistics.

Phase locking is stronger at the E to F than at the F to E transition in 16 out of 20 pairings (Fig. 5); the difference is highly significant ($p = 1.40 \times 10^{-4}$; E to F correlation minus F to E averages .559, range -.076 to .890), and knowing the direction of the transition (i.e. E to F or F to E) explains 27.4% of the variance in correlations at the transitions. Note that not only is phase locking stronger at the E to F transition vs. the F to E transition, it is also less variable (p=.0005).

Phase locking is weaker for shorter-cycle bouts than for longer-cycle bouts. This is true for both the transition from E to F and from F to E (for E to F p=.0068; mean correlation in short-cycle bouts = .811, range = .701 to .853; mean correlation in long-cycle bouts = .994, range = .8191 to ..9830; for F to E p=.0017; mean in short-cycle bouts = .073, range = -.227 to .411; mean in long-cycle bouts = .8358, range = .409 to .965).

The flexor EDL appears to be different from the cotemporaneous flexors in the way it phase-locks with extensors. Although the numbers are small, in 5 of 6 cases where EDL is paired with an extensor, phase locking at the transition from E to F is *weaker* than at the transition between F to E (p=.125; Fig. 5 circles with +).

Latencies and Phase Locking at Transitions

In examining the differences at the E to F and F to E transitions, we noticed that there was often a short period of overlap between bursts at the E to F transition, whereas there was short 'gap' between bursts at the F to E transition. We will call the time of subsequent burst onset minus the time of previous burst onset the 'latency' between bursts at the given transition. Positive latencies correspond to gaps and negative latencies to burst overlaps. For cotemporaneous nerves latencies at the F to E transition tend to be positive and large (i.e. burst do not overlap; mean = .0398 sec., range = .0002 to .0714 sec), whereas those at the E to F transition tend to be negative, and short (mean = .0025 sec, range = -.0405 to .0711 sec.; Fig. 6a). The differences across nerve pairs is significant (p = .0017; mean E to F minus F to E -.0373 sec, range –0.887 to .0422 sec)

Again, the pattern of latencies for EDL is the opposite of the pattern for other flexors. The offsets of EDL bursts tend to occur after the onset of extensor bursts (mean latency = -.0481 sec. , range = -.0898 to -.0264 sec., Fig 6a open circles with +). Conversely, EDL onset tends to occur appreciably later than extensor offset (mean latency = .0796 sec., range = .0048 to .1567 sec.; gray). These differences between EDL and other flexors are significant (p = .0131 for E to F latencies; p = 7.74×10^{-4} for F to

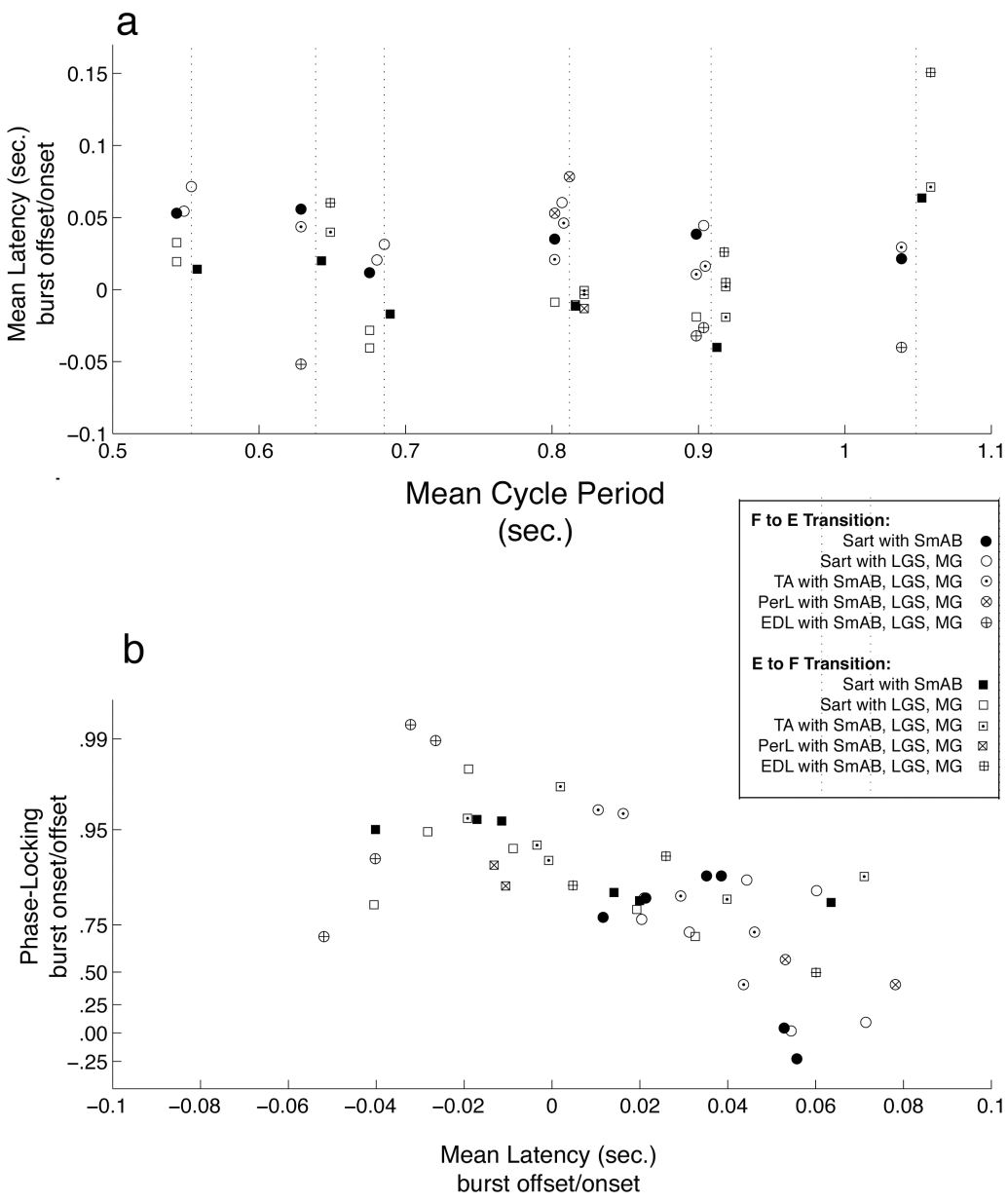

Fig. 3.6, Relationship between Phase-Locking and Latency. All data points labeled as in Fig. 5. 6a shows weak relationship between mean cycle period and latency. Latencies between flexor offset and extensor onset (F to E; circles above) tend to be positive and large. EDL is an exception having bursts offset which overlap with extensor onsets (6a: circles with +, have latencies at the F to E transition which are negative). Extensor offset and flexor onset tend to overlap (6a: squares have negative latencies). 6b exhibits relationship between latencies and strength of phase locking. Bursts having periods of overlap (negative latencies) tend to have strong phase-locking between burst offsets and onsets. Latencies between relative phase of burst offset and burst onset which are positive and large tend to be weakly phase-locked.

E). More importantly, differences are such that the relationship between phase locking at

the transition and latency for EDL (Fig. 6b, gray markers), matches the overall trend for the other flexors. This consistency argues that the factors determining the latency between burst offset and onset are closely related to those that determine phase locking at transitions.

Parameter Dependence of Phase Locking

In our data set, the degree of phase locking at the transitions between phases varies systematically with both mean cycle period and with the mean latency between bursts at the transitions. Separating out the two transitions, mean latency explains 27.2% of the variance in the E to F transitions (p=.0184), whereas cycle duration explains 22.1% (p=.0366). For the F to E transitions, mean latency explains 48.4% of the variance (p=.0007), whereas cycle duration explains 57.2% (p=.0001). The fact that both variables explain less of the variance in the E to F transitions is likely due to the fact that the phase locking at this transition is more consistent across all bouts. Putting all the data together, cycle duration explains 28.8% of the variance in phase locking (p=.0004). This reduction is to be expected, since a prediction based on mean cycle duration cannot capture the asymmetry in the E to F vs. F to E transitions. On the other hand, mean latency does capture this asymmetry, explaining 47.1% of the overall variance in phase-locking ($p= 9.19 \times 10^{-7}$). The fact that the mean latency is able to explain such a high fraction of the variance over the entire set of data suggests a strong functional relationship between phase-locking and mean latency, with differences in the degree of phase-locking reflected by differences in mean latency and vice versa.

Discussion

We describe four properties of MLR induced fictive locomotion: 1, Correlation between burst durations is weak within bouts containing short cycle periods and strong within bouts containing long cycle periods. 2, Phase locking at the E to F transition is strong both within and across the flexor and extensor phases, 3, Phase locking at the F to E transition is weak, especially within bouts containing short cycle periods. 4, Strength of phase locking between burst onset/offset times is strongly related to latency duration.

Changes in Correlations Between Bursts Across Experiments

Previously it has been shown that ENGs from the multiple nerves making up a phase have well correlated activity (Bayev, 1978). Here we report that the amount of correlation between burst durations within both the flexor and extensor phases vary across bouts of fictive locomotion.

One possible explanation for changes in strength of correlations between burst durations is that different bouts exhibit different levels of random noise in motor neurons. However, since it is known that ENGs recorded in the ventral root are produced by the interaction of a linear MN threshold with phasic excitation and inhibition from the sCPG in the form of the locomotor drive potential (LDP) (Krawitz, et. al. 2001), one expects for an increase in random noise at the level of motor neurons to increase overall variability within burst durations. However, we observe the opposite effect, burst durations within bouts containing short cycle periods are both less correlated (Fig. 3) and less variable (Fig. 2).

Another source of difference in correlation between burst durations could be changes occurring within the LDPs at pre-motor neuronal levels A previous study has shown that ENGs closely follow LDP activity (Hamm et. al. 1999). One way such changes could occur is through changes in coupling between multiple oscillators each associated with unique LDPs sent to different MN pools. These changes in coupling between sub-oscillators would have the effect of increasing or decreasing phase locking between LDPs. Within bouts containing shorter cycle periods coupling between oscillators would be weaker and variance within ENGs would be strongly influenced by the natural variability of the individual oscillators. Bouts having long cycle periods would have functional coupling that is strong, and variance that is well correlated within the LDPs received by multiple motor neuronal pools. Changes in excitatory coupling between multiple oscillators could be associated with a positive feedback loop explaining the increase in variance observed across bouts.

Asymmetry at Transitions Between Phases

The E to F transition is strongly phase locked across all observed experimental outputs with the offset of extensors being closely coupled to the onset of flexors. From a functional perspective this is intuitive given that initiating the transition from the stance (extension) to the swing (flexion) phase of locomotion at an inappropriate time can cause maladaptive behavior. The strong influence of sensory inputs on the initiation/inhibition of the E to F transition has been well studied in a variety of preparations (Rossignol, et. al. 2006, Whelan, 1996). Evidence presented here implies that much of the tight coupling of the offset of extensors with the onset of flexors doesn't require sensory input and is

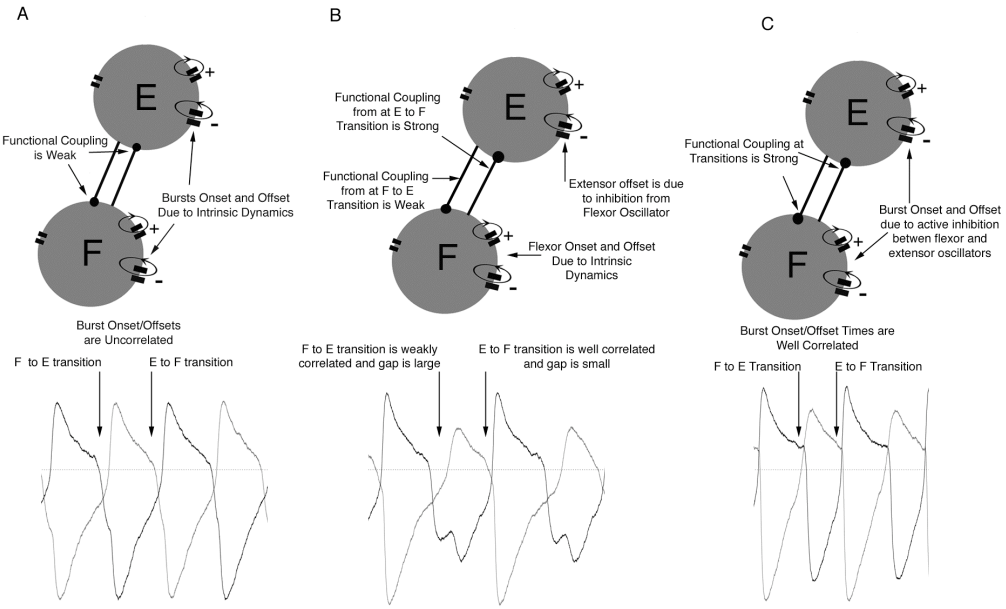

Fig. 3.7, Strength of Phase-Locking Hypotheses. 7a. Weak phase locking at the transitions between bursts could be caused oscillators by within a half-center offsetting due to their own intrinsic properties. 7b. The half-center could then be modulated such that network behavior now consists of one transition which is caused by synaptic inhibition from the opposing set of neurons. This transition would begin to exhibit strong phase locking. **7c.** Activity within each oscillator now 'fills' up the cycle and both transitions are mediated by active inhibition from opposing neurons.

hard wired into the connectivity of the spinal locomotor network. While phase locking at the E to F transition remains strong, phase locking at the F to E transition changes across observed experiments. We hypothesize that observed asymmetry between the E to F and the F to E transitions (Fig. 5) is due to intrinsic differences between the internal dynamics of the flexor and extensor oscillators within a half-center like organization.

It is uncontroversial that the most basic building block of the sCPG is a half-center (Lundberg, 1969, Grillner, 1981, Rybak et. al. 2006). What is and remains controversial is determination of both how many half-centers there are, and the connectivity of these half-centers in making up the entirety of the sCPG network. Within this section this issue is tangential in the sense that asymmetries in the organization of the

basic network would be observable in the output of the entire network regardless of its structure.

The basic organization of the half-center is such that there are two related but different ways in which the transition between the flexor and extensor phases can occur: 1, Each oscillator can turn off due to its own intrinsically oscillatory properties associated with a transition that is weakly coupled, or 2, Onset of the opposing oscillator can cause the currently active oscillator to turn off associated with a transition which is strongly phase locked (Fig. 7). We propose that within experiments containing short period cycles the relative duty cycles of the underlying oscillators are asymmetric. This asymmetry in duty cycles is such that at the F to E transition the flexor oscillator is turning off due to its own intrinsic oscillatory dynamics. Interaction at the F to E transition is then increased by modulation of the duty cycle of either oscillator such that the F to E transition begins to occur through mutual inhibition between the underlying oscillators. . At the opposing transition from E to F the extensor oscillator is always being actively turned off by the onset of flexion. The strong association of mean gap length with strength of phase locking at the transition is likely indicative of increased competition between flexor and extensor oscillators making up a half center (Fig. 7).

Relationship Between Gaps and Cycle Period

While mean cycle period is varying across bouts, mean gap durations are remaining relatively fixed. This effect is asymmetric, with gap durations at the E to F transition being invariant and near zero, while differences in cycle period are weakly associated with decreases in gap duration at the F to E transition. One possible

explanation for the weak influence of cycle period on gap durations could be that there is a maximal level of correlation that can be attained between burst onset/offset times. If we imagine the relationship between gaps and strength of phase locking to be a continuum then as the gap shortens (from large and positive) phase locking increases in strength. At some point before the mean gap duration reaches zero, the phase locking is as strong as possible. The mean gap durations may continue to shorten (into overlap), but the strength of phase locking will not change appreciably. If this is the case then large scale changes in the state of the sCPG associated with lengthening or shortening of cycle period could be associated with relatively small changes in gap duration. However, when this lengthening or shortening occurs near the transition to maximal correlation it would engender a large change in strength of phase locking at the transition.

Previously it has been hypothesized that thesCPG consists of a set of flexor oscillators interacting with a non-oscillating extensor network (Duysens, 1977). We find this unlikely since it implies that either 1, strength of phase locking at the transitions would be invariant since functionally the underlying cause of the transition i.e. onset or offset of the flexor oscillator would be constant, or 2, That changes in phase locking at the transitions would be related to the state of the flexor oscillator in which case one would expect for the to be a strong relationship between flexor burst durations and both the gap duration and strength of phase locking, which is not what we observe here.

Relative Fractionation of EDL

Of particular interest in determining the influence of gap durations on the amount of phase locking observed at the transitions between the flexion and extension phases is

the gap and correlation structure of EDL. Previously it has been shown that EDL responds differentially to stimulation from the periphery (Degtyarenko, et. al. 1999, and Burke, 2001), and that LDPs received by cotemporaneously active flexors such as PerL are uncorrelated with ENGs recorded from EDL (Hamm, 1999). These differences in behavior between EDL and cotemporaneous flexors has lead to speculation that activity in EDL could be produced by a separate pattern formation network, giving impetus to the idea that the sCPG is composed of multiple sub-oscillators (Grillner and Wallen, 1985). Here we report similar differences in the pattern of activation of EDL. Where cotemporaneous flexors have large gaps and malleable phase locking at the F to E transition, EDL has small or negative gaps and strong phase locking across all.

This result implies that EDL is not simply phase advanced or phase delayed relative to cotemporaneous flexors. If EDL were simply phase delayed at the F to E transition, then one would expect that EDL offset would retain the same level of phase locking with the onset of extension observed in cotemporaneous flexors regardless of duration of latencies. I.e. if activity in cotemporaneous extensors is such that they are slightly delayed, then EDL should be delayed by the same amount, but the correlation of EDL with extensor onset shouldn't qualitatively change.

Additionally, the current results show that the relative fractionation of bursting activity reported here in the form of gap durations, determines the strength of phase locking between activity within the various nerves more strongly than does the identity of that nerve as a flexor or extensor.

Summary and Future Directions

Although, currently the authors believe that it is likely that the sCPG for locomotion is composed of multiple sub-oscillatory units, we are unable to prove this to be the case given the relative fractionation of nerves presented here. Although it is rarely directly stated within the literature, the criterion for showing the existence of multiple oscillatory units entails finding cases where the qualitative structure of the output cannot be explained in terms of a simple phase advance or phase delay on a unitary signal. The most obvious way to show that burst onset/offsets are not simply phase advanced or phase delayed is to show that although the relative fractionation of two events are similar, i.e. say onset of flexors, the strength of phase locking of between these events and another event elsewhere in the step cycle is such that one is well phase locked and one is not. The existence of events that share timing but do not share phase locking would provide powerful evidence that there are separate networks underlying these temporally related events. As discussed earlier, since events occurring close together in time tend to be well correlated, the strongest case would be made for events which are well separated in time.

CHAPTER FOUR: MODELING ASYMMETRIES IN THE FICTIVE LOCOMOTOR CYCLE USING STOCHASTIC HALF-CENTER OSCILLATORS

Abstract

Functional relationships between simulated neuronal networks composed of oscillatory and non-oscillatory units are at present poorly characterized. Here we examine differences in the behavior of half-centers composed of the non-intrinsically oscillatory leaky integrator, and the oscillatory Morris-Lecar neuron. In order to induce natural variability in the models we inject a continuous and small noise current into each simulated neuron. We then track four properties of the output of the network over multiple parameter regimes: 1, Strength of phase locking between burst offset and onset times; 2, Relative timing of burst offset and burst onset; 3, Correlations between burst durations; and 4, Cycle period.

We find that for all parameters tested the leaky integrator half-center oscillator has strongly phase locked burst offsets and burst onsets. Within the Morris-Lecar half-center, strength of phase locking is malleable and depends upon the balance of excitation and inhibition within each simulated neuron. Changes in phase locking are largely determined by the latency or temporal distance between burst offsets and onsets.

Through manipulating the relative levels of excitation and inhibition in the Morris-Lecar neurons making up a half-center one can create a variety of qualitatively different states that can then be compared directly to the statistics of biological neuronal systems. One such state of particular interest to the authors (c.f. Boothe, et. al. Chpt 2) is asymmetric outputs where one transition is strongly phase locked and one transition is weakly phase locked. The Morris-Lecar half-center exhibits such a strongly asymmetric

state when one simulated neuron receives high levels of both tonic excitation and self-inhibition relative to the opposing neuron in the half-center.

Introduction

The behavior of many rhythmic neuronal networks from the spinal central pattern generator for locomotion (sCPG) to the stomatogastric ganglion of lobster's are thought to derive important functional properties from a core set of mutually inhibitory neurons (Grillner, 1999, Marder, 2005). The simplest such network consists of two mutually inhibitory interneurons termed a half-center (Lundberg, 1969). Deterministic models of the half-center organization have been well studied within both a mathematical context (Izhikevitch, 2001, Skinner et. al. 1994, Wang and Rinzel, 1992) as well as having been applied directly as an aid in understanding the structure and function of the spinal central pattern generator (sCPG) for locomotion (Jung, et. al, 1996, Rybak, et. al. 2006a-b). While current understanding of the behavior of such deterministic half-centers is well developed, understanding of the behavior of stochastic versions of these same networks is still evolving (Boothe, et. al., 2006).

Here we explore the possibility that half-centers composed of different types of simulated neurons might have substantial qualitative differences in the structure of their outputs. One of the most intuitive distinctions that can be made between simulated neurons is that they can be either intrinsically oscillatory, or incapable in isolation of generating a rhythmic pattern of output. If the oscillatory or non-oscillatory properties of simulated neurons strongly influence model output, then many properties of biological

neuronal networks may only be accurately reproduced in networks composed of simulated neurons of the proper type.

Previously we hypothesized that the intrinsically oscillatory properties of neurons making up the biological sCPG might be responsible for differences in the strength of phase locking between relative phase of burst offset and burst onset within the output of the sCPG during fictive locomotion (Boothe et. al. Chapter 3). In order to explore how differences in phase-locking could occur within a half-center organization we have performed a set of mathematical simulations using both the intrinsically oscillatory Morris-Lecar neuron, and the non-intrinsically oscillatory leaky integrator. These simulated neuronal types have been broadly used both in the context of modeling the sCPG for locomotion (Boothe, et. al. 2006, Jung et. al. 1996) and models of cortical function.

To induce measurable natural variation in the models we injected white noise currents into each simulated neuron. This method has the advantage of allowing one to measure the strength of phase locking within each simulation directly by measuring correlation between relative phase of burst onset and burst offset. Changes in phase locking can then be tracked across parameter changes that qualitatively alter the structure of each model's output. Of particular interest is the relationship between asymmetric sets of parameters and strength of phase locking.

We find that for all parameters tested phase locking in a half-center composed of leaky integrators is strong. Within a half-center composed of Morris-Lecar neurons we find individual parameters have specific effects upon strength of phase locking, specifically: 1, increases in excitatory currents (self-excitation or tonic drive) tend to

increase phase locking at multiple transitions between phases, while 2, decreases in self inhibition tend to increase phase locking at the following transition between phases, but not the previous transition.

Methods

Models presented here are designed to elucidate how changes in phase locking at the transitions between bursts might be accomplished within the context of a half-center organization. Previously we hypothesized that differing strength of phase locking at the transition from extension to flexion and flexion to extension may be caused by underlying differences in the state of the oscillators responsible for each phase of locomotion (Boothe, et. al., Chapter 3). Here we test the plausibility of this hypothesis through the construction of two sets of stochastic models.

Half-Center Composed of Leaky Integrators

We have performed an in depth analysis of the behavior of a half-center composed of neurons of the leaky integrator type (Boothe, et. al. 2006). The model presented here uses different parameters (c.f. below) but is otherwise identical to that presented earlier.

Within the leaky integrator half-center model neuron *i* is governed by two internal variables: a normalized membrane voltage variable V_i that takes values between -1 and 1, and a slow self-inhibitory conductance $g_{di}D_i$, where D_i ranges between 0 and 1. Voltage dynamics are based on the following differential equation:

$$(1) \qquad \frac{dV_i}{dt} = g_{ri}\,(0 - V_i) + g_{ti}\,(1 - V_i) + \sum_{j=1}^{n} h(V_j)\, g_{syn}^{ij}\,(v_{syn} - V_i) + g_{di}\, D_i\,(-1 - V_i) + I_i$$

The terms on the right hand side of equation (1) represent the following currents: a leak current with conductance g_{ri} and reversal potential V=0; a tonically active excitatory current with conductance g_{ti} and reversal potential V_i=1; synaptic input from other neurons as represented by the sigmoid firing rate function $h(V_j)$ times a maximal synaptic conductance g^{ij}_{syn} and reversal potential v_{syn}; the slow self-inhibitory current with conductance g_{di} D_i and reversal potential Vi= -1; and a perturbation current I_i. Perturbation currents for this set of simulations take the form of a Gaussian white noise process ξ_i scaled by σ_i. The slowly acting inhibitory conductance $g_{di}D_i$ was governed by an exponential decay to a cells output firing rate $h(V_i)$ with time constant t_i:

$$(2) \qquad \frac{dD_i}{dt} = (h(V_i) - D_i)/\tau_i$$

A similar schema for self-inhibition was used in Pribe, et. al. (1997), where the slow self-inhibitory current was construed as an additional neuron providing inhibitory feedback.

The firing frequency of a simulated neuron is a function of the membrane voltage and is determined by a non-linear sigmoid rate function $h(V_i)$. We chose to use a piecewise polynomial function with the following properties (Jung, et. al. 1996): (i) outputs rates range from 0 to 1; (ii) there exists a true threshold (V_i = 0) below which output rate is equal to 0; (iii) the function is sufficiently smooth to facilitate currently unpublished bifurcation analyses.

$$(3) \qquad h(V_i) = \begin{cases} 0 & if \quad V_i < 0 \\ -20\,V_i^7 + 70V_i^6 - 84\,V_i^5 + 35\,V_i^4 & if \quad V_i \geq 0 \end{cases}$$

Parameters were selected such that output of the model would conform to previously reported experimental observations (Boothe et. al. Chapter 3). Specifically the model should have parameter regimes where one burst is significantly longer than the opposing burst, and have bursts whose coefficients of variation (standard deviation of the burst duration divided by mean burst duration) are approximately the same size as those observed in both the output of the biological system (3 to 7%; Boothe, et. al. submission, Chapter 3), as well as the half-centers composed of Morris-Lecar neurons described below. Default parameters were chosen such that the symmetric model (in the parameters below) could transition into the asymmetric behaviors we are interested in with minimal changes. Default parameters of the leaky integrator half-center presented here are: $g_{ri} = 3.5$; $g_{ti} = 7$; $g^{ij}_{syn} = 30$; $g_{di} = 20$; $v_{syn} = -1$; $\beta = 5$.

Half-Center Composed of Morris-Lecar Oscillators

Morris-Lecar type neurons, while originally proposed as a model of barnacle muscle (Morris, and Lecar, 1981), have become a standard way to model neurons having intrinsically oscillatory properties and have been applied to a wide range of phenomenon (Rinzel and Ermentrout, 1987, Wang and Rinzel, 1995). As in the leaky integrator half-center the simulated voltages described here are assumed to linearly represent aggregate spiking rates in a population of neurons.

Each model neuron i is described by two internal variables: V_i representing membrane voltage, and W_i representing activation within a slow self-inhibitory conductance. Voltage dynamics are described by:

(4)
$$\frac{dV_i}{dt} = g_{ei}\, m_{inf}(V_i)\,(v_e - V_i) + g_{ki}\, W_i\,(v_k - V_i) + g_{li}\,(v_l - V_i) + h(V_j)\, g^{ij}_{syn}(v_{syn} - V_i) + \sigma_i \xi_i + I_i$$

The terms on the right side of (4) represent the following currents:

A fast self-excitatory current with maximal conductance g_{ei}, and activation dynamics $m_{inf}(V_i)$ and reversal potential v_e; a slow self inhibitory current with maximal conductance g_{ki}, activation dynamics W_i and reversal potential v_k; a synaptic current from the other neuron of the half-center with maximal conductance g^{ij}_{syn}, and activation dynamics determined by the sigmoid firing rate of the opposing neuron represented by $h(V_j)$ and reversal potential v_{syn}= -1; a leak conductance with maximal conductance g_l and reversal potential v_l; a term for stimulating current or in our terms tonic drive I_i; and a Gaussian white noise process ξ_i scaled by a factor σ_i.

The slowly acting self inhibitory conductance $g_{ki}W_i$ is governed by an exponential decay to the maximal activation of the self-inhibition $w_{inf}(V_i)$with time constant $\tau(V_i)$.

(5)
$$\frac{dW_i}{dt} = \phi_i \frac{[w_{inf}(V_i)_i - W_i]}{\tau_i(V_i)}$$

The activation dynamics of the fast self excitation $m_{inf}(V_i)$ are represented by a sigmoid function with activation between 0 and 1, as is $w_{inf}(V_i)$.

$$m_{inf}(V_i) = .5\,[1 + \tanh\{(V_i - v_i)/v_2\}$$

(6)

$$w_{inf}(V_i) = .5\,[1 + \tanh\{(V_i - v_3)/v_4\}$$

Firing frequency of simulated neurons is determined by a non-linear rate function $h(V_i)$ (Equation 3 above). Unlike in the previous model τ_i depends upon the current voltage, and is represented by equation (7) below.

(7)

$$\tau_i(V_i) = \frac{1}{\cosh\{(V_i - v_3)/2v_4\}}$$

Default parameters were similar to those used by Rinzel and Ermentrout (1989). Unless otherwise noted in the text parameters were symmetric and as described below: g_{ei}= 1.1; g_{ki}= 2; g_{li}= .5; g^{ij}_{syn}= 10; v_e= 1; v_k= -1; v_l= -.5; v_{syn}= -1; I_i= .26; v_1= .01; v_2=.145; v_3=.1; v_4=.15.

Analysis of Network Behavior

Bursts were detected using an automated procedure similar to that reported in Yakovenko et. al. 2005. For each simulated output from 30 to 300 thresholds were tested at equal intervals (from .01 to .001 V_i) within regions of model output where the slope of V_i was large. From each of these measurements the total number of threshold crossings was obtained for each threshold. When the threshold was applied at regions of simulated voltage that had large individual differences between bursts or were noisy, the total number of threshold crossings is large. Thresholds that only detected burst onsets

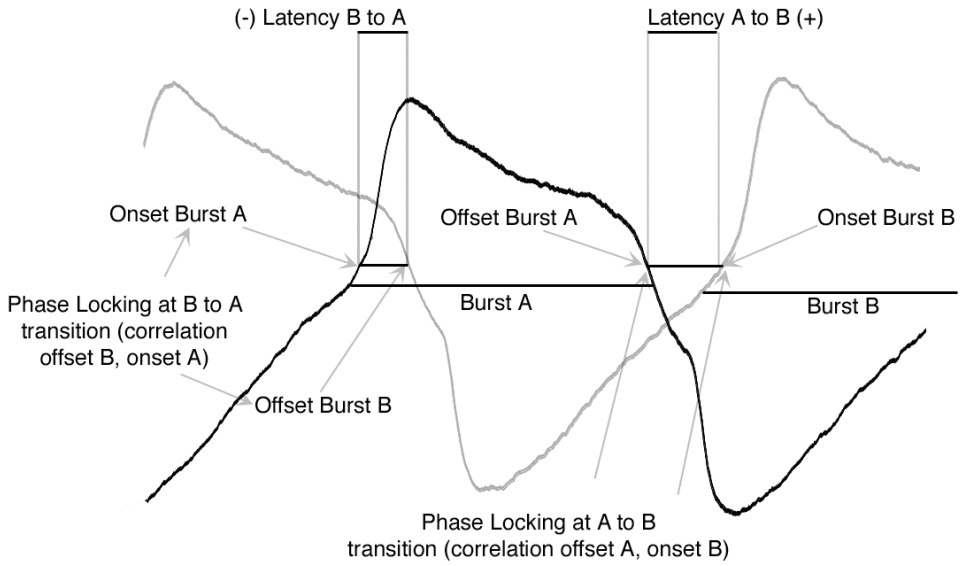

Fig. 4.1, Schematic Representation of Model Analysis. Here we report four measurements: Model output contains two transitions, i.e. from B to A, and from A to B. Since all parameter changes reported were performed in the neuron underlying behavior in burst A, the B to A transition is always the preceding the burst of interese, and the A to B transition is always following. For each transition we measure relative phase of burst onset and offset (time of burst onset/offset-cycle onset/cycle length). Strength of phase locking at each transition is then defined as the correlation coefficient between relative phase of burst offset with burst onset. Latencies between bursts are defined as relative phase of burst onset minus burst offset. Negative latencies indicate periods of overlap (pictured at B to A transition above), while positive latencies indicate a period of quiescence between bursts (A to B transition above). Burst duration is defined as burst onset time minus burst offset time and is not reported in relative phase. Burst correlation is the correlation coefficient of the duration of burst A and burst B.

and burst offsets yield the smallest possible number of threshold crossings. Once each threshold was tested, It was then determined whether or not contiguous thresholds also detected the smallest number of total threshold crossings. For the sake of consistency we then chose the smallest threshold possible having contiguous thresholds with the minimum number of threshold crossings.

Statistics performed on time dependent phenomena require setting an arbitrary time as time zero. Measurements taken without comparison to a standard are unreliable since time is itself monotonically increasing, leading to artificially high co-variances and correlations. Additionally, measurements of time dependent phenomena in ‘real’ or

absolute time are strongly influenced by cycle to cycle variability. In order to accurately measure regularity in temporal relationships we have used a relative phase measure of burst onset and burst offset times.

We have named the neurons in the half-center neuron A and neuron B (Fig. 1, Fig. 2. a-b). We then define the cycle period as the time from onset in neuron A the time of next onset in neuron A. Relative phases of burst onset and offset can then be computed relative to this cycle definition. Relative phase of offset of burst A is then defined as the length of time from the beginning of the burst in neuron A to the offset of the burst in neuron A divided by the cycle period. Relative phase of the burst onset within neuron B is then defined as the difference in onset times of neurons A and B, divided by the cycle period. Since, we are only analyzing the statistics of one transition; neuron A is always turning off (offset) and neuron B is always turning on (onset) for this set of simulations.

Strength of phase locking between burst A offset and burst B onset can then be computed directly using the correlation coefficient on the relative phase of offset burst A and relative phase of onset of burst B. Pearson's correlation coefficient (r) for any two variables X and Y ranges from –1 to +1 and is defined by:

(8) $$r = \frac{Cov(X,Y)}{\sqrt{Var(X)Var(Y)}}$$

where $Cov(X,Y)$ is the covariance of X and Y and $Var(X)=Cov(X,X)$ is the variance of X.

We report three additional measures of model output (Fig. 1). One which we term the 'latency' is defined as the mean distance in relative phase between the offset of burst

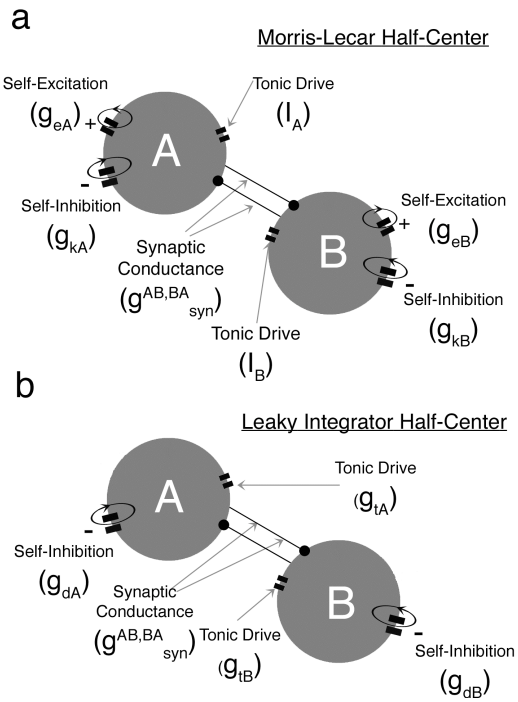

Fig. 4.2, Summary of Model Parameters. 1a. Morris-Lecar neurons composed of two excitatory currents (conductances: g_{ei}, I_i) and two inhibitory currents (conductances: g^{ij}_{syn}, g_{ki}). 1b. Leaky integrator half-center composed of one excitatory current (conductance g_{ti}), and two inhibitory currents (g^{ij}_{syn}, g_{di}).

A and onset of burst B (Fig. 1). A positive latency indicates a short off period or 'gap' between burst A offset and burst B onset, while a negative gap indicates that the bursts overlap with burst B onset occurring before burst A offset. A second reported measure is the 'burst correlation' which we define as a pairwise comparison of covariance between burst duration A and burst duration B using the correlation coefficient (Fig. 1). The third is the 'burst ratio' which is defined as the mean length of burst duration A divided by the mean length of burst duration B (Fig. 1).

Naming and the Transitions Between Bursts

Since reported parameter changes all occur within a single neuron, with parameters within the opposing neuron remaining constant, the B to A transition is by definition equivalent to measuring changes as above only now having parameters within the opposing neuron remain constant (now neuron A), and making identical parameter

changes within neuron B. When we report measures of the B to A transition this is the method we have used.

Simulations

Stochastic simulations were run on a Linux based Dell E-310 using xpp.aut (Bard Ermentrout, www.math.pitt.edu/~**bard**/xpp/xpp.html). Differential equations used in the model were solved numerically using the Euler-Maruyama method for solving stochastic differential equations (Oksendal, 2000). Simulations were originally run using a variety of time steps and methods with little change in model outputs; reported simulations used a time step *dt* =0.004. Noise added to the models takes the simplest possible form, an additive current into the membrane voltage. At each time step of width *dt,* noise values in the term ξ_i were drawn from a Gaussian distribution with standard deviation equal to one and then scaled by the quantity σ_i/sqrt(*dt*). The final value for σ_i was set so that the variability in cycle length was approximately the same for all models.

Statistical analysis was performed in Matlab (*Mathworks, Natick, MA*). In order to run xpp.aut from within matlab we relied on a very usefull m-file entitled ChangeXppOde.m (http://www.cam.cornell.edu/~rclewley/research. html) written by Dr. Robert Clewley.

Results

The creation of oscillatory behavior in simulated neuronal networks takes two general forms: 1, the oscillatory behavior can be a property of a network composed of non-intrinsically oscillating simulated neurons; or 2, the individual neurons used within the simulations can themselves have intrinsically oscillatory dynamics.

The simplest oscillatory network composed of non-oscillating units is the half-center. In order to give a rhythmic output such models must contain within their dynamics a way of turning off activity in one neuron, and turning on activity in the opposing neuron. This can be performed in many ways, but the simplest is for each neuron to have some form of self-inhibition. Self-inhibition slowly builds up strength while the simulated neuronal voltage is above an arbitrary threshold. When the self-inhibition is sufficiently strong, there is a reduction in voltage within the currently active neuron. This reduction in voltage causes a reduction in inhibition upon the opposing neuron. The combination of the currently active neuron being self-inhibited, and the opposing neuron being released from inhibition, has the effect of terminating activity in the currently active neuron, and causing onset of activity in the other neuron in the half-center. This process then begins again for the opposing neuron. Since active inhibition from the opposing neuron is always necessary for the transition in activity between the neurons of the half-center we hypothesize that phase locking between burst offset in one neuron and burst onset in the opposing neuron will always be strong. This strong phase locking will be associated with small latencies between bursts (Fig. 1).

Half-centers composed of intrinsically oscillating neurons can be in one of two regimes which form a continuum. If the burst duration of each neuron is short relative to the cycle period, bursting in each neuron will be anti-phasic, due to mutual inhibition. Within this regime the offset of neurons in the network is caused by interplay within the individual neuron's internal dynamics of self-excitation and self-inhibition. When one neuron offsets, the other neuron simply turns on due to its own intrinsic oscillatory properties. Here, since the time of offset of each neuron is due to its own intrinsic state,

modulated by independent noise, we expect for phase locking between the offset and onset of each neuron to be weakly phase locked. Additionally, since burst offset is occurring due to internal dynamics, burst offset and onset can occur well separated in time, giving a large and positive latency.

When intrinsically oscillating neurons within a half-center are in a state where burst durations are large relative to the cycle period, they act much like the non-intrinsically oscillating network described above, i.e. bursting within the currently active neuron is actually terminated by the interaction of its own self-inhibition with onset bursting activity within the opposing neuron, causing a transition where phase-locking is strong.

Consistent Properties Across Simulations

As described above, in the leaky integrator model there is only one route to oscillatory behavior, namely winner-take-all dynamics that is biased by an alternating buildup of slow self-inhibition. Since the offset of every burst is dependent upon the onset of competitive inhibition coming from the other neuron, we expect burst offsets and onsets to be strongly phase locked at transitions. Furthermore, since both neurons are active during the period of competition, we expect that the latencies at burst to be negative. These expectations are borne out in our simulations, with negative latencies and near perfect phase locking for all transitions and across all parameter values for this model.

Less obviously, we consistently find that the correlation in burst duration is near zero across simulations (figs 3-5, panel d). This result holds for both models.

Asymmetries in Self-Inhibition

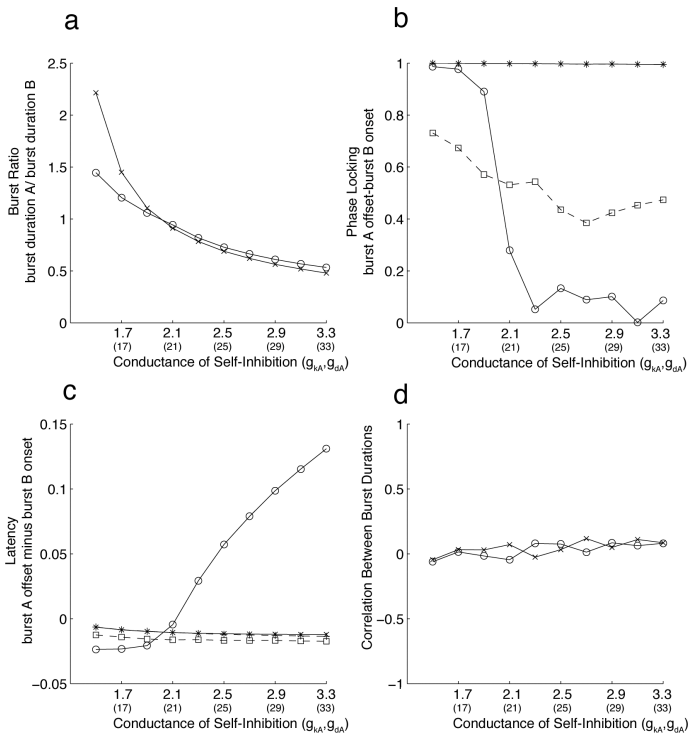

Fig. 4.3, Influence of Changes in Self-Inhibition. 3a. Ratio of mean burst A/mean burst B. Increases in self-inhibition, (g_{kA}) from 1.5 to 3.3 in Morris-Lecar half-center, and 15 to 33 (g_{dA}) in leaky integrator half-center decrease length of burst A relative to burst B (open circles and solid line indicate Morris-Lecar; x with solid line indicates leaky integrator). 3b. Leaky integrator half-center has no change in strength of phase-locking due to increasing g_{dA} (overlapping + and x = *), while within the Morris-Lecar half-center changes in self-inhibition (g_{kA}) strongly decrease phase locking at the A to B transition (circles with solid line), while weakly decreasing phase-locking at the B to A transition (squares dashed line). 3c. Within the Morris-Lecar half center increasing g_{kA} causes the latency between burst A offset and burst B onset to increase from overlapping (negative latency) to a period of inactivation (positive latency). The B to A transition shows only a weak increase in latency. 3d. Burst durations are always weakly correlated for both models.

In both the Morris-Lecar and leaky-integrator models, the build up of self-inhibition (Fig. 2) plays a dominant role in burst termination. Consistent with this notion, increasing the strength of self-inhibition in neuron A causes the duration of bursting in this neuron to decrease relative to that in neuron B (Fig. 3a). However, the effect of early termination of the burst in neuron A has different consequences in the two models. In the leaky integrator, the early termination of activity in neuron A results in an early release from inhibition in neuron B. Latencies remain negative and phase locking

remains strong. In the Morris-Lecar model, at higher levels of self-inhibition the burst in neuron A terminates before the intrinsic oscillatory dynamics enable burst onset in neuron B. This leads to a positive latency between neuron A offset and neuron B onset (fig. 3c, open circles). Furthermore, as the termination of bursting in A and the onset of bursting in B become separated in time, they are dominated by mechanisms that are intrinsic to each neuron. Therefore, the transition to positive latencies is accompanied by a precipitous drop in phase locking at the A to B transition (fig 3b, open circles).

The situation at the B to A transition is quite different. The strength of self-inhibition in A only affects the lingering self-inhibition inhibition that was recruited during the previous neuron A burst, which occurred more than half a cycle earlier than the B to A transition. As a result, changing the strength of self-inhibition in A causes little change in the latency from burst B to A, and only a minor decrease in phase-locking at the B to A transition (fig 3b and 3c, open squares).

Asymmetries in Tonic Drive

Increasing the tonic drive to a neuron within the half-center is expected to lengthen bursting within that neuron and shorten the period of inactivation between bursts. Consistent with this straightforward interpretation, increasing tonic excitation (Fig. 2) in neuron A causes an increase in the burst duration of neuron A relative to neuron B (Fig 4a).

In the Morris Lecar model, as the tonic drive (I_A) to neuron A becomes *lower* than for neuron B (left side of plot in fig 4), the burst duration of neuron A can become shorter than the natural period of inactivation in neuron B. Neuron A's burst can then "fit

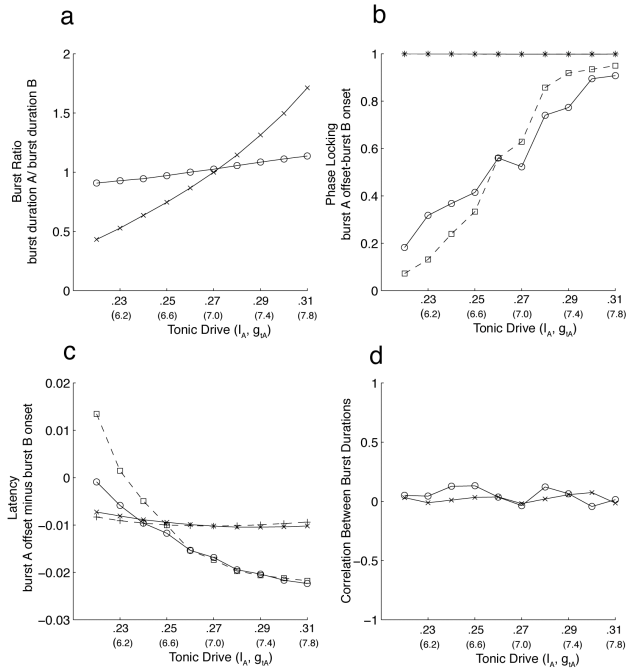

Fig. 4.4, Effect of Increasing Tonic Excitation. 4a, Increases in tonic excitation (I_A in Morris-Lecar, g_{tA} in leaky integrators) increase burst durations (circles indicating Morris-Lecar half-center, and x indicating leaky integrators). 4b, Phase-locking within leaky integrators is always strong, increasing self-excitation in Morris-Lecar neurons increases phase-locking at A to B and B to A transitions. 4c, Increasing strength of phase-locking is associated with a reduction in latency. 4d, Burst Durations remain uncorrelated for all parameter changes.

inside" this period of B inactivation. So at low levels of tonic drive, the latency between B offset and A onset as well as the latency between A offset and B onset grow (fig. 4c, left). As the onset and offsets in A become separated from the offsets and onsets in B, these events become largely decoupled, and the phase-locking at the transition is weak (Fig. 4b, left). Note that while asymmetries in tonic drive cause asymmetries in burst duration, tonic drive lengthens the burst at "both ends," causing effects at the A to B and B to A transitions. Although these effects are largely symmetric, is does appear that changes in tonic drive in neuron A have a slightly greater impact on the preceding (B to A) transition (Fig. 4b, dashed lines).

Asymmetries in Self-Excitation

In the Morris-Lecar model, burst duration can also be extended by increasing the excitatory feedback parameter g_{ei} (Fig. 2a). When a neuron is active, reducing self-excitation will lead to a shorter period of activation before the build up in self-inhibition causes a termination of the burst. Consistent with this expectation, decreasing excitatory feedback strength (g_{eA}) decreases the duration of bursting in neuron A relative to neuron B (fig. 5a, left). Furthermore, large reductions in feedback excitation lead to a termination of bursting in neuron A before the onset of neuron B. This causes positive latencies and weak phase locking at the A to B transition (fig. 5b and 5c left, circles). An increase in feedback excitation will also make neuron A more sensitive to changes in inhibition received from neuron B, and will speed the activation of neuron A at the beginning of a burst. In the simulations, increasing positive feedback increases phase locking and causes a slight decrease in latency at the B to A transition (5b and 5c right, squares).

Modeling Multiple Asymmetries: Self-Excitation

Previously we have shown that within fictive locomotion there are significant differences in strength of phase locking observed between the transition from flexion to extension and extension to flexion (Boothe, et. al., Chapter 3). The transition from extension to flexion is always strongly phase-locked, while the transition from flexion to extension is weakly phase-locked in cycles having short durations. In order to give an output qualitatively similar to these previous observations two preliminary criterion must be met: 1, Tested parameter regimes must contain one burst duration which is substantially longer than the other (1.5 to 3 times), and 2, Model output must have one

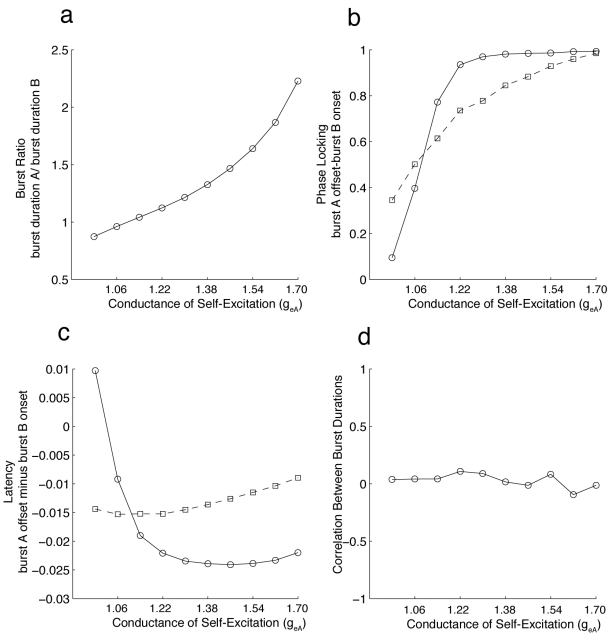

Fig 4.5, Effect of Increasing Self-Excitation. 5a. Increasing self-excitation (g_{eA}), increases burst durations. 5b, Increases phase locking at both transitions. 5c Shortens latencies, and 5d doesn't effect correlations between burst durations.

transition that is invariant and strongly phase locked over many parameters changes, and one transition that is weakly phase locked for some of those same parameters but is strongly phase-locked for others.

Since phase locking between burst offset and burst onset was always strong for the parameters tested within the leaky integrator half-center, we conclude that this model is unlikely to generate outputs qualitatively similar to the biological system. Therefore, we focused our analysis on the Morris-Lecar model.

Based on the previous simulations, we hypothesized that a half-center containing one Morris-Lecar neuron having high excitatory currents (to produce asymmetric burst durations), combined with a high level of self-inhibition (in order to de-correlate one transition but not the other) was likely to give behavior qualitatively similar to the experimental data. We examined the combined effect of changing both the strength of self-excitation, g_{eA}, and the strength of self-inhibition, g_{kA}, and measuring the relative burst length, latencies, and phase locking for each combination of parameters (Fig 6).

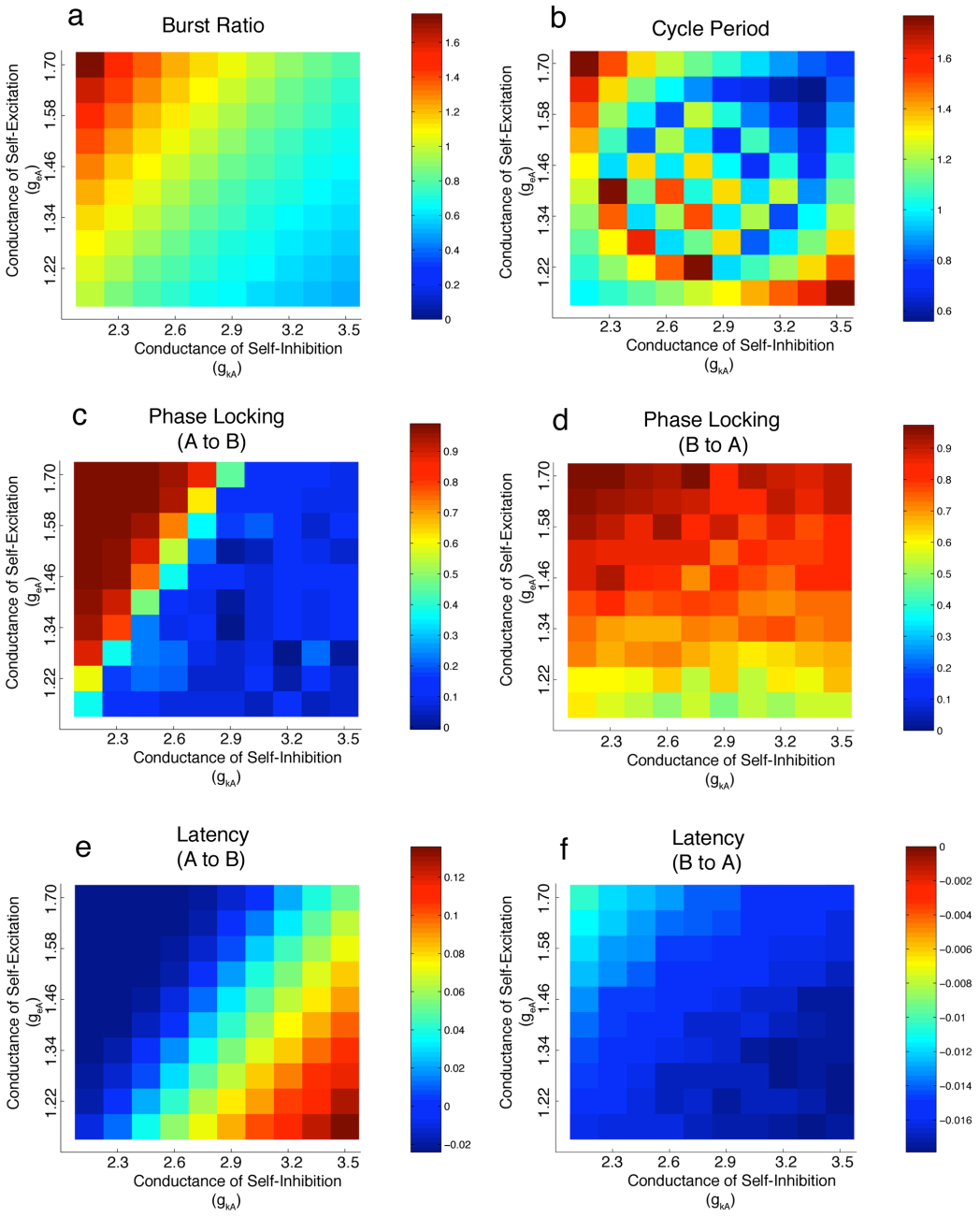

Fig. 4.6, Interaction of Self-Excitation and Self-Inhibition. Morris-Lecar Half-Center. 6a. Relative strength of self-excitation (g_{eA}) and self inhibition (g_{kA}) interact to determine burst length. 6b. Changes in burst duration are reflected in overall cycle period, shown here as the ratio of cycle duration for the given asymmetric parameters divided by cycle period in symmetric (default parameters) case. 6c. When self-excitation is strong relative to self-inhibition following transition is well phase locked (A to B). Increasing self-inhibition balances this effect and weakens phase locking. 6d. Because strength of self-excitation effects the previous transition (B to A) more strongly than does the self-inhibition, this transition B to A remains well correlated. 6e-f. Latencies at the A to B transition are variable (as expected given the changes in phase locking), while those at the B to A transition are always negative.

The strengths of self-excitation and self-inhibition affect the relative duration of

burst A and B as above with increases in self-excitation increasing the relative burst duration of A whereas increases in self-inhibition decrease relative burst duration in A (fig 6a). The two affects are largely additive in that parameters that give rise to a given relative duration correspond to a diagonal line in parameter space going from the bottom left to the top right of Fig. 6a. Latency changes at the following (A to B) transition show a similar pattern with larger latencies for strong self-inhibition and weak self-excitation (Fig 6e, lower right). Phase locking also shows a similar pattern with phase locking of saturating near zero for strongly positive latencies, and saturating near 1 for strongly negative latencies, with a relatively narrow transition region corresponding to latencies slightly below 0 (Fig. 6c). Increasing burst durations tend to increase overall cycle period (Fig. 6b).

Changes at the B to A transition show a different pattern. The effects of parameter changes on the B to A latency have a similar pattern as those on the A to B latency, but the magnitudes are much smaller. Latencies remain negative for all parameters explored, ranging between -.011 and-.017 sec (Fig 6f). As with the single parameter simulations, phase locking at the B to A transition are dominated by changes in self-excitation, with self-inhibition playing only a minor role (Fig 6d).

Modeling Multiple Asymmetries: Tonic Excitation

Given the strong similarities in influence on model output between self-excitation and tonic drive (Figs 4 and 5), we hypothesized that strength of tonic drive (I_A) and strength of self-excitation (g_{eA}) should interact with self-inhibition (g_{kA}) in a similar manner. Changes due to modulation of tonic drive and self-inhibition at the A to B

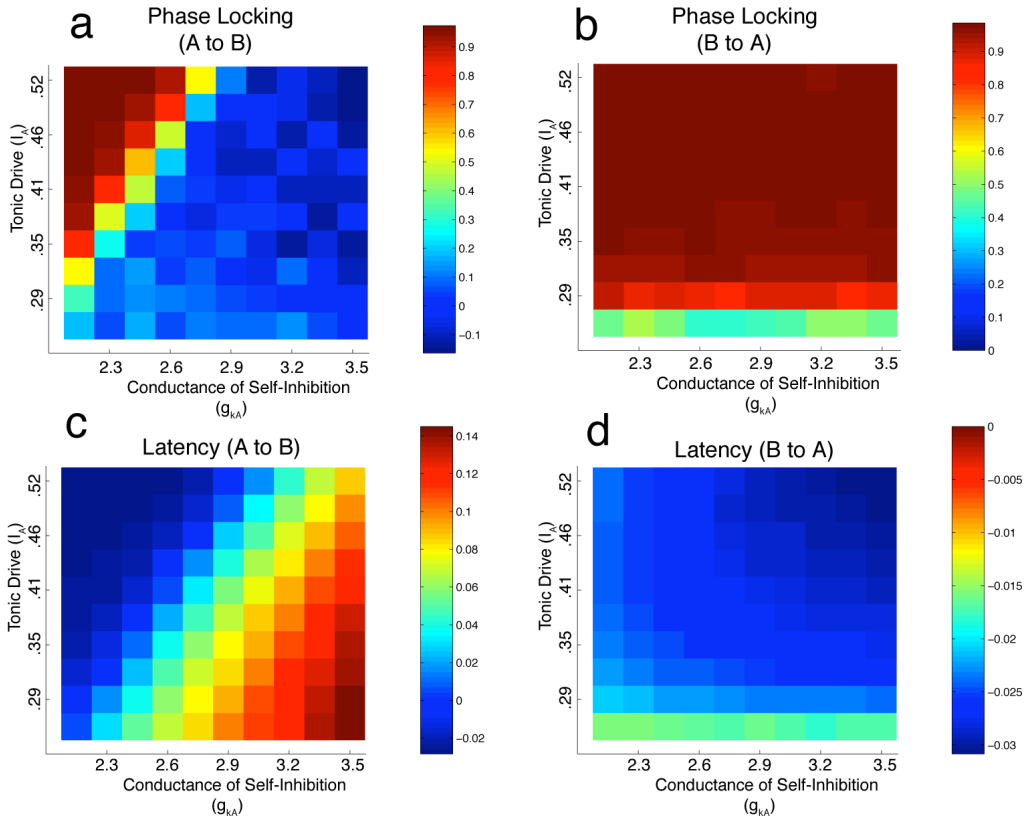

Fig. 4.7, Interaction of Tonic Drive and Self-Inhibition Morris-Lecar Half-Center. 7a Changes in tonic drive (I_A) has the same relationship with self-inhibition (g_{kA}) as does self-excitation at the A to B transition (Fig. 6a). 7b Since increasing tonic drive effects both transitions equally the B to A transition is more well phase locked than observed changing self-excitiation. 7c-d Latencies at the B to A transition are more invariant than observed in changing self-excitation.

transition are nearly identical to those observed in the relationship between self-excitation and self-inhibition above (Fig. 7a and c). However there appears to be less variation in latency and phase locking at the B to A transition (Fig. 7b and d).

Symmetric Parameter Changes in Asymmetric Networks

From the previous sets of simulations we hypothesized that the relationship between latencies and strength of phase locking might be somewhat malleable. To determine if this was the case, we altered strength of mutual inhibition between the

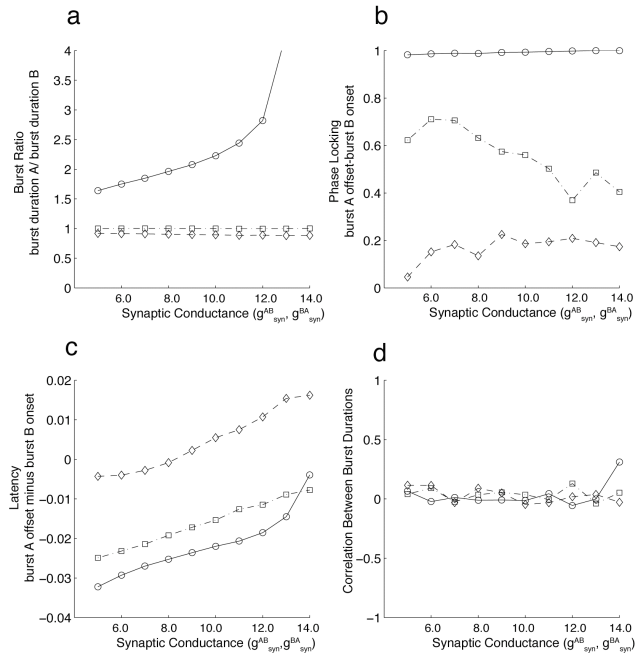

Fig. 4.8, Influence of Synaptic Strength. Morris-Lecar Half-Center. 8a. Increasing synaptic conductance (g^{AB}_{syn}, g^{BA}_{syn}) increases burst duration in neuron A when neuron A has high levels of self-excitation (g_{eA}=1.7, circles with solid line), but has no effect when self excitation is symmetric (g_{eA}=g_{eB}=1.1, squares with dot-dash line), or when self excitation is weak (g_{eA}=1.0, diamond with dashed line). 8b. Changes in synaptic strength do not change strength of phase-locking when g_{eA} is high, but weakens phase locking in the symmetric case. 8c, Increasing synaptic strength has a strong influence on latency in the symmetric case, however also of interest is that latencies can shift slightly when strength of phase locking is saturated. 8d. Burst correlations remain invariant during changes in synaptic strength.

simulated neurons (on both sides A to B and B to A) under three conditions, the model was asymmetric with one neuron having strong self-excitation (g_{eA}=1.7), a symmetric model at the default parameters (g_{eA}=g_{eB}=1.1), and an asymmetric model where strength of self-excitation in neuon A was weaker than neuron B.

Interestingly even though modulation of mutual inhibition was equal for both sets of synapses, burst duration of the neuron with more self-excitation was increased dramatically (Fig. 8a).

Modulation of synaptic strength had very little effect on the strength of phase locking when the network was already in a state where phase locking was either very strong, or very weak (Fig. 8b). However when phase locking was of medium strength increasing mutual inhibition

tended to increase the latency (Fig. 8c), and decrease the strength of phase locking (Fig. 8b). Additionally, when neuron A had more self-excitation, strength of phase locking was high and invariant, but changes in strength of mutual inhibition still engendered small changes in the latencies between bursts (Fig. 8c).

Discussion

Here we have shown that half-centers composed of a pair of leaky integrator neurons have strong invariant phase locking at the transitions between bursts. Pairs of intrinsically oscillatory Morris-Lecar type neurons exhibit strength of phase locking at the transitions that are parameter dependent. Sets of parameters where burst termination is caused by onset within the opposing neuron have transitions between bursts which overlap and which are strongly phase locked, while those having burst terminations which are caused by self-inhibition tend to have transitions between bursts which do not overlap and are weakly phase locked.

Previously we hypothesized that changes in strength of phase locking observed within the output of fictive locomotion were likely due to differences in the internal dynamics of the flexor and extensor oscillators (Boothe, et. al. Chapter 3). Here we assess this hypothesis with concrete examples describing what sorts of differences one might expect between the flexor and extensor oscillators making up the sCPG for locomotion within the context of the current models.

Summary of Experimental Observations

Previously we have reported that strength of phase locking between burst offset and burst onset within the output of MLR induced fictive locomotion is strongly asymmetric. Phase locking at the transition from extension to flexion (E to F) is: 1, Always strong; 2, Associated with periods of overlap between bursts (i.e. negative latencies); and 3, Latencies do not vary across experiments containing short or long cycle periods (Boothe, et. al. Chapter 3). Phase locking at the transition from flexion to extension (F to E) is: 1, Weak in bouts containing short cycle periods but strong in bouts containing long cycle periods; 2, Latencies between bursts offset and onset which are both positive and long are weakly phase locked while shorter latencies are strongly phase locked; and 3, Cycle period and latencies are negatively correlated. We will discuss each of these in the context of assessing model adequacy below.

Given the fact that all parameters tested here within the leaky integrator half center have transitions which are strongly phase locked, we do not believe it is possible to successfully model previously observed experimental statistics using a model of this type.

Asymmetries in Strength of Phase Locking

The two overarching qualities that any model purporting to explain asymmetries in the output of fictive locomotion must have are: bursts which are asymmetric in length, combined with invariant phase locking between burst offsets and onsets at one transition and variable phase locking at the opposing transition. These overall changes should be weakly associated with changes in overall cycle period.

Models reported here behave similarly through the introduction of substantial asymmetries within neurons making up the half-center. To meet the above criterion neurons, however must have differences in at least two parameters, one of which must be an excitatory influence (either self or tonic) combined with changes in self-inhibition. Changing a symmetric half-center through modulation of a single parameter fails to qualitatively simulate the output of the biological system.

Increasing or decreasing the strength of self-inhibition alone asymmetrically modulates strength of phase locking at the transitions, with the previous transition being weakly effected by these changes, and the following transition being strongly effected (Fig. 3b). However, the same changes which create strong phase locking at the following transition also tend to shorten the current burst duration (Fig. 3a), making it unlikely that changes in self-inhibition alone are responsible for the combination of long burst durations having a weakly phase locked transition at offset observed in the output of the biological system (Boothe, et. al. Chapter 3).

Modulating excitatory currents alone is also inadequate. Networks containing one neuron having stronger excitatory currents (either self or tonic), tend to have strongly asymmetric burst durations like those observed within fictive locomotion (Figs. 4-5a). However these same increases in burst duration tend to cause increases in phase locking at both the leading and following transitions simultaneously (Figs. 4-5b).

Asymmetries within two parameters are sufficient to produce asymmetric burst durations combined with offset of the longer burst having variable strength of phase-locking with onset in the opposing burst. Possible parameter regimes are: 1, one neuron has high excitation and then self-inhibition is changing, 2, one neuron has strong self-

inhibition and excitiation is changing, or 3, both self excitiation and self-inhibition are changing (Figs. 6-7).

Latencies and Phase Locking

Within the output of the Morris-Lecar half-center strength of phase locking is largely dependent upon relative timing between burst offset and burst onset. Large positive latencies are associated with weak phase locking, while latencies which are negative or positive and near zero are strong. This strong relationship implies that many functional properties of the models are parameter independent. I.e. any set of parameters which effects the latencies will also effect the strength of phase locking at the transitions. This is illustrated by the strong similarity in the relationship of both types of excitation (tonic or self) and strength of self-inhibition (Fig. 6 and Fig. 7).

While the strength of phase locking depends critically upon the latency, this relationship is weakly influenced by the strength of mutual inhibition (Fig. 8). When the network is in a state of maximal correlation there is still some compression of the latency that is insufficient to increase phase locking past its current maximal state.

Within the biological system, the strongest indicator of strength of phase locking was latency duration (Boothe, et. al. Chapter 3). However, the biological system had two interesting properties that were difficult to explain in terms of differences in internal state of oscillators making up the sCPG, 1, The strong relationship between latency and phase locking was stronger for the positive latencies observed at the F to E transition than it was at the negative latencies observed at the E to F transition; and 2, There was a relationship between cycle period and latencies at the F to E transition, but not at the E to F transition.

One property the models possess that could help explain these observations is the continuing malleability of latency under conditions of very strong phase locking (Fig. 8). Once the latencies become sufficiently small they are resistant to compression, and are no longer associated with increased phase locking. However, when the latencies are positive the same changes that extend the cycle, i.e. lengthening of the burst durations, tend to also compress the positive latencies since there is still 'room' between the bursts.

Source of Variance in the Biological System

The current set of models points to underlying differences in internal state between intrinsically oscillating flexor and extensor units organized in a half-center as the likely source of variation observed across bouts of fictive locomotion (Boothe, et. al. Chapter 3). Specifically it is likely that the flexor oscillator has stronger levels of both excitation and self-inhibition, when compared to the extensor oscillator. Since correlation at the F to E transition changes across bouts, it is likely that the relative balance of these excitatory and inhibitory currents is also changing.

Given what is known about the functioning of the biological system, we believe that it is likely that there is an underlying asymmetry within strength of self-inhibition across the flexor and extensor oscillators with flexors having strong self-inhibition and extensors having weak self-inhibition. Changes in phase locking and increasing burst durations could then be explained in terms of different levels of tonic drive across bouts. In short cycle bouts tonic drive to the flexors, while being higher than the extensors would not be sufficiently strong to swamp the higher levels of self-inhibition in the flexor oscillator and create an F to E transition that is strongly phase locked (Fig. 7). However

the difference in levels of tonic drive would be sufficient to make the flexor burst longer than the extensor burst (Fig. 7). Bouts exhibiting longer cycle periods would contain flexor oscillators receiving increased levels of tonic drive (increases in tonic drive also increase cycle period (Fig. 6b). This increased level of tonic drive would have the additional effect of strengthening correlations at the F to E transition. This could potentially all take place in the absence of changes to the strength of phase locking at the E to F transition (Fig. 7b)

MLR induced fictive locomotion isn't always flexor dominated (i.e. flexors are on for more than 50% of the cycle), it is occasionally extensor dominated (Yakovenko, 2005). If the source of asymmetry in the network is self-excitation then levels of self-excitation would vary widely across bouts, i.e. sometimes the flexor oscillator has more self-excitation and sometimes the extensor oscillator has more. On this explanation the internal state of the sCPG would be need to be highly plastic.

Changes in tonic drive on the other hand are thought to derive from supra-spinal sources, so ultimately on this hypothesis the spinal cord itself could be relatively unchanging across bouts but how it is being activated by supraspinal networks would vary.

On our hypothesis where the spinal cord itself is asymmetric is in the levels of self-inhibition within the flexor and extensor oscillators. We find this especially plausible when one considers that within normal locomotion the flexor phase is substantially shorter than the extensor phase. Our current hypothesis can account for this by assuming that in normal locomotion the tonic drive to each oscillator is symmetric. Under such conditions the extensor oscillator would have bursts (owing to weak self-

inhibition) which are substantially longer than the flexor burst (having strong self-inhibition).

Conclusion

Given the complicated nature of the vertebrate nervous system, clearly models like those presented here are unlikely to be literally true. However, they do aid in sharpening intuitions about what sorts of explanations are plausible and which are not. Models presented here can serve as a usefull starting point for modeling more complicated behaviors. For instance if sets of half-centers like those described here are organized in a hierachal fashion as has been suggested by Grillner (1981) and recently by Rybak (2006) how do the statistics of the output of the networks change. This question should keep those interested in modeling the sCPG buys for quite some time.

CHAPTER FIVE: SUMMARY AND CONCLUSIONS

The current work advances our understanding of both simulated and biological central pattern generators. Novelty in this dissertation includes: 1, Development of model systems with behaviors which are both complex and biologically relevant; 2, A detailed statistical study of the biological sCPG. This analysis has generated a set of plausible hypotheses regarding sCPG structure and function; and 3, The development of statistical tools which can be used to measure natural variability within both simulated and real biological systems.

Within the main body of the chapter below, I will first address the general finding explored in Chapter 3 regarding observed differences in transitions between flexion and extension and vice-versa. First I will focus on analyses similar to those performed in Chapter 3 within the mammalian sCPG literature. I will then discuss sensory control of phase transitions (flexion to extension and vice versa) in the intact/semi-reduced cat. Finally I will discuss a recent paper that when interpreted in the light of our evidence from Chapter 3, strongly implies the existence of multiple oscillators in the structure of the sCPG in mammals.

Comparing Across Preparations

The nearest point of contact for the statistical description of MLR induced fictive locomotion presented in Chapter 3, is a series of papers published by Grillner and Zangger from 1979 to 1984. Grillner and Zangger (1979, 1984) present an overview of the output of the reduced spinal cord, and use a methodology similar to that presented in Chapter 3. However there are significant qualitative differences in the output of the

preparation used by Grillner and Zangger (1979, 1984) and the MLR preparation presented in Chapter 3. A discussion of these differences is presented below focusing on the work of Engberg and Lundberg,(1969) and Forssberg et. al. (1980a-b).

Kinematically Defined Phases within the Locomotor Cycle

The first studies of cat locomotion characterized the basic pattern of EMGs for both intact and chronic spinal cats (Engberg and Lundberg 1969). Within intact cat the locomotor cycle can be divided into four kinematically defined phases: Flexion (F) and Extension I (E1) during the swing phase, and Extension II and III (E2-3) during the stance phase. Flexion (F) occurs when the limb is lifted off the ground and actively moved forward (Forssberg et. al. 1980a-b). The end of the swing phase begins with activation of the extensors (E1). E1 serves to move the limb towards ground contact while the limb is still off of the ground. E1 is associated with activation of both ankle (including LGS, and MG in Chapter 3) and hip extensors (SmAB). The beginning of the stance phase of locomotion (E2) is associated with ground contact. E2 is characterized by a short period of coactivation between flexors and extensors to support the weight of the body. This is called the yield. Once ground contact occurs (E3) force is then applied to the substrate pushing the animal forward. This period of ground contact combined with the animal moving forward is final phase of stance, termed E3. In intact/spinal locomotion the extensors (SmAB, LGS, MG) are active throughout E1, E2 and E3 (Forssberg, et. al. 1980a-b). Activity within the extensors is terminated at the onset of the next flexion phase, and the entire cycle begins all over again. These findings are identical to those reported for extensors in Chapter 3.

Differences in Relative Timing Between Intact and MLR Fictive Locomotion

Interestingly, while activity within the extensor nerves during MLR induced fictive locomotion, is identical to that reported in intact (Engberg and Lundberg 1969, Krouchev et. al. 2006) and stepping chronic spinal cats (Forssberg, 1980a-b), timing of flexor bursts exhibits striking differences. In the stepping chronic spinal cat, tibialis anterior (TA) bursts run into E1 and have a short period of overlap with the onset of the extensor bursts (SmAB, LGS, and MG, ENGs) (Forssberg, et. al. 1980a-b). Within intact locomotion TA burst offset occurs prior to/and or simultaneous with the onset of extensors in the middle of E1 (SmAB, LGS, and MG) (Forssberg, et. al. 1980a-b, Krouchev et. al. 2006, Quevedo et. al. 2005a). Within the output MLR induced fictive locomotion reported in Chapter 3, TA burst offset is identical to that observed during normal locomotion (i.e. TA offsets prior to extensor onsets, Fig. 6, Chapter 3).

Additional differences occur across preparations within the relative timing of both the hip flexor sartorious (Sart), and the ankle/toe flexor extensor digitorum longus (EDL). During both intact and spinal locomotion burst offset of both Sart and EDL occur shortly after the transition to E3 (Forssberg et. al. 1980a-b, Krouchev, 2006). If MLR induced fictive locomotion is similar to intact/spinal locomotion then one expects for Sart and EDL offset to overlap with the onset of extensors creating a long period of negative 'latency' or 'gaps'. However our observations of MLR induced fictive locomotion indicate that the Sart burst offset is associated with a short silent period before the extensor burst onset. This silent period is observed as a positive latency in Fig. 6, Chapter 3. So within MLR induced fictive locomotion the phase of Sart offset has a

different functional relationship with the onset of extensors than observed in normal locomotion.

While Sart bursts become cotemporaneous with TA bursts during MLR induced fictive locomotion, EDL retains some of the differences in relative timing observed during intact locomotion. Specifically EDL exhibits a short period of overlap with the onset of extensors at the F to E transition (negative latencies, Chapter 3, Figure 6). So, while the phase of offset of both EDL and Sart shift within MLR fictive locomotion to become more similar to that observed in TA, EDL retains some timing aspects from normal locomotion.

In summary, significant differences across preparations occur mainly in regards to the timing of the offset of flexion and the onset of extension (i.e. the F to E transition). Both phase of offset and the relationship of flexor offsets with extensor onsets differ for flexors across all three reported preparations. The opposing transition from extension to flexion appears to remain fairly stable across multiple experimental conditions.

Statistics of Fictive Locomotion in the Low Spinal Cat

Grillner and Zangger (1979) describe the output of the reduced spinal cord using the following procedures: 1, The spinal cord was transected between L3-L6. 2, All dorsal roots below L2 were cut. 3, Spinal cords were treated with DOPA and Nialamide to make them easier to activate. 4, Stimulation was applied to the cut dorsal roots at 30-50 hz in .2 ms pulses. Two sorts of behaviors were then recorded, 1, stepping output of the cord as EMGs, and 2, Ventral root electroneurograms while the animals limbs were paralyzed with both curare and Flaxedil.

Pertinent results are 1, The variance of the extensor bursts are more strongly correlated with the variance of the cycle than the extensors are, and 2, Burst midpoints of two flexors and one extensor have phase relationships that are consistent and similar to those in intact animals.

Interestingly, Grillner and Zangger (1979) used a measure of latencies, which is very similar to that used in Chapters 3 and 4. Cycle duration was taken as the midpoint of TA burst to the midpoint of the next TA burst. Burst midpoints were normalized relative to that definition of the cycle. The authors then reported the differences in phase within their normalized cycle between the midpoints of the flexors TA and tenunisimus. The authors observed that flexors were 'tightly' phase locked since the standard deviations of the normalized phase were small. A similar result regarding the output of MLR fictive locomotion was observed in the 'strong' phase locking between flexor burst onset and offset times (Fig. 4, Chapter 3). Prima facie the Grillner and Zangger (1979) results seems to imply strong correlation between flexor burst durations, however if burst durations and relative timing of the bursts within the cycle are controlled by separate neuronal mechanisms then midpoints of the bursts could be tightly phase locked while burst durations themselves would be uncorrelated.

Grillner and Zangger (1979) also reported the 'tightness' of phase locking between the midpoint of a flexor burst (TA) and the midpoint of the following extensor burst (LG). Phase locking between flexor and extensor bursts was found to be 'looser' than that observed between flexors. 'Loose' phase locking between flexor burst midpoints and extensor burst midpoints could be caused by a highly variable transition from F to E (Chapter 3), such as that observed in Chapter 3. If the transitions between

phases in low spinal fictive locomotion are produced by the same functional mechanisms as those observed within MLR induced fictive locomotion, then one would predict that the 'tightness' of phase locking would depend on the order in which two bursts are being compared. When one compares the midpoint of LG with the midpoint of the following TA burst, one would expect for there to be 'tight' phase locking since now the phase locking is dominated by the E to F transition.

Statistics of MLR Induced Locomotion During Treadmill Walking

A second paper by Grillner and Zangger (1984) used a preparation in which locomotion was induced via stimulation of the MLR in a decerebrate animal. EMGs were then recorded while the cat was walking on a treadmill. The effects of later deafferentation on the qualitative structure of EMGs were also reported.

The authors (Grillner and Zangger, 1984) report that the timing of the output of MLR induced treadmill locomotion is qualitatively similar to that observed within intact locomotion. However some of the figures within the text clearly show that some of the cycles are 'flexor' dominated like those reported in Chapter 3 and in Quevedo, 2005a.

Using a technique similar to that employed in Chapter 3, the Grillner and Zangger (1984) compared raw latencies between extensor and flexor offsets and onsets for the ankle flexor tibialis anterior (TA), and the ankle extensor lateral gastrocnemius (LG). One important difference between these EMGs and the ENGs reported in Chapter 3 is that the nerve (LGS) also innervates the synergistic soleus muscle as well as the lateral gastrocnemius.

Latencies observed differ from those reported in Chapter 3, in that the overall variance and latency of the E to F transition is larger than that of the F to E transition. Additionally, the latency between TA to LGS at the F to E transition is sometimes negative. However since there is no direct report of the std's of the latencies and/or 'strength' of phase locking of TA and LGS offset/onset it is impossible to know how similar/dissimilar the two results actually are. Specifically since error bars on the Grillner figures are a measure of standard error, one cannot discern whether or not they are most strongly influenced by the number or cycles being compared or the variance of the latencies.

Some likely possibilities for the divergent observations include: First, there are likely strong influences on the relative timing of the nerves derived from the prep and experimental conditions themselves. Although both sets of data (Grillner and Zangger, 1984, and Chapter 3) use MLR stimulation to induce locomotion, one data set is derived from EMGs and one from ENGs which themselves may contribute small differences in relative timing. Difficulty in comparing results directly is compounded by the author's combining both flexor and extensor dominated experimental outputs into one data set. Potentially with all extensor dominated locomotor outputs removed the output of MLR induced treadmill walking could be identical to that observed in the fictive preparation and reported in Chapter 3.

Sensory Inputs Regulating Phase Transitions

As described above walking consists of two main phases: swing which is associated with activity in flexor muscles and stance which is associated with activation

of extensors. The influence of sensory inputs upon these two transitions has been well studied (Rossignol, et. al. 2006). First I will discuss the influence sensory inputs on the termination of extension and the onset of flexion, and then the opposing flexion to extension transition.

As walking animals change speed extensor burst duration is lengthened and shortened (Whelan, 1996). Multiple sensory inputs have been implicated in the transition from stance to swing including: Unloading of the extensor muscles through activation of Ib golgi tendon organs (Duysens, 1980); Protraction of the limb creating hip joint angles past 95^{o} (Grillner and Rossignol, 1978); Vibration of the extensors activating group Ia afferents can cause elongation of the extensor burst (Whelan, et. al. 1995); In a similar manner stretch of ipsilateral flexor muscles both shortens the extensor bursts as well as initiates activity within the flexors (Hiebert et. al. 1996).

Sensory regulation of the opposing transition from swing to stance has only recently been explored in detail (Rossignol, et. al. 2006). In walking decerebrate cats enhancing protraction of the limb during the swing phase of locomotion shortens hip flexor burst length (Lam and Pearson, 2001). Slowing/impeding protraction of the limb during the swing phase enhances hip flexor burst duration (Lam and Pearson, 2001). Recently there is evidence that these same perturbations advance the onset of extension (McVea, et. al. 2005). Oddly, though the authors compare the off times between extensor bursts from one cycle to the next with the burst durations of the flexors. They then compare the two measures (off times between extensor bursts and flexor burst durations) using a linear regression. However they seem unaware that this statistic has a confound in that 1, The flexor burst duration contributes to both, and 2, While the slopes of their

linear regressions are statistically significant (r^2=.804, and .829) these are not the same as showing that the slope of the reported regression lines are significantly different than the expected slope of 1. A better measurement would have been to show that mean 'gap' duration shrinks relative to a normalized cycle for the perturbed and unperturbed cycles.

In conclusion, while much is known about how sensory inputs effects both burst durations and overall timing of the transition from flexion to extension and vice versa, no studies have reported how unitary or fragmented these perturbation induced transitions are for synergistic muscles. Non-synergistic muscles such as PBSt and the flexor nerves reported here (Sart, TA, EDL, PerL) are known to be differentially activated during both the stumble corrective response (Forssberg, 1980a-b, Quevedo, et. al. 2005a), and due to other forms of sensory input (Rossignol, 2006).

Interpreting Differences in Phase Locking at the Transitions

So in the end what does our finding that the transition from extension to flexion is more strongly phase locked really mean for the background literature regarding the influence of sensory inputs on the relative timing of transitions between flexion and extension?,

One possibility is that there is a natural step cycle imbedded within the output of MLR induced locomotion beginning and ending at a specific phase of the step cycle. The natural onset point for such a cycle would be the strongly phase locked E to F transition. Once the cycle is started, the relative timing of other events in the cycle form part of a stereotyped motor plan. As this 'plan' unfolds noise begins to make the relative timing of

burst onset/offset 'looser'. One such event is the transition from flexion to extension, the phase locking between which is now weak.

Evidence against the existence of such an imbedded cycle is two-fold: First, If there is such a natural cycle embedded in the structure of the sCPG then one would expect for resetting of the step cycle to occur preferentially at either the transition from flexion to extension or extension to flexion. However, peripheral perturbations of sensory afferents are equally capable of resetting the step cycle to either the onset of flexion or extension (Rossignol, et. al. 2006). Secondly, if there is some set of neurons within the sCPG clocking the cycle duration, then one would expect for the cycles where one of the burst durations (a flexor for instance) is a little bit longer, to be associated with shortening of the following burst (in the extensors). This push-pull relationship would lead to negative correlations between flexor and extensor burst durations. However in the output of the MLR prep, the burst durations of flexors and extensors are not consistently positively or negatively correlated with one another. Both of the above arguments seem to rule out the existence of a natural step cycle explaining differences in strength of phase locking at the transitions.

A second plausible explanation is that while sensory input to the spinal cord contributes to the timing of the transitions between flexion and extension, it does not influence the phase locking of these transitions. The transitions consist of a stereotyped set of sequential offsets and offsets that are hard wired into the sCPG. On this hypothesis one would expect for the 'strength' of phase locking to be identical in both normal and MLR induced fictive locomotion. Furthermore, he lack of sensory input in the case of MLR induced fictive locomotion is therefore causing the relative lengths of the bursts to

be pathological. This has the effect of moving from extensor dominated normal locomotion to the flexor dominated pattern seen during MLR induced fictive locomotion. This story is complicated by the fact that the relative timing of flexor offset (see comparison of offset times of TA, EDL and Sart above) changes drastically between normal and MLR induced ficitive locomotion.

A third possibility is that the phase locking itself is changing between normal and MLR induced fictive locomotion. On this hypothesis sensory inputs during normal locomotion would create strongly phase locked transitions between flexion and extension. One would then interpret strong phase locking in MLR induced fictive locomotion as an indicator that that transition is 'hardwired' into the structure of the sCPG. Weak phase locking would then be evidence that that transition relies on sensory input within the intact animal. Part of this interpretation suggests that in the case of normal locomotion the strength of phase locking would be itself a product of online response to sensory inputs on a very fine time scale.

In the end interpretation of the observed differences in strength of phase locking between the E to F and F to E transition seen in MLR induced fictive locomotion depend on the strength of phase locking within the intact system. Since this is an empirical question that is itself unresolved within the literature, any conclusions made in Chapter 3 are at best speculative. However the results of Chapter 3 do bring up interesting questions regarding the influence and timing of sensory input upon motor outputs. If sensory inputs modify the 'when' but not the 'how' of the transitions between flexion and extension as one would conclude if the strength of phase locking during intact locomotion was identical with that observed in MLR induced fictive locomotion, it is

likely that these transitions are created by a feed forward motor plan. One would then argue that sensory inputs are not themselves regulating and contributing to many aspects of the fine grained timing of motor output. On the other hand if both the strength of phase locking and the relative timing of events are different within normal locomotion then one would conclude that during normal locomotion sensory inputs are really updating and filtering the output of the sCPG on a very fine time scale.

Burst Durations and the Multiple Oscillators

A recent paper from the lab of Trevor Drew (Krouchev et. al. 2006) combined with our results from Chapter 3, could be interpreted as evidence for multiple oscillators in the structure of the sCPG for locomotion. Krouchev et. al. (2006) reports a cluster analysis performed on the timing of cat hindlimb EMGs during intact treadmill walking. He finds that TA is likely controlled by a separate synergy from Sart and EDL, which are controlled by the same underlying network. Interestingly synergistic muscles (as defined by the cluster analysis) are those that have strong similarities in the timing of onset and offset normalized to the cycle duration. If one were to interpret evidence for muscles being synergistic as possible candidates for multiple muscles being controlled by separate unit pattern generators (like those described by Grillner, 1981), then there is good evidence that TA and Sart/EDL are independently controlled within normal locomotion.

Within MLR induced fictive locomotion TA, Sart and EDL all share very similar timing. If one were to apply a similar cluster analysis to the output of MLR induced fictive locomotion one might or might not pick up that EDL offset occurs a fraction of the cycle later on average than TA and Sart, and therefore is controlled as part of a separate

synergy. Within Chapter 3 we have shown that while TA, Sart, and EDL share some timing relationships (positively correlated burst durations, and onset/offset times), that EDL has a qualitatively different relationship with the extensors. In Chapter 3 we argue that EDL is controlled by a separate oscillator from those controlling the other flexors.

Combining the evidence from the MLR and normal locomotion argues for a sCPG for locomotion that is highly flexible and dynamic. Relationships between individual nerves/muscles are highly variable. Under conditions of normal locomotion TA is independent of EDL and Sart, and during MLR induced fictive locomotion EDL is independent from TA and Sart. Two of the three nerves therefore are independent under different conditions and one (Sart) switches its synergy depending upon the preparation. Taken together, the most parsimonious interpretation of both sets of data is that each muscle is controlled by its own independent oscillator. What is changing on this interpretation is the relationships between these independent oscillators. Changes like those observed across normal and MLR induced fictive locomotion are most easily explainable in terms of the strength of the coupling between these independent oscillators.

Concluding Remarks

The major difficulty in drawing further conclusions regarding the results of Chapter 3, is the unknown nature of strength of phase locking within normal locomotion. Without such a benchmark to compare with the statisitics of MLR fictive locomotion it is impossible to concretely assess the structure/function relationships within the sCPG.

Understanding the same relationships within normal locomotion should differentiate the relative contributions of the sCPG and sensory input in creating locomotion.

BIBLIOGRAPHY

Bayev KV (1978) Central locomotor program for the cat's hindlimb. Neuroscience 3:1081-1092

Bem T, Cabelguen JM, Ekeberg O, and Grillner S (2003) From swimming to walking: a single basic network for two different behaviors. Biol Cybern 88(2):79-90

Boothe DL, Cohen AH (2001) Testing a set of neural network models for cat locomotion with electroneurograms. Soc Neurosci Abst 26: 730 29 (2001)

Boothe DL, Cohen AH (2002) A model of limbed locomotion for a four muscle system. Neurocomputing 44-46: 743-752

Boothe DL, Cohen AH, Troyer TW (2006) Temporal correlations in a stochastic model of bouble bursting. J Neurophysiol 95: 1556-1570

Bretzner F, Drew T (2005) Contribution of the motor cortex to the structure and timing of hindlimb locomotion in the cat: a microstimulation study. J Neurophysiol 94: 657-672

Buchanan JT (1992) Neural network simulations of coupled locomotor oscillators in the lamprey spinal cord. Biol Cybern 66: 367-374

Burke RE (1999) The use of state-dependent modulation of spinal reflexes as a tool to investigate the organization of spinal interneurons. Exp Brain Res 128: 263-277

Burke R, Degtyarenko M, and Simon E (2001) Patterns of locomotor drive to motoneurons and last order interneurons: clues to the structure of the CPG. J Neurophysiol 86:447-462

Brown TG (1911) The intrinsic factors in the act of progression in the mammal. Proc Roy Soc Lond B Biol Sci 84: 308-319

Cohen AH, Boothe DL (2002) Sensorimotor interactions: Principles derived from central pattern generators. In: Handbook of Brain Theory and Neural Networks, MIT press (Boston)

Drew T, Prentice SD, and Schepens B (2004) Cortical and brainstem control of locomotion. Prog Brain Res 143: 239-49

Duysens J, (1977) Reflex control of locomotion as revealed by stimulation of cutaneous afferents in spontaneously walking premammilary cats. J Neurophysiol 40: 737-751

Duysens J, Pearson KG (1980) Inhibition of flexor burst generation by loading ankle extensor muscles in walking cats. Brain Res 187:321-332

Duysens J, Stein RB (1978) Reflexes induced by nerve stimulation in walking cats with implanted nerve cuff electrodes. Exp Brain Res 32: 213-224

Edgley SA, Jankowska E (1987) An interneuronal relay for group I and II muscle afferents in the midlumbar segments of the cat spinal cord. J Physiol (Lond) 389: 647-674

Eide AL, Glover J, Kjaerulff O, Kiehn O (1999) Characterization of commissural interneurons in the lumbar region of the neonatal rat spinal cord. J Comp Neurol 403: 332-345

Engberg I, Lundberg A (1969) An electromyographic analysis of muscular activity in the hindlimb of the cat during unrestrained locomotion. 75:614-630

Forssberg H (1979) Stumbling corrective reaction: a phase dependent compensatory reaction during locomotion. J Neurophysiol 42: 936-953

Forssberg H, Grillner S, Halberstama J (1980a) The locomotion of the low spinal cat I. Coordination within a hindlimb. Acta Physiol Scand 108:269-281

Forssberg H, Grillner S, Halberstama J (1980b) The locomotion of the low spinal catII. Interlimb coordination. Acta Physiol Scand 108:283-295

Golubitsky M, Stewart I, Buono P, Collins J (1999) Symmetry in locomotor central pattern generators and animal gaits. Nature 401:693-695

Grillner S (1975) Locomotion in vertebrates: Central Mechanisms and reflex interaction. Physio Rev 55: 247-304

Grillner S (1979) On the central generation of locomotion in the low spinal cat Exp Brain Res 34: 241-261

Grillner S (1981) Control of locomotion in bipeds tetrapods and fish. Handbook of Physiology- The Nervous system II pgs 1179-1227

Grillner S (1999) Bridging the gap- from ion channels to networks and behaviour. Curr Opin Neuro 9: 663-669

Grillner S, Rossignol S (1978) On the initiation of the swing phase of locomotion in chronic spinal cats. Brain Res 146:269-277

Grillner S, Zangger P (1979) On the central generation of locomotion in the low spinal cat. Exp Brain Res 34:241-261

Grillner S, Zangger P (1984) The effect of dorsal root transection on the efferent motor pattern in the cat's hindlimb during locomotion. Acta Physiol Scnad 120:393-405

Hamm TM, Trank TV, Turkin VV (1999) Correlations between neurograms and locomotor drive potentials in motoneurons during fictive locomotion: implications for the organization of motor commands. Prog Brain Res 123: 331-339

Hiebert GW, Whelan PJ, Prochazka A, Pearson K G (1996) Contribution of the hind limb flexor muscle afferents to the timing of phase transitions in the cat step cycle. J Neurophys 3:1126-1137

Huang A, Noga B, Carr P, Fediruchuk B, Jordan L (2000) Spinal cholinergic neurons activated during locomotion: localization and electrophysiological characterization J Neurophys 83: 3537-3547

Izhikevich EM (2001) Synchroniztion of elliptic bursters. SIAM Review 43(2): 315-344

Jung R, Kiemel T, and Cohen AH (1996) Dynamic behavior of a neural network model of locomotor control in the lamprey J Neurophys 75: 1074-1086

Kiehn O, Johnson BR , Raastad M (1996) Plateau properties in mammalian spinal interneurons during transmitter induced locomotor activity Neuroscience 73(1): 263-273

Kiemel T, Gormley KM, Guan L, Williams TL, Cohen AH (2003) Estimating the strength and direction of functional coupling in the lamprey spinal cord. J Comput Neurosci 15(2): 233-45

Kiemel T, and Cohen AH (1998) Estimation of coupling strength in regenerated lamprey spinal cords based on a stochastic phase model. J Comp Neurosci 5: 267-284

Krawitz S, Fedirchuk B, Dai Y, Jordan LM, McCrea DA (2001) State-dependent hyperpolarization of voltage threshold enhances motoneurone excitability during fictive locomotion in the cat. J Physiol 532: 271-281

Krouchev N, Kalaska JF, Drew, T (2006) Sequential activation of muscle synergies during locomotion in the intact cat as revealed by cluster analysis and direct decomposition. J Neurphysiol 96:1991-2010

Lafreniere-Roula M, McCrea DA (2005) Deletions of rhythmic motoneuron activity during fictive locomotion and scratch provide clues to the organization of the mammalian central pattern generator. J Neurophysiol 86: 1321-1332

Lam T, Pearson KG (2001) Proprioceptive modulation of hip flexor activity during the swing phase of locomotion in the decerebrate cat. J Neurophysiol 86:1321-1332

Lundberg A (1969) Reflex control of stepping. The Nansen Memorial Lecture V 5-42 Universitetetsforlaget: Oslo

Marder E (2000) Motor pattern generation. Curr Opin Neuro 10:691-698

McVea DA, Donelan J, Tachibana A, Pearson KG (2005) A role for hip position in initiating the swing to stance transition in walking cats. J Neurophysiol 94:3497-3508

Mellon N, Kiemel T, Cohen AH (1995) Correlational analysis of fictive swimming in the lamprey reveals strong functional intersegmental coupling. J Neurophysiol 73: 1020-1030

Morris C, Lecar H (1981) Voltage oscillations in the barnacle giant muscle fiber. J Biophys 35(1): 193-213

Oksendal B (2000) Stochastic Differential Equations Springer-Verlag (Berlin, Heidelberg) 5th edition

Orlovskii G, Feldman D (1973) Classification of lumbarsacral neurons by their discharge pattern during evoked locomotion. Neirofiziologiya 4:410-417

Pribe C, Grossberg S, Cohen MA (1997) Neural control of interlimb oscillations II Biped and quadraped gaits and bifurcations. Biol Cybern 77: 141-152

Quevedo J, Stecina K, Gosgnach S, McCrea DA (2005a) Stumbling corrective reaction during fictive locomotion in the cat. J Neurophysiol 94: 2045-2052

Quevedo J, Stecina K, McCrea DA (2005b) Intracellular analysis of the stumbling corrective reaction during fictive locomotion in the cat. J Neurophysiol 94: 2053-2062

Rinzel J, Ermentrout GB (1989) Analysis of neural excitability and oscillations. In: Methods in Neuronal Modeling Boston MA: MIT Press 135-171

Rossignol S, Drew T (1988) Phasic modulation of reflexes during rhymic activity. In: Neurobiology of Vertebrate Locomotion London: Macmillan 517-534

Rossignol S, Dubuc R, Gossard JP (2006) Dynamic sensorimotor interactions in locomotion. Physiol Rev 86: 89-154

Rybak IA, Shevtsova NA, Lafreniere-Roula M, McCrea DA (2006a) Modelling spinal circuitry involved in locomotor pattern generation: insights from deletions during fictive locomotion J Physiol 577: 617-39

Rybak IA, Stecina K, Shevtsova NA, McCrea DA (2006b) Modelling spinal circuitry involved in locomotor pattern generation: insights from the effects of afferent stimulation. J Physiol 577: 641-58

Saltiel P, Rossignol S (2004a) Critical points in the forelimb fictive locomotor cycle and motor coordination: effects of tonic proprioceptive perturbations in the cat. J Neurophysiol 92:1329-1341

Saltiel P, Rossignol S (2004b) Critical Points in the forelimb fictive locomotor cycle and motor coordination: effects of phasic retractions and protractions of the shoulder in the cat. J Neurophysiol 92:1342-1356

Shefchyk SJ, McCrea DA, Kriellaars D, Fortier P, Jordan L (1990) Activity of interneurons within the L4 spinal segment of the cat during brainstem-evoked fictive locomotion Exp Brain Res 80: 290-295

Sherrington CS (1913) Further observations on the production of reflex stepping by combination of reflex excitation with reflex inhibition J Physiol 47:196-214

Skinner F, Kopell N, and Marder E (1994) Mechanisms for oscillation and frequency control in networks of mutually inhibitory relaxation oscillators J Comput Neurosci 1:69-87 (1994)

Taga G, Yamaguchi Y, Shimzu H (1991) Self-organized control of bipedal locomotion by neural oscillators in unpredictable environment. *Biol Cybern* 65:147-159

Traven H, Brodin L, Lasner A, Ekeberg O, Wallen P, and Grillner S (1993) Computer Simulations of NMDA and non-NMDA Receptor-Mediated Synaptic Drive: Sensory Supraspinal Modulation of Neurons and Small Networks. J Neurophysiology 70(2)

Wang XJ, Rinzel J (1995) Oscillatory and bursting properties of neurons. In: Handbook of Brain Theory and Neural Networks Boston MA: MIT Press 686-691

Whelan PJ, (1996) Control of locomotion in the decerebrate cat. Prog in Neurobiology Vol 49 pgs 481-515

Whelan PJ, Hiebert GW, Pearson KG (1995) Stimulation of the group I extensor afferents prolongs the stance phase in walking cats. Exp Brain Res 103:20-30

Williams TW (1992) Phase coupling by synaptic spread in chains of coupled oscillators. Science 258: 662-665

Winfree AT (2001) The Geometry of Biological Time 2nd ed Springer New York

Yakovenko S, McCrea DA, Stecina K, Prochazka A (2005) Control of locomotor cycle durations J Neurophysiol 94: 1057-1065